ADDIS ABABA UNIVERSITY

COLLEGE OF HEALTH SCIENCE

SCHOOL OF PHARMACY

DEPARTMENT OF PHARMACEUTICS AND SOCIAL PHARMACY

GREEN SYNTHESIZED ZINC OXIDE NANOPARTICLES USING *MORINGA STENOPETALA* LEAF WATER EXTRACT FOR CIPROFLOXACIN DELIVERY AGAINST RESISTANT *ESCHERICHIA COLI*

BY:

Mesay Wondaya Bahiru

January, 2022

Addis Ababa, Ethiopia

GREEN SYNTHESIZED ZINC OXIDE NANOPARTICLES USING *MORINGA STENOPETALA* LEAF WATER EXTRACT FOR CIPROFLOXACIN DELIVERY AGAINST RESISTANT *ESCHERICHIA COLI*

BY
Mesay Wondaya Bahiru

A Thesis Submitted to the Department of Pharmaceutics and Social Pharmacy, School of Pharmacy, College of Health Sciences, Addis Ababa University for the partial Fulfillment of the Requirements of the Degree of Master of Science in Pharmaceutics.

Under the supervision of:

Gebremariam Birhanu (PhD)

Eyobel Mulugeta (PhD)

January, 2022

Addis Ababa, Ethiopia

Declaration

I the undersigned, declare that the thesis entitled "Green synthesized zinc oxide nanoparticles using *Moringa Stenopetala* leaf water extract for ciprofloxacin delivery against resistant *Escherichia coli"*, is a result of my own investigation and has not been done in substance for the award of any degree in any other university. All sources of the materials used in this thesis have appropriately been acknowledged.

	Signature	Date
Mesay Wondaya	_____	_____

Addis Ababa University

School of Graduate Studies

This is to certify that the thesis prepared by Mesay Wondaya, entitled: "Green synthesized zinc oxide nanoparticles using *Moringa Stenopetala* leaf water extract for ciprofloxacin delivery against resistant *Escherichia coli"* and submitted in partial fulfillment of the requirements for the degree of Master of Science in Pharmaceutics complies with the regulations of the University and meets the accepted standards with respect to originality and quality.

Approved and signed by the examining committee:

Name	Signature	Date
1. Dr. Gebremariam Birhanu (Advisor)	_____	_____
2. Dr. Eyobel Mulugeta (Advisor)	_____	_____
3. Dr. Yitayal Admasu (Examiner)	_____	_____
4. Dr. Nisha Mary Joseph (Examiner)	_____	_____

Head, Department of Pharmaceutics and Social Pharmacy, School of Pharmacy, AAU

Acknowledgments

First and above all, I would like to thank the Almighty God who gave me the courage and strength to complete my thesis.

Successful completion of this thesis was possible due to the support of many people and organizations. It is therefore a pleasant opportunity for me to express my gratitude for all of them.

My sincere and deepest gratitude and appreciation goes to my advisors Dr. Gebremariam Birhanu and Dr. Eyobel Mulugeta for their valuable guidance, comments, follow-up and inspiring words throughout the course of this work.

I extend my heartfelt thanks to Cadila pharmaceuticals (Ethiopia) P.L.C. for their provision of ciprofloxacin. I am grateful to Microbiology and Parasitology Laboratory of Microbiology Department, College of Health Sciences, Addis Ababa University for their gift of clinical isolates of ciprofloxacin resistant *Escherichia coli* and for provision of their laboratory facilities to conduct antimicrobial susceptibility test. I also thank Ethiopian Biotechnology Institute for providing me the necessary materials and equipments.

I would also like to thank Wollo University and Addis Ababa University for sponsoring my study.

Finally, my gratitude goes to my instructors, friends and families for their support and encouragements throughout the entire work.

Table of Contents

List of Figures

List of Tables

Acronyms

AMR	Antimicrobial Resistance
AR	Antibiotic Resistance
AST	Antimicrobial Susceptibility Testing
CDC	Centers for Disease Control and Prevention
CFU	Colony Forming Units
CLSI	Clinical and Laboratory Standards Institute
DDS	Drug Delivery System
DLS	Dynamic Light Scattering
DNA	Deoxyribonucleic Acid
DSC	Differential Scanning Calorimetry
EARS-Net	European Antimicrobial Resistance Surveillance Network
EE	Entrapment Efficiency
EPHI	Ethiopian Public Health Institute
FTIR	Fourier Transform-Infra Red
FWHM	Full-Width Half-Maximum
GDP	Gross Domestic Product
GLASS	Global Antimicrobial Surveillance System
GRAS	Generally Recognized as Safe
HIV	Human Immunodeficiency Virus
LC	Loading Content
MDR	Multi Drug Resistance
NPs	Nanoparticles
PDI	Polydispersity Index
PSD	Particle Size Distribution

ROS	Reactive Oxygen Species
SEM	Scanning Electron Microscope
SPR	Surface Plasmon Resonance
TEM	Transmission Electron Microscope
TGA	Thermo Gravimetric Analysis
US-FDA	United States - Food and Drug Administration
UTIs	Urinary Tract Infections
UV/Vis	Ultra-Violet/Visible
WHO	World Health Organization
XRD	X-ray Diffraction
ZnO	Zinc Oxide
ZnONPs	Zinc Oxide Nanoparticles
ZOI	Zone of Inhibition

Abstract

Antimicrobial resistance is a critical public health issue in the world which is now challenging the effectiveness of drugs and successful treatment of infectious disease as well as poverty eradication due to its significant financial burden. Urinary tract infection is the most common nosocomial infection which is mostly caused by *Escherichia coli*. Like other infectious disease, its management has become challenging due to antimicrobial resistance. To tackle this problem researchers develop various suitable alternatives including inorganic nanoparticles like zinc oxide nanoparticles (ZnONPs) which are known for their antimicrobial activity, and use of these nanoparticles for the delivery of antibiotics to benefit from the synergetic effect against resistant microbials. Therefore, our study aimed to synthesize ZnONPs using water extracts of *Moringa Stenopetala* leaf which is an endemic plant to Ethiopia, north Kenya and east Somali. Nanoparticles were characterized using ultraviolet-visible spectroscopy, X-ray diffraction (XRD), dynamic light scattering (DLS), scanning electron microscope (SEM), differential scanning calorimetry-thermogravimetric (DSC-TGA) analysis and fourier transform infrared spectroscopy (FTIR). Then, nanoparticles were loaded with ciprofloxacin and characterized using ultraviolet-visible spectroscopy, DLS and FTIR to confirm the effective loading of ciprofloxacin on nanoparticles. Nanoparticles were also evaluated for their drug delivery potential. The drug loading content and drug entrapment efficacy were 49.1% and 96.5 %, respectively. The drug loaded nanoparticles were also evaluated for their drug releasing behavior at four different pH conditions (1.2, 6.0, 6.8 and 7.4 to simulate gastric, *E.coli* infected urinary tract, intestine and blood pH values, respectively). The result revealed that the loaded ciprofloxacin were efficiently released from ZnONPs at the site of *E.coli* infected uroepithelium environment in a sustained manner but with instant release in acidic pH due to the higher solubility of the drug and the nanoparticle in acidic pH. Finally, the antimicrobial activity of ZnONPs and ciprofloxacin loaded NPs was evaluated and compared with ciprofloxacin alone by the disc diffusion method. Accordingly, the drug loaded ZnONPs showed promising result against ciprofloxacin resistant *E.coli* and significantly enhanced the antibacterial activity of ciprofloxacin against this pathogen compared with ciprofloxacin and the unloaded NPs.

Key Words: Antimicrobial resistance**;** Drug delivery; Green synthesis; *Moringa Stenopetala*; Zinc oxide nanoparticles.

1. INTRODUCTION

1.1. Antimicrobial resistance overview

Antibiotics exert their actions on their targets which are generally conserved across the bacterial domain of life but absent or sufficiently different in eukaryotic cells. Keeping the specific mechanism vary from antibiotic to antibiotic, they inactivate bacterial target through mechanisms which include: inhibition of protein synthesis like aminoglycosides; alteration of cell wall synthesis like β-lactams; metabolic disruption like sulfonamides and interference with deoxyribonucleic acid (DNA) replication like fluoroquinolones (Crofts et al., 2017); the latter are known to interact with DNA gyrase and topoisomerase IV enzymes (Hooper, 2001).

After long period of success in treating bacterial infections, conventional and last resort antibiotics are now facing resistant bacteria (Alawieh et al., 2015). While the specific vary from bacteria to bacteria, they utilize a few common approaches to resist antibiotics to survive their effect. Their resistance to antibiotics is demonstrated by the antibiotics inactivation through enzymatic degradation or modification of enzymatic scaffold, alteration of antibiotics targets, reducing the permeability of cell membrane and expression of efflux pump, in which the latter two mechanisms are to keep the intracellular concentration of antibiotics below inhibitory level (Crofts et al., 2017). Moreover, some bacteria and fungi may develop new cell processes that avoid using the antibiotics target. Sadly, when the exposed bacteria develop resistant genes, they share it with other pathogens that have not been exposed to antibiotics (CDC, 2019).

Antimicrobial resistance (AMR) can be defined as the ability of microbes to grow in the presence of a class of drugs known as antimicrobials that would normally kill microbes or limit their growth. It occurs when microorganisms such as bacteria, viruses, fungi and parasites change in ways that render the medications used to cure the infections they cause ineffective (CDC, 2019, ECDC, 2018).

Antimicrobial resistance is a critical public health issue in the world and is now challenging the effective and successful treatment of infectious disease (WHO, 2017). It is a global crisis which can affect any person at any stage of life and once it is developed somewhere in the world, it can

be spread to the other parts through people, goods and animals with a remarkable speed (CDC, 2019). It was the fourth health issue to be discussed by United Nations General Assembly in September 2016 (Roope et al., 2019). The first report from the World Health Organization's (WHO) Global Antimicrobial Surveillance System (GLASS) in 2017 showed that there was a widespread occurrence of antibiotic resistance in 500,000 people with only eight suspected bacteria across 22 countries. According to this report, resistance to ciprofloxacin in urinary tract infection caused by *E.coli*, as an example, was between 8 and 65% (WHO, 2017). With under estimation due to poor reporting and surveillance, it is estimated that 700,000 people die every year globally from drug resistance bacterial infection, human immunodeficiency virus (HIV) and malaria (Ibrahim et al., 2018). This figure may be increased to 10 million deaths in 2050, from which 4.15 million will be the contribution of Africa, if nothing is done for the containment of AMR (Osman et al., 2019, Safdari et al., 2017, Roope et al., 2019, O'neill, 2014). According to 2019 Antibiotic Resistance (AR) Threats report of Centers for Disease Control and Prevention (CDC), more than 2.8 million antibiotic resistant infections occurs in the United States which ends up with the death of 35,000 people each year (CDC, 2019). Similarly, in Europe, more than 670, 000 infections occur due to bacteria resistant to antibiotics and around 33,000 people die each year (ECDC, 2018).

Antimicrobial resistance is a problem for developing countries, like Ethiopia, too. A systematic review about bacterial infections and their antibiotic resistance pattern and which encompasses publications before April 2018 showed that, majority of the bacterial isolates were resistant to commonly used antibiotics (Reta et al., 2019). Another cross-sectional study conducted in Hawassa University Comprehensive Specialized Hospital indicated that, almost all isolates were with substantial rates of resistance to most of the antibiotics that are commonly used in the study area (Alemayehu et al., 2019). Similarly, a cross-sectional study conducted in Gondar town revealed that there were high multiple drug resistant bacterial pathogens for commonly used antibiotics from Gondar university teaching hospital waste water (Moges et al., 2014a). Treatment options for infectious disease have become limited due to the wide spread occurrence of resistant pathogens for frequently prescribed antimicrobials in some countries including Ethiopia (Moges et al., 2014b).

Antimicrobial resistance has also a significant financial burden due to longer treatment duration, additional laboratory test and use of expensive medicines, especially in developing countries (Sweileh et al., 2018, Ibrahim et al., 2018). By considering only the direct health care costs, it was estimated that AMR costs from 5 to 55,000 additional US dollar per patient episode (Roope et al., 2019). Worldwide, it may cause a loss of 100 trillion US dollar through 2015 to 2050, which negates the eradication of poverty (Ellen et al., 2019), and by 2030, due to AMR, more than 24 million people may be forced into extreme poverty, of which many will come from developing countries (FAO, 2018). It is also expected that the world's gross domestic product (GDP) may be 0.5% and 1.4% smaller by 2020 and 2030, respectively with 100 million people's premature death for the latter (O'neill, 2014). In Europe also, there is an estimated 1.1 billion EUR costs related to AMR annually (ECDC, 2018).

Among the most common bacterial infections, urinary tract infections are the one with significant economic and clinical burden. Regarding its financial burden, merely in United States, it costs 1.6 – 3.5 billion US dollar annually (Steiger et al., 2017).

1.2. Urinary tract infections

Urinary tract infection (UTI) is the inflammation of any tissue from renal cortex to urethral meatus due to invasions of both gram negative and gram positive bacteria or due to candida infections (Zhou and Lv, 2020). UTIs are the most common nosocomial infection (Tielen et al., 2011). Globally, the annual incidence is around 150 million cases (Arslan et al., 2005, Fasugba et al., 2015, Flores-Mireles et al., 2015) and whatever the sterility of hospital conditions, 10% of all hospitalized cases contract these infections (Fahimmunisha et al., 2020). It is responsible for 25% of the health care related infections (Rajivgandhi et al., 2019) and is the second common causes of morbidity in the population only preceded by respiratory infections (Rajivgandhi et al., 2019, Reis et al., 2016). In comparison with men, it is more common in women (Walsh and Collyns, 2017) and approximately half of all women have had a UTI during their late 20s' (Marrs et al., 2005).

It is caused by both gram-positive and gram-negative bacteria including *Staphylococcus aureus*, *Enterococcus faecalis*, *Escherichia coli*, *Proteus mirabilis*, *Pseudomonas aeruginosa*, *Enterobacter sp.* and *Klebsiella pneumonia* (Rajivgandhi et al., 2019) but most commonly it is

caused by *E.coli* (80-90% of all UTIs) (Nielsen et al., 2017, Abejew et al., 2014, Kudinha, 2017, Robino et al., 2014).

E.coli, which causes common hospital and community acquired infections worldwide, is among the eight pathogens selected for WHO's Global AMR Surveillance System (GLASS) early implementation phase (WHO, 2017). It is also among the three pathogens prioritized for surveillance in Ethiopia as part of WHO's GLASS early implementation phase (Ibrahim et al., 2018). In addition, it is included in the list of WHO global priority pathogens for research and development to address antibiotic resistant bacteria (WHO, 2017).

1.3. Ciprofloxacin hydrochloride

Quinolones are family of antibiotics containing a bicyclic core structure related to the compound 4-quinolone. Due to their high potency, broad spectrum of activity, favorable bioavailability, convenient formulations, high serum concentrations and low incidence of side effects, they have been favored for more than five decades (Pham et al., 2019). They are under critically important column in the list of critically important antimicrobials for human (Van Giau et al., 2019).

Ciprofloxacin is the second generation quinolone drug with the chemical formula of 1-cyclopropyl-6-fluoro-1,4-dihydro-4-oxo-7-(1-piperazinyl)-3-quinolinecarboxylic acid and ciprofloxacin hydrochloride is the monohydrochloride salt of it, as it is indicated in Figure 1. In short, it is resulted from additions of piperazine ring to C_7 position, fluorine to C_6 position and cyclopropyl at the N_1 position of the pharmacophore of the class. The addition of fluorine and piperazine ring is to improve the gram negative potency and cyclopropyl is to improve the overall activity.

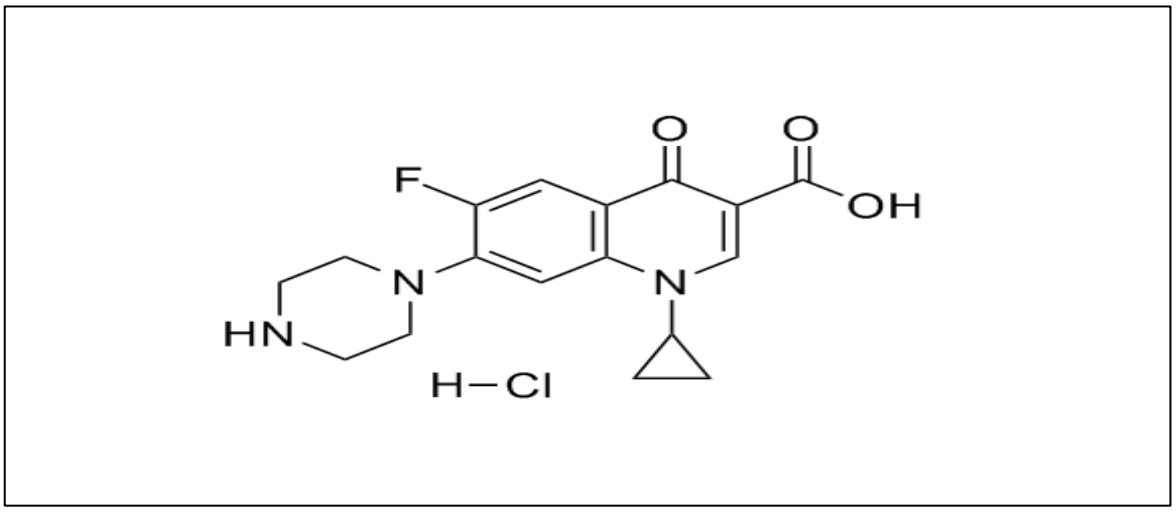

Figure 1: Chemical Structure of Ciprofloxacin Hydrochloride

Ciprofloxacin is a faintly yellowish to light yellow crystalline substance. It is a zwitterionic molecule with pK_a values of 6.2 and 8.59 at 37^0C and 6.8 and 8.73-8.76 at 25^0C for pK_{a1} and pK_{a2}, respectively. It is with a "U" shaped pH-solubility profile with a minimum solubility near the isoelectric point (close to neutral) and maximum solubility at pH values of less than 5 and greater than 10 (Olivera et al., 2011). It is soluble in water, slightly soluble in methanol, very slightly soluble in ethanol and practically insoluble in acetone, in ethyl acetate and in methylene chloride (Avramescu et al., 2017).

Ciprofloxacin is effective against all gram-negative and some atypical pathogens (Pham et al., 2019). It is the most potent fluoroquinolone, being aerobic gram-negative bacilli especially enterobacteriaceae and *Neisseria* are the most susceptible organisms for it (Sharma et al., 2010). It is approved for the treatments of 14 types of infections (Olivera et al., 2011) and it is among the most commonly used antibacterial agents for treatment of community acquired UTIs (Pham et al., 2019, Fasugba et al., 2015); even it is the first option to treat UTIs empirically (Reis et al., 2016). Likewise, according to Ethiopian standard treatment guidelines for general hospitals, it is the first line drug for the treatment of both acute non-complicated as well as complicated UTIs (FMHACA, 2014). It is also among antibiotics selected for antimicrobial susceptibility testing (AST) for the GLASS early implementation phase (WHO, 2017).

1.4. AMR as a challenge for UTIs treatment

Managing UTIs caused by *E.coli* has become challenging over the years due to the increased resistance to commonly used antibiotics (Kudinha, 2017). The result of the study that analyzed global research output in AMR among uropathogenes, which were published between 2002 and 2016, revealed that there was a noticeable increase in AMR (Sweileh et al., 2018). It was also indicated that, in all WHO regions, there was higher rates of *E.coli* resistance for antimicrobials (Fasugba et al., 2015). The origin of fluoroquinolones resistant *E.coli*, though it is not defined, may be from the proliferation of spontaneous fluoroquinolones resistant *E.coli* mutants in human gut as a result of fluoroquinolones use or it may be due to human acquisition of preexisting fluoroquinolone resistant strains from exogenous sources (Johnson et al., 2006). In a systematic review which aimed to compare ciprofloxacin resistance to hospital and community acquired UTIs by *E. coli*, indicated that there was resistance in all parts of the world being the higher resistance rate was in developing countries compared with developed countries (31% for Africa only preceded by Asia which was 43%). The main reasons for higher resistance in developing countries are poverty and lack of knowledge which in turn increases the empirical and over-the-counter uses of antibiotics. Patient expectation is also another factor which enforces 40% of general practitioners to prescribe antibiotic only to meet their patients need, which again leads to antimicrobial resistance (Zhou and Lv, 2020). In another study which aimed to investigate the level of AMR in *E.coli* isolate causing UTI in female outpatients from six European countries also indicated that there was a higher rate of resistance for ampicillin, trimethoprim, amoxicillin/clavulanic acid, trimethoprim/sulfamethoxazole and ciprofloxacin (Ny et al., 2019). More than half of the *E.coli* isolates reported to European Antimicrobial Resistance Surveillance Network (EARS-Net) for 2018 were resistant to at least for one of aminopenicillins, fluoroquinolones, third-generation cephalosporins, aminoglycosides and carbapenems. There was also a significant increase in resistance between 2015 and 2018 for fluoroquinolones and third generation cephalosporin. Both in number of cases and attributable disease in Europe, antimicrobial resistant *E.coli* contributed the most for the burden of AMR (ECDC, 2018). In Brazil also 35% of *E.coli* was resistant to ciprofloxacin (Reis et al., 2016). A study conducted to assess the antimicrobial resistance patterns of bacteria isolated from the urine samples for six years starting from 2012 in Ayder comprehensive specialized hospital, found in Tigray region of Ethiopia, indicated that there was a high level of antimicrobial resistance to commonly

prescribed antibiotics. This study also revealed that there was a significant resistance of *E. coli* to all tested antibiotics including ciprofloxacin except for imipenem and nitrofurantoin (Tuem et al., 2019). According to Ethiopian Public Health Institute (EPHI) (EPHI, 2017), there was a multiple antibiotic resistance (resistance for more than 5 antibiotics) gram negative isolates including *E.coli* and even pan-antibiotic resistant *E.coli* when study was conducted from surgical site infections in St. Paul Specialized Hospital Millennium Medical College and Yekatit 12 Referral Hospital Medical College since 2016. There was also *E.coli*, isolated from cloacal swab of broiler chickens, which showed multi drug resistance (MDR) for two or more antimicrobials in a study conducted in eastern Harerge zone selected farms since 2013. A systematic review and meta-analysis conducted by considering five year back publications from 2019 indicated that many bacteria were resistant to commonly prescribed drugs and numerous pathogens were develop multidrug resistance. According to this study, there was resistance *E.coli* to ceftriaxone, ciprofloxacin, and norfloxacin and also there was multi drug resistant strain (Muhie, 2019). All in all, there is a wide spread resistance of *E.coli* to fluoroquinolones, which in turn can has serious clinical impacts due to they are one of few available options to treat serious *E.coli* infections (Fasugba et al., 2015).

In the era of antimicrobial resistance development, therefore, it is very important to develop suitable alternative strategies which may include discovery of new generation antibiotics, combined therapy, use natural antibacterial agents like plant extracts, and application of nanotechnology in addition to proper utilization of the available antibiotics (Jelinkova et al., 2019). The rapid development of AMR for the available antimicrobials made the researchers to constantly search efficient antimicrobial agents that prevent the microorganisms getting resistance to it (Barui et al., 2018, Raj and Jayalakshmy, 2015). Nanotechnology, in this regard, opens a new gateway in producing new antibacterial agents that can inhibit the growth of or kill the resistant organisms. In between 2018 and 2020, there were about 99,000 scientific publications about searching new antimicrobial compounds of which 5,900 were searching for antimicrobial compounds based on metallic compounds like zinc, copper, nickel, cobalt, manganese, chromium and silver (Gudkov et al., 2021).

1.5. Nanotechnology

The term nanotechnology, invented by Norio Taniguchi, Professor of Tokyo University, in 1974 (Rajoriya et al., 2017), is defined as a science which deals with the manufacture and application of materials with size of up to 100 nm (Siddiqi et al., 2018). It is the creation and utilization of particles which fall between individual molecule and corresponding bulk material through the control of properties and structure of matter at the nanomertic scale (Bhumi et al., 2014). It is sixth most revolutionary and promising technology with varieties of applications (Chandra et al., 2019). It has an application in various sections of biological, medicine, cosmetics, renewable energies, environmental remediation and biomedical devices (Thatoi et al., 2016).

Nanoparticles (NPs), on the other hand, according to European Commission, can be defined as "are such that 50% or more of the particles in a sample have a dimension in 1-100 nm size range" (Maguire et al., 2018). The word "nano", which is derived from the Greek word "dwarf", indicates the billions parts of a meter and it means extremely small (Rajoriya et al., 2017). When they are synthesized from their bulk equivalent, the physical, chemical, mechanical and biological properties are improved significantly (Akbar et al., 2020).

These NPs can be classified primarily as organic and inorganic NPs. The former is for NPs of carbon and the latter is for a collection of magnetic, noble metal and semiconductor NPs. The noble metal NPs include platinum, gold and silver NPs; semiconductor NPs contain titanium dioxide, zinc oxide and zinc sulfide NPs (TC et al., 2010, Selvam and Sivakumar, 2015); and magnetic NPs include iron, nickel and cobalt (Akbarzadeh et al., 2012). From nanotechnology outputs, nowadays, many researches have been focused on the inorganic NPs due to their reduced toxicity, better antimicrobial activity and stability (Barui et al., 2018, Raj and Jayalakshmy, 2015). From inorganic NPs, metal and metal oxide NPs are emerging as potential candidates due to their wide range of applications (Muthuvel et al., 2020) like catalysis (e.g. titanium oxide NPs, manganese oxide NPs, copper oxide NPs) (Akbari et al., 2018), sensors (e.g. copper oxide NPs, zinc oxide NPs) (Chavali and Nikolova, 2019), antibacterial (e.g. silver NPs, zinc oxide NPs, titanium oxide NPs, copper oxide NPs (Dizaj et al., 2014), luminescent materials (e.g. gold NPs) (Zheng et al., 2012) and drug delivery (e.g. silver, iron (Venkatesh et al., 2018), zinc oxide NPs (Nagarajan and Kuppusamy, 2013, Rajendran et al., 2021)).

1.5.1. Zinc oxide nanoparticles

Zinc oxide (ZnO), one of inorganic metal oxides, is a member of the group II-VI semiconductor family (Matinise et al., 2017) which exhibits unique properties like a wide range of radiation absorption, piezoelectric, pyroelectric and possesses high catalytic activity. It is available in three crystalline forms namely hexagonal wurtzite, rock salt and cubic structure (Aldalbahi et al., 2020) from which wurtzite is most common and thermodynamically stable at surrounding conditions (Beg et al., 2020, Agarwal et al., 2017), the cubic structure is meta stable and rock salt structure is only stable under extreme pressure (Agarwal et al., 2017). In hexagonal wurtzite structure, each tetrahedral zinc atoms are surrounded by four oxygen atoms and vice versa (Sirelkhatim et al., 2015). Zinc oxide has been listed as "Generally Recognized as Safe" (GRAS) by US Food and Drug Administration (US-FDA) due to its non-toxic properties which in turn make it safe to be used on human and animals (Yusof et al., 2019, Sharma et al., 2019). In addition ZnONPs are biodegradable, biocompatible (Matinise et al., 2017) and with low cost (Vijayakumar et al., 2020).

Among ten different known engineered nanomaterials, ZnONPs are the third highest nanoparticle produced and utilized in different fields globally only preceded by nano-silicon dioxide and nano-titanium dioxide (Piccinno et al., 2012). This wide scientific and industrial application of ZnONPs is due to their good conductivity, chemical stability, catalytic properties, antifungal, antimicrobial and antiviral activities (Akbar et al., 2020). Because of its high surface-to-volume ratio, it is with high surface reactivity (Aldalbahi et al., 2020) and hence it is widely used in solar cells, Ultraviolet (UV) light emitting devices, gas sensor, photocatalysts, cosmetics industries, optoelectronic, varistors, photodetectors, pharmaceutical and other biological applications (Muthuvel et al., 2020, Sangeetha et al., 2011). The NPs have been reported in morphologies like nanoflower, nanobelt, nanoflake, nanoroads and nanowire (Agarwal et al., 2017).

1.5.2. Synthesis of metallic nanoparticles

Nanoparticles can be synthesized in two approaches namely, top-down and bottom-up approaches. The top-down approach, as the name implies, is formulating or creating a nano scale structure starting from larger ones by reducing their size through "cutting" to required values while bottom-up approach is synthesizing NPs by starting at the molecular, atomic or ionic level

with precise control of molecular structure (TC et al., 2010, Pryshchepa et al., 2020). Based on processes had been used, synthesis techniques can be categorized as; physical, chemical and biological methods in which the former two methods are concidered as traditional methods. Physical approaches utilize physical agents like, heat, electrical discharge, plasma or electromagnetic radiation for the production of nanomaterials. It includes mechanical milling/ball milling, laser ablation, sputter deposition, lithography and spray pyrolysis. Chemical method, on the other hand, implies NPs production through chemical transformations of the starting materials (metal precursor, reducing agent, and stabilizing/capping agents). It includes hydrothermal mediated, precipitation, chemical reduction, micro-emulsion and sol-gel synthesis (Pryshchepa et al., 2020). However, both physical and chemical methods are with limitations of; they are costly, with low production rate, need highly restricted laboratory environment, require high temperature and pressure, consume high energy for synthesis, produce toxic by-products and in case of chemical method, since toxic chemicals are used for synthesizing and stabilizing of NPs, they may be adsorbed on the surface which makes difficult for biological applications of NPs (Akbar et al., 2020). In addition there is a need of additional capping and stabilizing agents in these methods (Sharma et al., 2020).

In order to deal with these limitations, it is obvious to need an alternative which is cost-effective, safe and environmentally sound method for NPs synthesis. Green synthesis method is a feasible alternate in this regard. It is a bottom-up approach which may be microbial mediated (use bacteria and bacterial extracts), natural extract mediated (use plant or algae extracts) and biomolecule/biopolymer mediated (utilizes biomolecules isolated from living organisms/structural biopolymers) (El Shafey, 2020). Due to the difficulty of selection and cultivation of suitable bacterial strain, scaling laboratory process to industry and additional stage of purification of microorganism mediated NPs production, plant mediated green synthesis is gaining popularity over it (Ivanova et al., 2018, Zhu et al., 2019). In addition, this microorganism mediated synthesis needs microorganism culture maintenance, highly aseptic conditions and high cost associated with media and process (Agarwal et al., 2017). Plant mediated green synthesis method utilizes natural extracts mainly phytochemicals (including sugars, lignans, polyphenols, flavonoids, aromatic acids, xanthones, terpenes, quinones, proteins and alkaloids) obtained from

plants, leaves, fruits, peels, flowers, and seeds for the synthesis of inorganic NPs including metal oxide NPs (Zhu et al., 2019, Isık et al., 2019).

In general, green synthesis method reduces the negative effect of the production and applications of nanomaterials; in other words, it lowers nanotechnology riskiness. It is an eco-friendly approach, with reduced cost of synthesis because of utilization of biological components which acts as both reducing and capping agent, with reduced energy consumption and it can be used at large scale production of NPs (El Shafey, 2020). But, as a limitation for this method, the difficulty to point the exact compound from phytochemicals which is responsible to the formation of NPs and the variability of phytochemicals levels in plants based on climate change and location can be concidered (Zhu et al., 2019).

1.5.2.1. Green synthesis of ZnONPs

Due to the above aforementioned advantages and popularity of green synthesis method, different works had been done to synthesize ZnONPs using plant extracts. These includes synthesis of ZnONPs using extracts from *Azadirachta indica, Agathosma betulina, Aloe vera, Anisochilus carnosus, Calatropis gigantean, Cocus nucifera, Coptidis rhizome, Moringa Oleifera, Parthenium hysterophorus* (Agarwal et al., 2017), *Calotropis procera , Aloe barbadensis miller, Corriandrum sativum, Acalypa indica, Sargassum myriocystum, Cassia auriculata, Vitex negundo, Camelia sinensis, Olea europea, Catharanthus roseus, Hybanthus enneaspermus, Hibiscus rosa-sinensis, Citrus paradise, Morinda pubescens, Tabernaemontana Divaricate, Murraya koeininggi, Cassia densistipulata taub, Cassia fistula, Ficus benghalensis, Trifolium pretense, Emblica Officinalis, Hibiscus subdariffa, Hemidesmus indicus, Punica granatum, Lawsonia inermis Melia azedarach* L., *Micrococca mercurialis, Passiflora edulis* and *Duranta erecta* L. (Akbar et al., 2020).

Although the ability of plant extracts to reduce metal ions has been known since the early 1900s (Kavitha et al., 2017), defining a precise mechanism route of synthesizing metal and metal oxide NPs using them is still a challenge because of a problem to analytically determine the exact amount of all molecules extracted from plant which are found in enormous variety and in different concentrations (Bandeira et al., 2020, Sangeetha et al., 2011). Phytochemicals present in plant extract with antioxidant property are the basis for ZnONPs preparation (Kavitha et al.,

2017). One plausible mechanism for the formation of ZnONPs involves the formation of intermediate $Zn(OH)_2$ due to reduction of Zn^{+2} ions to its stable form when it is chelated with antioxidant phytochemicals like polyphenols and flavonoids and latter ZnONPs will be formed due to heat treatment (calcination) of this intermediate product (Ezealisiji et al., 2019, Yuvakkumar et al., 2014, Matinise et al., 2017, Suresh et al., 2018, Gawade et al., 2017). Another estimated mechanism is Zn^{+2} may be reduced by these antioxidant phytochemicals to zero-valent states without forming coordinated complex with them and this reduced zero-valent zinc atom reacts with dissolved oxygen in the solution to form ZnO nuclei, which is stabilized by those plant compounds (Sutradhar and Saha, 2016, Singh et al., 2018, Jan et al., 2020, Akintelu and Folorunso, 2020). The latter proposed mechanism of formation for ZnONPs may be the mechanism involved in our NPs formation because they were formed without heat treatment (calcination) and the plausible mechanism is illustrated in Figure 2.

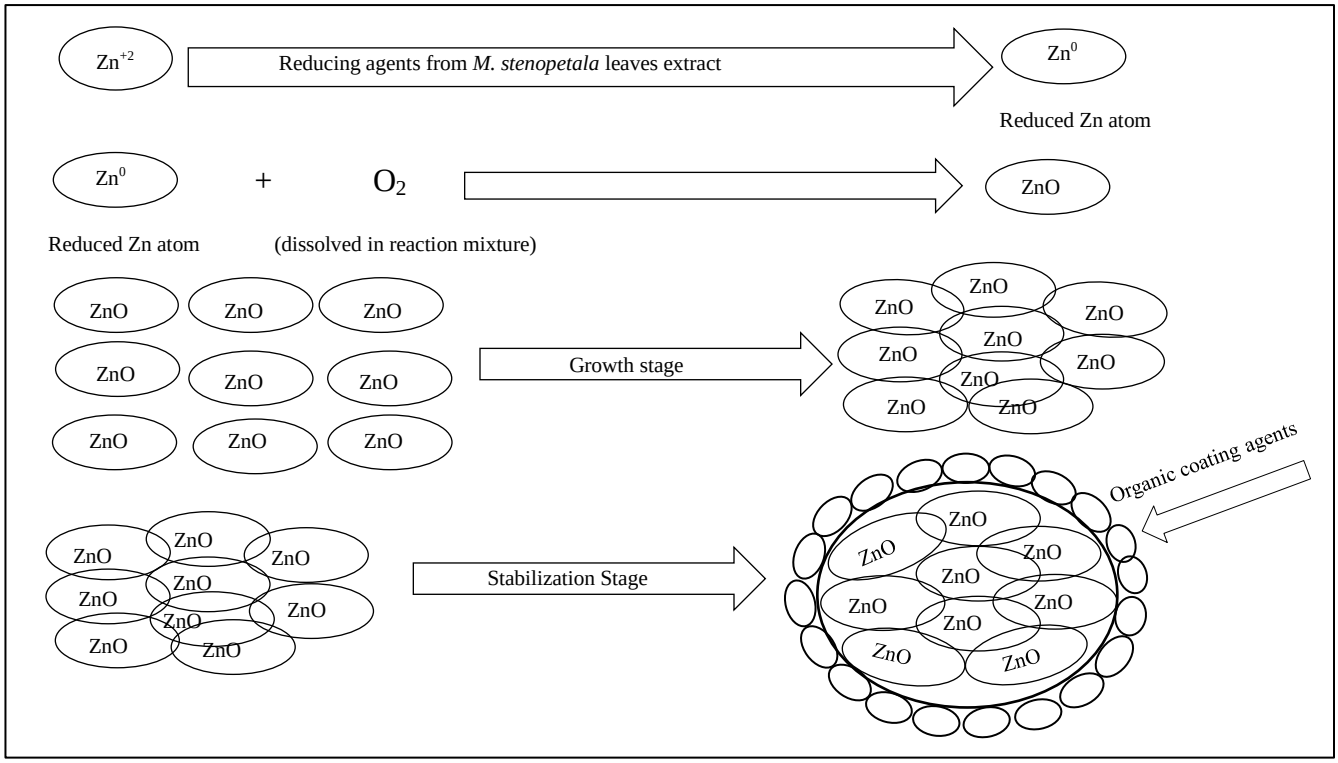

Figure 2: Probable mechanism of ZnONPs synthesis using *M. Stenopetala* leaf extract (Singh et al., 2018).

1.5.2.2. ZnONPs as an antimicrobials agent

The antibacterial properties of ZnO is known since antiquity and historical records show it was used in many ointments for the treatment of injuries and boils even in 2000 BC (Siddiqi et al., 2018). It is demonstrated that ZnONPs have strong bactericidal properties against broad spectrum of pathogenic bacteria (Isık et al., 2019, Ghasemi and Jalal, 2016) and it is with interesting antibacterial activities against both gram negative and gram positive bacteria (Muthuvel et al., 2020). Due to this, it is utilized in antiseptic creams, cosmetic products, calamine lotion, shampoos and surgical tapes (Happy et al., 2019). Its antimicrobial activity is proposed through destruction of cell integrity due to its direct contact with cell walls, reactive oxygen specious (ROS) formation, and release of antimicrobial ions mainly Zn^{+2}, as shown in Figure 3 (Shaikh et al., 2019, da Silva et al., 2019). These broad spectrums of mechanisms create a difficulty for microorganisms to develop resistance for these NPs (Kora and Arunachalam, 2011).

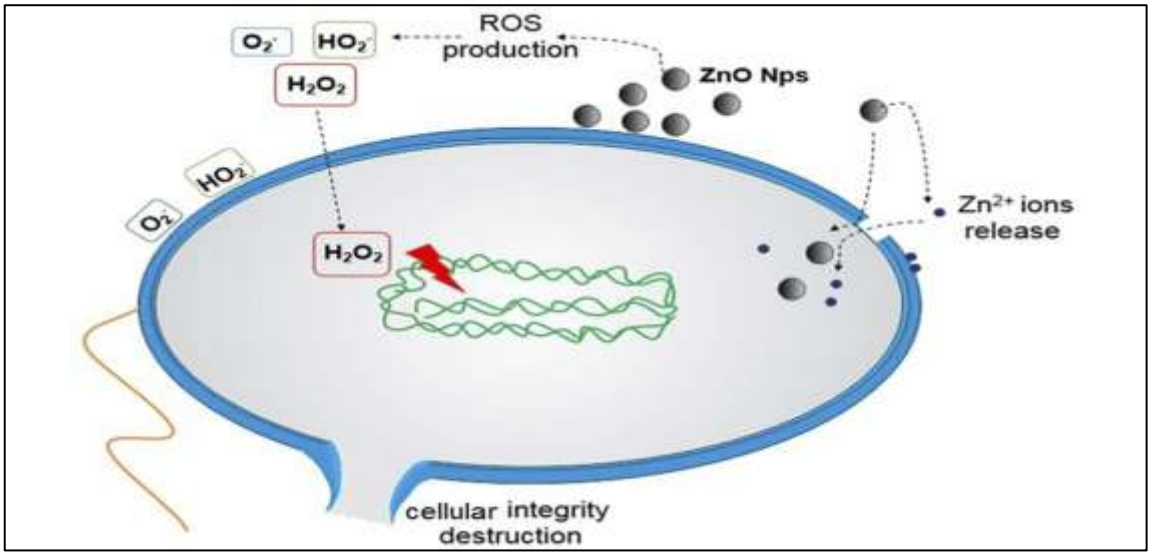

Figure 3: Suggested mechanisms of action of ZnONPs against bacteria (da Silva et al., 2019).

In addition to their own antimicrobial activity, they enhance the activities of antibiotics when they are conjugated with them with simultaneous antibiotic dose reduction (Shaikh et al., 2019, Van Giau et al., 2019, Kalita et al., 2016). Conjugation enhances the ability of killing the antibiotic resistant bacteria, increases antimicrobial concentration at the sites on which it interact with bacteria, aids the binding of antimicrobials with bacteria (Shaikh et al., 2019), and shields the antimicrobial from pathogens resistance mechanism (Van Giau et al., 2019). Conjugation

also reduces development of antimicrobial resistance. As it is reported, in comparison with the drug alone, microbes are unlikely to develop resistance to drug-NP conjugates (Sreedharan and Singh, 2019).

1.5.2.3. ZnONPs as drug delivery devices

Metallic NPs can act as an effective system for the delivery of drugs. Since the surface of green synthesized metallic NPs is covered with functional groups come from phytochemicals, they can easily bind or interact with target molecule of interest which is to be delivered (Sreedharan and Singh, 2019). Due to this, biosynthesized ZnONPs have been used as a drug carrier (Nagarajan and Kuppusamy, 2013, Rajendran et al., 2021) and ZnO based nanostructures are now being established in drug delivery system (DDS). They are good nano platform for drug delivery (Król et al., 2017). In one study, ZnONPs were synthesized by green method using *Borassus flabellifer* fruit extract and they were with high drug loading capacity and drug delivering efficiency (Vimala et al., 2014).

1.6. *Moringa Stenopetala*

Moringa Stenopetala (M. Stenopetala), originally discovered by Donadson Smith in 1895 (Habtemariam, 2017), is a massive tree which attains a height of 6 - 12 meters with a diameter at breast height of 60 cm. It is with many leafy branches and the leaves are green, 3.3 - 6.3 cm long and 1.8 - 3.3 cm wide and they are di- or tri-pinnate with five pairs of pinnae and three to nine elliptic to ovate leaflets on each pinna (Hamza and Azmach, 2017).

In Ethiopia it is locally called, amongst others, *aleko* or *Shiferaw;* or ‘cabbage tree’ in English (Habtemariam and Varghese, 2015). Its taxonomy is given as (Hamza and Azmach, 2017):

Kingdom	Plantae
Division	Magnoliophyta
Class	Magnoliopsida
Order	Moringales
Family	Moringaceae
Genus	*Moringa*
Species	*stenopetala*

M. Stenopetala is among 13 species of *Moringaceae* family which is endemic species to Ethiopia (mainly in southern part), Northern Kenya and Eastern Somali (Murali et al., 2014, Tekle et al., 2015) and due to this it is also called East African Moringa tree (Mitiku and Yilma, 2017). Although, in recent years, it is distributed nearly in all parts of the midlands and lowlands of Ethiopia (Abiyu et al., 2018), it is widely cultivated and distributed in Konso, Keffa, Borena, Gamo Gofa, Wolayita, Sidama, Debub Omo zone, Dherashe areas and the adjoining provinces.

M. Stenopetala is resistant for drought, insects and pests (Abuye et al., 2003). It grows best in hot, semi-arid tropical region, at an altitude below 600 m and in a temperature range of 25-35^{0}C. It can grow in an area with annual rain fall of 250 -1500 mm (Hamza and Azmach, 2017) and can grow in poor soil (Habtemariam and Varghese, 2015). Once it is established, it will not show any sign of moisture stress in areas with a harsh agro-ecology for tree growth (Jiru et al., 2006). It is with the ability to be harvested in a short period of time (Habtemariam and Varghese, 2015).

Figure 4: *M. stenopetala* tree

Almost all parts of the tree (roots, flowers, pods, seed oil, leaves, seed and fruits) have been used in traditional medicine preparation to treat various human diseases (Hamza and Azmach, 2017). It is widely used as a traditional medicine for treatment of diarrhea, hypertension, diabetics, stomach pain, malaria, leprosy, epilepsy, asthma, cold, emetic, for wound healing and as an

antioxidant in addition to its utilization as source of diet (Habtemariam and Varghese, 2015). It is also used for water purification, hedges, fences, wind breaks and for animal food (Habtemariam, 2017).

Unlike ZnONPs synthesized by other methods, there is a scarcity of studies about the antimicrobial effects of antibiotics loaded ZnONPs prepared by green synthesis and more specifically, to the best of my knowledge, there is no study yet on the antibacterial effect of ZnONPs and antibiotics loaded ZnONPs synthesized using *M. Stenoptala.* In addition, ZnONPs, fabricated by green synthesis, are less explored for their drug delivery potential. Based on these facts, the aim of this study was to prepare ZnONPs using water extracts of *M. stenoptala* leaf for ciprofloxacin delivery and to evaluate the antimicrobial effect of drug loaded NPs against ciprofloxacin resistant *E.coli*.

1.7. Significance of the study

Antimicrobial resistance is a critical public health issue in the world with significant social and economic burden on the society especially in developing countries. Currently, the problem becomes even more severe because of reduced pharmaceutical interest in developing new antimicrobial agents (Alawieh et al., 2015) and resistance occurrence is outplaced the development of new drugs. One of the approaches currently used by different researchers to solve this global concern is the development of novel strategies that can alleviate the challenge. One of the strategies is development of antimicrobial nanomaterials for the delivery of the antibiotics to have a synergetic antimicrobial effect when conjugated with the antibiotics. Therefore, the aim of this study was to synthesize antimicrobial ZnONPs from water extract of *M. Stenopetala* leaf for the delivery of ciprofloxacin against ciprofloxacin resistant *E.coli.*

Therapeutic drug molecules have different limitations like poor solubility, non-specificity and faster clearance from the body (Barui et al., 2018). For example, 70% of the oral dose of ciprofloxacin is excreted unchanged in the urine which necessitates frequent administration which in turn associated with numerous side effects (Isa et al., 2016). These limitations can be solved using NP based drug delivery system which allows sustained release and delivery of drugs to desired area of the body (Barui et al., 2018). Therefore, our study was aim to find alternative approach for the delivery of ciprofloxacin by synthesizing ZnONPs with good drug

loading and entrapment efficiency, and with sustained releasing profile at the pH value of the intended site of action.

Many conventional ZnONPs synthesis routes like physical and chemical methods require a particular set-up, high cost, high temperature-pressure conditions and chemicals which can't easily disposed of due to their non-ecological nature. Hence, ZnONPs synthesis procedures that eliminate the use of toxic chemicals and apply environmentally friendly routes are becoming demand of the time. In line with this, in our study, we aimed to synthesize ZnONPs from *M. Stenopetala* leaf extract by green synthesis method which is cost effective, simple, rapid, and safe route.

1.8. Objectives

1.8.1. General Objective

- To prepare ZnONPs from water extract of *M. Stenopetala* leaf for ciprofloxacin delivery and to evaluate the antibacterial effect of drug loaded NPs against ciprofloxacin resistant *E. coli*.

1.8.2. Specific Objectives

- To synthesize and characterize ZnONPs using *M. Stenopetala* leaf extract and $Zn(NO_3)_2.6H_2O$.
- To load ciprofloxacin on ZnONPs and to characterize drug loaded ZnONPs.
- To determine the drug loading and encapsulation efficiency of ZnONPs.
- To determine the *in vitro* drug release profile of the drug loaded NPs.
- To evaluate the *in vitro* effect of drug loaded NPs against ciprofloxacin resistant *E.coli*.

2. MATERIALS AND METHODS

2.1. Materials

Ciprofloxacin HCl (98.28%) was kindly donated by Cadila pharmaceuticals (Ethiopia) P.L.C. Clinical isolates of ciprofloxacin resistant *Escherichia coli* was obtained from microbial stock cultures, Microbiology and Parasitology Laboratory, College of Health Sciences, Addis Ababa University. Other materials and chemicals that were used in the study include zinc nitrate hexahydrate ($Zn(NO_3)_2.6H_2O$) (96%, Loba Chemie Pvt. Ltd., India), absolute ethanol (97%, Dallul Pharmaceuticals PLC), chloroform AR (Reagent Chemical Services Ltd., UK), sulfuric acid (98%, Loba Chemie Pvt. Ltd., India), hydrochloric acid (35.4%, Loba Chemie Pvt. Ltd., India), potassium iodide (99-100.5%, Loba Chemie Pvt. Ltd., India), ferric chloride (99%, Loba Chemie Pvt. Ltd., India), sodium carbonate (Sigma chemical company, USA), sodium chloride (99.8%, UNI-CHEM chemical reagent), iodine (Reagent Chemical Services Ltd., UK), sodium citrate (99%, UNI-CHEM chemical reagent), copper sulfate (98.5%, Banbury, UK), gelatin powder (Blulux Laboratories Ltd., India), sodium hydroxide (99.8% Norbright, China), potassium chloride (99% BDH Limited Poole, England), potassium dihydrogen orthophosphate (99%, TITAN BIOTECH LTD., India), distilled water, Whatman No.1 filter paper, Whatman No.3 filter paper, dialysis Sack (an average flat width of 35 mm, and 12 kDa molecular weight cutoff, SIGMA-ALDRICH, USA), universal indicator (Effective laboratory supplies, India), thermometer, petri plate, Müller-Hinton agar (Sisco Research Laboratories Pvt. Ltd.) and other common laboratory equipments and supplies were used for this work. All chemicals and reagents used in this work are of analytical grade and they were used without any further purification. All aqueous solutions were prepared using distilled water.

2.2. Collection and identification of *M. Stenopetala* leaves

In September 2020, fresh leaves of *M. Stenopetala,* without any infestation were collected from Southern Nations Nationalities and Peoples Regional State of Ethiopia, Gamogofa zone, Arbaminich City (Latitude: 6° 01' 59.99" N and Longitude: 37° 32' 60.00" E). The collected leaves were botanically identified (authenticated) using the standard morphological characteristics features by department of plant biology and biodiversity management, Addis Ababa University.

2.3. Preparation of *M. Stenopetala* leaf extract

The preparation of *M. Stenopetala* leaf extract was done according to (Rad et al., 2019). The collected *M. Stenopetala* leaves were washed with tap water and distilled water to remove unwanted impurities. Then, the leaf sample was shadow dried at room temperature for 10 days. The dried leaves were ground using high speed multifunction comminutor RRH-A350 (Shanghai Yuanwo Industrial and trade Co., Ltd.) and sieved using 125µm size sieve. About 5 g of the powder was weighed and boiled with 100 mL of distilled water for 10 min at 60^0C while stirring under magnetic stirrer. Then, it was allowed to cool at room temperature once the time allowed for boiling was over. Finally, the extract was filtered by using Whatman No.1 filter paper and stored in refrigerator at 4^0C for further experimental use.

2.4. Qualitative phytochemical analysis

The presence of various phytoconstituents in aqueous extracts of *M. Stenopetala* leaf was studied by conducting phytochemical analysis using standard chemical methods. The extract was screened for the presence of flavonoids, alkaloid, tannin, saponins, phenols, glycosides, proteins, carbohydrate, steroids, terpenoids and coumarins.

2.4.1. Test of alkaloids

Wagner's Test: Two milliliter of aqueous extract of *M. Stenopetala* leaf was treated with five drops of Wager's reagent (Emasushan and Britto, 2018, Uma and Sekar, 2014, Banu and Cathrine, 2015).

2.4.2. Test for flavonoids

Alkaline Reagent Test: Two milliliter of 2.0% sodium hydroxide solution was mixed with two milliliter aqueous extract of *M. Stenopetala* leaf (Emasushan and Britto, 2018, Uma and Sekar, 2014, Gul et al., 2017).

2.4.3. Test for tannins

Gelatin test: one percent (1 %) solution of gelatin containing 10% sodium chloride was added to 5 mL of *M. Stenopetala* leaf extract (Makhawi and Hamadnalla, 2019).

2.4.4. Test for saponins

Foam Test: Two milliliter of aqueous extract of *M. Stenopetala* leaf was diluted with 10 mL of distilled water and warmed gently. Then the mixture was shaken for 5 minutes.

2.4.5. Test for phenols

Ferric chloride test: Two milliliter of aqueous extract of *M. Stenopetala* leaf was treated with three drops of 5% ferric chloride solution (Emasushan and Britto, 2018, Uma and Sekar, 2014).

2.4.6. Test for glycosides

Glycoside Test: One milliliter of aqueous extract of *M. Stenopetala* leaf was treated with 1 mL water and shaken well. Then 2 mL of 2% sodium hydroxide solution was added to it (Emasushan and Britto, 2018).

2.4.7. Test for proteins

Biuret Test: Two milliliter of aqueous extract of *M. Stenopetala* leaf was treated with 5% sodium hydroxide (2 mL) and 1% copper sulfate solutions (2 mL) (Emasushan and Britto, 2018).

2.4.8. Test for carbohydrates

Benedict's test: To 0.5 ml of filtrate, 0.5 ml of Benedic's reagent was added. Then after the mixture was heated on a boiling water bath (GFL Gesellschaft für Labortechnik mbH, Germany) for 2 minutes (Uma and Sekar, 2014, Banu and Cathrine, 2015).

2.4.9. Test for steroids

Salkowski's Test: Two milliliter of aqueous extract of *M. Stenopetala* leaf was treated with 2 mL chloroform and 2 mL concentrated sulfuric acid (Emasushan and Britto, 2018, Gul et al., 2017).

2.4.10. Test for terpenoids

Salkowski's Test: Two milliliter of chloroform and 1 mL of concentrated sulfuric acid was added to 1 mL of *M. Stenopetala* leaf extract.

2.4.11. Test for coumarins

Two milliliter of aqueous extract of *M. Stenopetala* leaf was treated with 3 mL of 10% sodium hydroxide solution (Emasushan and Britto, 2018).

2.5. Synthesis of ZnONPs using *M. Stenopetala* leaf extract

Synthesis of ZnONPs synthesis from *M. Stenopetala* leaf extract was done according to (Liu et al., 2020). First, *M. Stenopetala* leaf extract was centrifuged (Beckman Coulter Allegra 64R, USA) at 10,000 rpm for 10 minutes to remove heavy biomaterials. Then, 25 mL of the extract was heated at 60^0C for 10 minutes and 25 mL of 1 M zinc nitrate hexahydrate solution was added to it. Then, 1 M NaOH was added drop wise to the mixture to enhance precipitation and to adjust the pH of a solution. The resulting mixture was then continuously stirred at 800 rpm using magnetic stirrer for 2 h at 60 °C that resulted in pale white suspension. The formed solid precipitate was collected with centrifugation at 10,000 rpm for 20 minutes and washed twice with distilled water followed by ethanol to remove any impurities. Finally, the pale yellow colored NPs were obtained after fully drying in oven at 60 °C overnight and meshed using mortar and pestle so as to get a finer nature for characterization and applications.

2.6. Optimization of physicochemical parameters for ZnONPs Synthesis

The properties of ZnONPs are strongly depends on bioprocessing conditions (Wahab et al., 2009, Alam et al., 2014). Smaller sized metal NPs with narrow size distribution are necessity for successful green route synthesis and application perspectives (Rao and Paria, 2015). The size, shape, dispersity, optical properties and stability of green synthesized NPs are controlled by some synthesis parameters like concentration of metal ions, pH of the solution, plant extract volume, reaction temperature and time (Samari et al., 2019).

Hence, in our study, the pH of the mixture, concentration of zinc nitrate hexahydrated solution, quantity of *M. Stenopetala* leaf extract, synthesis temperature and time were optimized to find the best condition for the synthesis of desired ZnONPs by identifying their impact on it. The synthesis process was optimized by varying these input variables sequentially by keeping all parameters constant except the one which was varied (one-factor-at-a-time) and the selected parameter for studied variable was used for the optimization of other consecutive variables. The formation of green synthesized ZnONPs and the influences of these impute variables on the

formed ZnONPs were investigated using UV/Vis spectrophotometer in addition to visual color changes.

Therefore, the optimum parameters were found by varying the pH of the mixture (4, 6, 8, 10, 12 and 14) using NaOH and HCl solutions, salt concentration (0.1, 0.5, 1 and 1.5 M), zinc nitrate hexahydrate solution to *M. Stenopetala* leaf extracts volume ratio (3:1, 2:1, 1:1 and 1:3), temperature (room temperature, 60^0C and 80^0C) and time interval (0.5, 1, 2 and 3h). Then, the optical properties, crystal structure, shape and size were investigated to characterize the NPs synthesized at the optimum conditions.

2.7. Characterization techniques

The as-synthesized ZnONPs and ciprofloxacin loaded ZnONPs were characterized using different techniques and instruments to study their physical, optical thermal properties and to confirm their formation (Ahmed et al., 2017).

2.7.1. UV–Visible spectrophotometry analysis

The optical properties of the synthesized ZnONPs and ciprofloxacin loaded ZnONPs was investigated by using ultraviolet and visible absorption spectrophotometer (Spectrophotometer carry 60, Agilent Technologies) in the range of 200-800 nm.

2.7.2. Fourier transform-infra red (FTIR) analysis

In order to determine the functional groups of leaf extract and their role in the synthesis of ZnONPs and to determine the functional groups involved in nanoparticle drug conjugate formation, FTIR spectrum of the leaf extract, ZnONPs, ciprofloxacin and ciprofloxacin loaded ZnONPs were measured using the KBr pellet method in the range of 4000-400 cm^{-1} on FTIR spectrophotometer (Perkin Elmer, spectrum 65).

2.7.3. Powder x-ray diffraction (XRD) analysis

To determine crystal structure, average crystalline size and composition of ZnONPs (phase purity), Powder X-ray diffraction analysis was performed. The XRD pattern of synthesized ZnONPs was determined using x-ray diffractometer (XRD-7000 X-RAY DIFFRACTOMETER, SHIMADZU Corporation, Japan) operating at a voltage of 40 kV and a current of 30 mA with CuKα radiation (k=1.541Å) in a scanning range between 10^0 and 80^0 of 2θ angel and with

scanning speed of 3^0 per minute. The result was analyzed using X'Pert HighScore Plus software (version 2.1, PANalytical B.V. Almelo, The Netherlands). The crystallite size of the NPs was estimated by using Debye-Scherrer formula:

$$D = 0.89\lambda / (\beta \cos\theta) \qquad \text{(Eq.1)}$$

Where, D is the mean size of the particle, λ is the wave length of X-ray, β is full width at half maximum intensity and θ is the diffraction (Bragg) angle (Raja et al., 2018).

2.7.4. Scanning electron microscope (SEM) analysis

SEM analysis was conducted to study the size, shape and surface roughness of synthesized ZnONPs by using scanning electron microscope (TESCAN VEGA 3 SBU, Brno, Czech Republic).

2.7.5. Dynamic light scattering (DLS) analysis

The hydrodynamic diameter and polydispersity index (PDI) of ZnONPs and ciprofloxacin loaded ZnONPs were assessed with 90 plus particle size analyzer (Brookhaven Instruments Corporation, USA). The aqueous suspensions of both ZnONPs and ciprofloxacin loaded ZnONPs were filtered through a 0.22 µm syringe driven filter unit and their size distribution was measured by using the principle of DLS technique.

2.7.6. Differential scanning calorimetry /thermogravimetry (DSC-TGA) analysis

The decomposition and thermal stability of the green synthesized ZnONPs was determined using a simultaneous differential scanning calorimetry and thermogravimetric (DSC-TGA) analysis (SDT Q600 V20.9 Build 20, Universal V4.5A TA instruments).

2.8. Drug loading on ZnONPs

2.8.1. Determination of λmax and construction of calibration curve

To draw a calibration curve for drug loading study, ciprofloxacin stock solution was prepared with a concentration of 1 mg/mL in distilled water. From this stock solution, serial dilutions were made with distilled water to obtain a series of standard solutions with a final concentration 1, 2, 3, 4, 5 and 6 µg/mL. The spectrum of standard solution was run from 200-400 nm using UV/Vis spectrophotometer (Spectrofluorimeter CM2203, Republic of Belarus) to determine the absorption maximum (λ_{max}=275 nm) of ciprofloxacin. Then, the absorbance of the above

dilutions was measured at 275 nm and the graph was plotted by taking concentration on X-axis and absorbance on Y-axis.

2.8.2. Drug loading

Ciprofloxacin was loaded on ZnONPs according to a method used previously (Vimala et al., 2014). Briefly, 6 mL of ZnONPs dispersion (1 mg/mL) was added to 2 mL aqueous solution of ciprofloxacin (2 mg/mL) and the resulting mixture was stirred at 200 rpm using magnetic stirrer for 12 h in dark atmosphere. Then, it was centrifuged at 10,000 rpm for 10 minutes in order to separate ciprofloxacin loaded ZnONPs and the drug loaded NPs were washed three times with distilled water to remove excess unadsorbed ciprofloxacin. Finally, the resulted drug loaded NPs were dried and stored in refrigerator for further experiment and the supernatant was used to determine the loading content and encapsulation efficiency of NPs.

2.8.2.1. Optimization for drug loading

In order to examine the effect of different factors on drug loading efficiency and loading content, optimization was done for time (6, 12 and 24 h) and ciprofloxacin quantity to be loaded (1.5, 2.0, 3.0 mg/mL, all in 2 mL of distilled water).

2.8.2.2. Drug loading and drug entrapment efficiency determination

Drug loading content (LC) and entrapment efficiency (EE) was evaluated using UV-Vis spectrophotometer (Spectrofluorimeter CM2203, Republic of Belarus). The concentration of free ciprofloxacin in the supernatant isolated during drug loading procedure was determined via a calibration curve (Woźniak-Budych et al., 2017) and the amount of loaded drug onto the NPs was determined indirectly by measuring the amount of drug that is not loaded on NPs. Both parameters were computed as:

$$\% \text{ EE} = \frac{\text{Amount of the drug added initially} - \text{Amount of drug in supernatant}}{\text{Amount of drug added initially}} \times 100 \quad \text{(Eq. 2)}$$

$$\% \text{ LC} = \frac{\text{Amount of the drug added initially} - \text{Amount of drug in supernatant}}{\text{Amount of drug loaded nanoparticles}} \times 100 \quad \text{(Eq. 3)}$$

Where, % EE is percentage entrapment efficiency and % LC is percentage loading content.

2.9. In-vitro drug release study

2.9.1. Determination of λmax and construction of calibration curve

Since the drug release tests were conducted at four different pH conditions (pH = 1.2, pH = 6.0, pH = 6.8 and pH = 7.4), the absorption maximum (λ_{max}) of ciprofloxacin was determined in buffer solutions at the pH values mentioned. Therefore, to determine λ_{max} of ciprofloxacin in all buffer solutions, stock solutions with different concentrations of ciprofloxacin were prepared to obtain the working solutions and these final solutions were scanned in the range of 200-400 nm. The absorption maximums (λ_{max}) of the drug were determined to be 276 nm, 276 nm, 270 nm and 268 nm in buffer solutions of pH 1.2, 6.0, 6.8 and 7.4, respectively.

Similarly, the calibration curve was also constructed for all pH conditions. To do this, stock solutions with 0.2, 0.1, 0.05 and 0.025 mg/mL of ciprofloxacin were prepared in buffer solutions with pH 1.2, 6.0, 6.8 and 7.4, respectively. Then, there was a serial dilution to obtain final concentrations of 1, 2, 4, 6, 8, 10 and 12 µg/mL of ciprofloxacin in all buffer solutions. After that, the absorbance of each resultant solution for each buffer solutions was measured at determined λ_{max} of ciprofloxacin in their corresponding buffer solutions and the values were plotted against concentration to obtain the calibration curve for all buffer conditions. Determination of λ_{max} and measurement of absorbance for all solutions of buffers' with different pH values were conducted using UV/Visible spectrophotometer (Spectrofluorimeter CM2203, Republic of Belarus).

2.9.2. Drug release test

In order to understand the manner and extent of drug release from drug loaded NPs, drug release test was conducted according to a method used by (Shaker and Shaaban, 2017). The cumulative drug release was studied at a pH value of 1.2 (pH values of gastric), 6.0 (pH values of *E.coli* infected uroepithelium) (Martín-Gutiérrez et al., 2016), 6.8 (pH values of intestine) and 7.4 (physiological pH including the blood pH). To do this, 15 mg ciprofloxacin loaded ZnONPs were dispersed in 5 mL of each buffer solutions with the above mentioned pH values and placed inside over-night soaked dialysis sacks. Then, the sacks were tied with thread at both of its ends and immersed in 50 mL of external buffer medium (with the pH value similar to the solution inside the sacks) in an Erlenmeyer flask which in turn was kept on the shaker (Heidolph Unimax

1010, Heidolph instruments, Germany) operating at 100 rpm. The drug release was monitored using UV/Vis. spectrophotometer (Spectrofluorimeter CM2203, Republic of Belarus) by measuring the absorbance of 5 mL samples from external buffers. Sink condition was maintained by replacing an equal volume of corresponding fresh buffers during every time of sample collection. The drug release tests were done in triplicates and the cumulative percentage of released ciprofloxacin was plotted as a function of time.

2.10. In-vitro antibacterial activity study

The antibacterial activities of ZnONPs, ciprofloxacin and ciprofloxacin loaded ZnONPs were tested separately by disc diffusion method. The procedures, except for filter paper disc preparation, were performed using a standard antimicrobial susceptibility testing procedures.

2.10.1. Preparation of filter paper discs

Here the filter paper discs were locally prepared according to a method used by (Vineetha et al., 2015). Briefly, Whatman filter paper No. 3 was punched using office paper punching machine to produce holes of approximately 6 mm in diameters. The resulting filter paper discs were then autoclaved at 15 pounds per square inch pressure for 30 minutes. Next, the working solutions for ciprofloxacin, ciprofloxacin loaded ZnONPs and ZnONPs were prepared, loaded on the autoclaved paper discs (5 µg ciprofloxacin, 10 µg ZnONPs - ciprofloxacin conjugate and 5 µg ZnONPs per disc) and the loaded filter paper discs were dried in incubator at 37^0C for 4 hours. The amount of ciprofloxacin to impregnate the disc was taken from Clinical and Laboratory Standards Institute (CLSI) guideline which was set based on a dosage regimen of 400 mg IV or 500 mg orally administered every 12 hours (CLSI, 2020) and the amount of ciprofloxacin loaded ZnONPs and ZnONPs were determined based on the loading content of NPs.

2.10.2. Inoculum preparation

Three well isolated colonies, from sub-cultured isolates for 24 hours, of the same morphological types were selected. The top of each colony was touched with a loop and was suspended in 2 mL of sterile saline (0.85%). Then the saline tube was vortexed in order to create the smooth suspension and the suspension was adjusted to match 0.5 McFarland turbidity standard (1 to 2 x 10^8 colony-forming units (CFU)/mL).

2.10.3. Test plates inoculation

Within 15 minutes after adjusting the turbidity of the inoculum suspension, a sterile cotton swab was dipped into the adjusted suspension. Then, a petri plate prepared with Muller Hinton Agar was inoculated by streaking the swab over its surface three times by rotating the plate approximately 60^0 each time. Finally, the lid was left ajar for 5 minutes and made ready for the applications of discs.

2.10.4. Disc applications to inoculated agar plates

To apply discs on the surface of inoculated agar plates, a forceps was used after immersed in alcohol and ignited. Then, all discs (one control disc inoculated with normal saline and discs inoculated with ciprofloxacin, ciprofloxacin conjugated ZnONPs and bare ZnONPs) were placed on the plate gently with sufficient distance between their centers and were pressed with the forceps. Finally, the plates loaded with those discs were inverted and were incubated at 37^0C for 18 hours.

2.10.5. Reading and interpreting results

After 18 hours of incubation, the resulting zones of inhibitions' (ZOI) diameters were measured including the diameters of discs using a ruler on the back of the inverted petri plate. The susceptibility or resistance of the organism was then determined by using CLSI 2020 guideline for comparing the obtained results. The AST experiment was done in triplicates and the mean values were presented.

3. RESULTS AND DISCUSSION

3.1. Qualitative phytochemical analysis

Qualitative screening of phytochemicals in aqueous extracts of *M. Stenopetala* leaf revealed the presence of different phytoconstituents as presented in Table 1.

Table 1: Phytochemical screening of aqueous extract of *M. Stenopetala* leaf

S/No	Phytochemicals	Test	Interference	Result
1	Flavonoids	Alkaline reagent	Concentrated yellow color	Positive
2	Alkaloid	Wagner's test	Reddish brown precipitate formation	Negative
3	Tannin	Gelatin test	Formation of any precipitate	Positive
4	Saponins	Foam test	Persistent foaming	Positive
5	Phenols	Ferric chloride	Bluish-black color formation	Positive
6	Glycosides	Glycoside test	Appearance of yellow color	Positive
7	Proteins	Biuret test	Violet coloration	Positive
8	Carbohydrate	Benedict's test	Orange red precipitate formation	Positive
9	Steroids	Salkowski's test	Red chloroform layer and greenish yellow fluorescent acid layer	Negative
10	Terpenoids	Salkowski's test	Reddish brown color formation	Negative
11	Coumarins	_____	Yellow coloration	Positive

The presence of phenols, flavonoids (Geleta et al., 2016, Assefa et al., 2015), saponins, tannins, glycosides and coumarins in aqueous extracts of *M. Stenopetala* leaf were also reported before (Geleta et al., 2016). Therefore, as it is stated above, since these phytochemicals are responsible for the formation of ZnONPs through the estimated mechanism in Figure 2, their presence in *M. Stenopetala* leaf extract confirms the ability of the plant extract for the production of the NPs.

3.2. Formation of green synthesized ZnONPs

3.2.1. Visual color change

Visual color change of the solution is the preliminary test for synthesis of NPs. Like other metallic NPs, during the ZnONPs synthesis processes, there was a typical color change patterns which confirm the formation of NPs in all runs except for synthesis process at pH value of 4 and 6.

When the pH of the mixture was adjusted to pH values other than 4 and 6, immediately the mixture color was changed to light brown and at about 5 minutes of stirring on hot plate at specified temperature, the color of the solution was completely changed to creamy yellowish which latter changed to pale white up on continuous heating (starting from 15th minutes of heating) (Figure 5). In line with our result, there was a formation of pale white precipitate when ZnONPs were synthesized using *Laurus nobilis* leaf (Vijayakumar et al., 2016), *Aloe socotrina* leaf (Fahimmunisha et al., 2020), *Malus pumila* and *Juglen regia* leaf (Mirza et al., 2019), *Corriandrum sativum* leaf (Hassan et al., 2015), *Solanum torvum* (L) leaf (Ezealisiji et al., 2019), *Ruta graveolens* (L.) stem (Lingaraju et al., 2016), *Ficus palmate* leaf (Sati et al., 2020), *Peganum harmala* (Mehar et al., 2019) and *Adhatoda vasica* leaf extract (Bhumi et al., 2014).

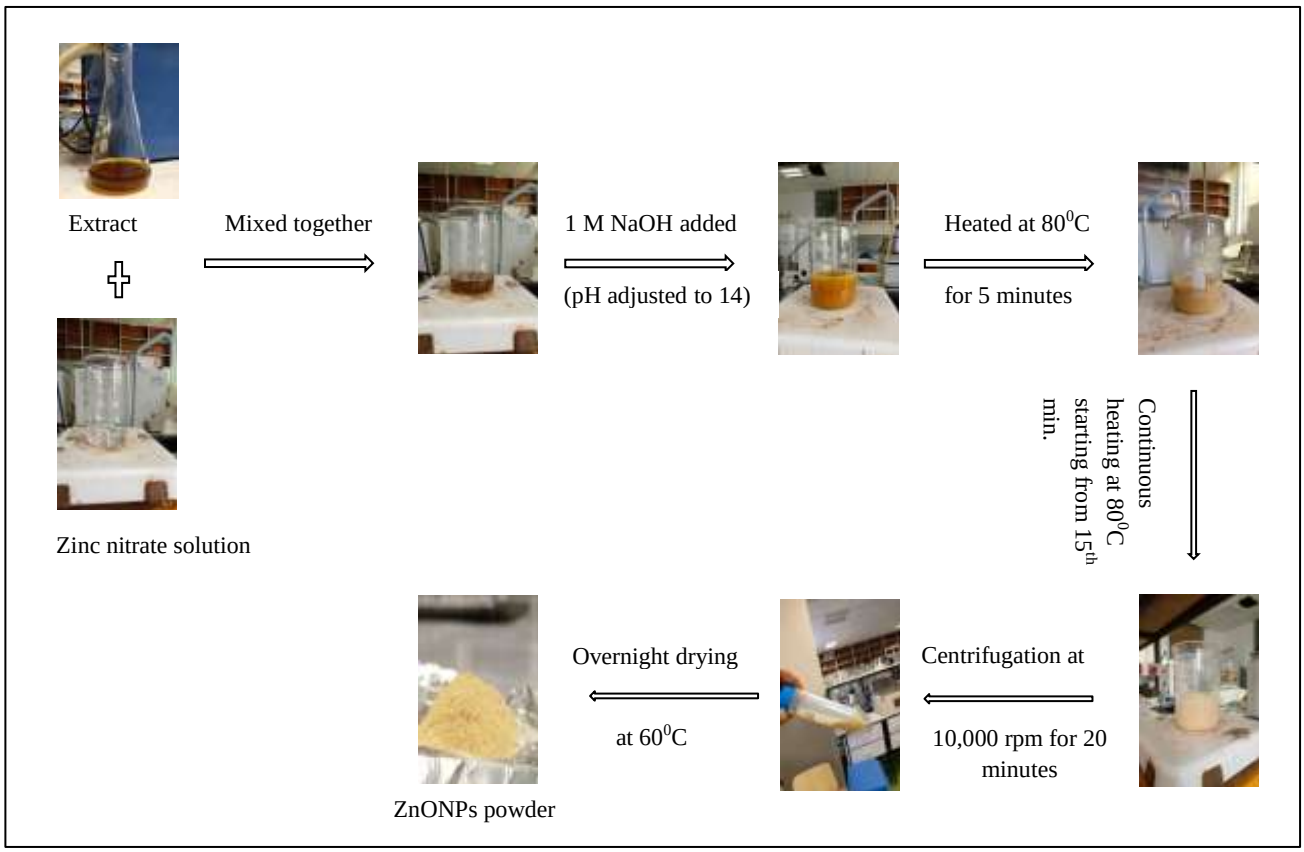

Figure 5: Schematic procedures for biosynthesis of ZnONPs from zinc nitrate hexahydrate and *M. Stenopetala* leaf water extract at optimum conditions.

.

3.2.2. UV-Visible spectrophotometry analysis

UV/Vis. spectrophotometer analysis is a method to confirm the formation of ZnONPs, because ZnONPs are associated with specific absorbance bands in characteristic spectra when the incident light enters into resonance with the conduction band electrons on the surface of the NP (Patra and Baek, 2014). The emergence of the peak is due to the Surface Plasmon Resonance (SPR) characteristic of ZnONPs (Abdullah et al., 2020, Chakraborty et al., 2020). SPR is a phenomenon ascribed to electron oscillation and transition from the valance band to conduction band upon interaction with the light of certain wave length and its occurrence between 310 and 380 nm is a characteristics feature of ZnONPs (Agarwal and Shanmugam, 2019, Hoseinpour et al., 2017). In our study, the synthesized ZnONPs in all runs were with the characteristics UV/Vis. absorption peaks within this range except for NPs synthesized at pH values of 4 & 6, and that synthesized at room temperature as it is clearly indicated in Figure 6 for the former two and Figure 9 for the latter. The position of this peak is attributed to the particle size, shape, degree of charge transfer between the medium and the particles, and the interaction with the medium (Abdullah et al., 2020, Chakraborty et al., 2020, Rao and Paria, 2015, Aboelfetoh et al., 2017, Mohammadi and Ghasemi, 2018, Yang and Li, 2013, Sivaraj et al., 2014, Devipriya and Roopan, 2017). Larger particles absorb light at higher wavelength with broad SPR band and smaller particles absorb light at shorter wavelength (Abdullah et al., 2020, Ibrahim, 2015, Siddiqui et al., 2018, Devipriya and Roopan, 2017). In addition, higher intensity of SPR band is a measure of higher concentration of produced NPs (Bar et al., 2009).

3.3. Optimization of synthesis parameters

3.3.1. Effect of pH on ZnONPs synthesis

The pH of the reaction mixture is a key factor in the formation of NPs, especially for a biochemical reaction (Abdullah et al., 2020, Samari et al., 2019) and even more numerous studies reported it as the most important parameters affecting NPs formation (Praburaman et al., 2016). As an example, during their optimized green synthesis of ZnONPs, (Agarwal and Shanmugam, 2019) found that size of ZnONPs was significantly affected by pH of the solution followed by temperature. Its influence is due to an increment of nucleation center development at higher pH value by affecting the protonation-deprotonation of active ingredients which finally leads to donation of electrons (Jameel et al., 2020). The major effect of pH is changing the

electrical charges of biomolecules which may change their reducing and capping ability and finally growth of NPs (Mohammadi and Ghasemi, 2018, Shabaani et al., 2020). In alkaline pH, many functional groups are ionized and are available for reduction and facilitate the formation of small size NPs (Velammal et al., 2016). At strongly basic pH, when compared with lower pH values, there will be more abundant hydroxyl ions in the solution which is important for the formation of ZnONPs and growth of formed NPs (Buazar et al., 2016). Also, (Aboelfetoh et al., 2017) confirmed that the reducing and capping ability of *C. serrulata* extract was enhanced in alkaline medium.

The result of our study also confirmed that the formation of ZnONPs is strongly dependent on the pH of the mixture. Figure 6 presents the UV/Vis. absorption spectra of ZnONPs synthesized at different pH values. The spectra revealed that, as the pH of the solution increased, the absorbance also increased and the peaks become narrower and hence, it suggests that more alkaline medium enhances the synthesis of ZnONPs. This result is in line with the findings of ZnONPs synthesized from banana peel extract which shows increased absorbance as the pH increased (Abdol Aziz et al., 2019). In another study, there was an increase in absorption of green synthesized ZnONPs as the pH of the mixture was increased from 8 to 12 (Rahaiee et al., 2020). Also, during optimized green synthesis of ZnONPs, stable NPs were produced at higher pH due to the presence of abundant hydroxyl groups (Shabaani et al., 2020). Similarly, there was an increased SPR peak intensity of silver NPs with narrower width as pH of a solution was increased (Siddiqui et al., 2018).

According to our study, at pH value of 4 and 6, both color change and characteristics SPR peaks of ZnONPs were not observed. The absence of SPR peaks was also reported during green synthesis of ZnONPs (Mohammadi and Ghasemi, 2018), gold NPs (Chandran et al., 2019) and silver NPs (Yang and Li, 2013) in acidic pH. This may be due to biomolecules which are assumed to be involved in green synthesis of NPs, are likely inactivated under acidic conditions (Yang and Li, 2013, Ibrahim, 2015). Similar justification was given when gold NPs were not synthesized at lower pH of the reaction medium by confirming the reducing and capping functional groups of biomolecules were blocked and deactivated in strongly acidic pH (Alam et

al., 2014). Therefore, for further investigations, the pH value of 14 was selected for the synthesis of high concentrations of ZnONPs.

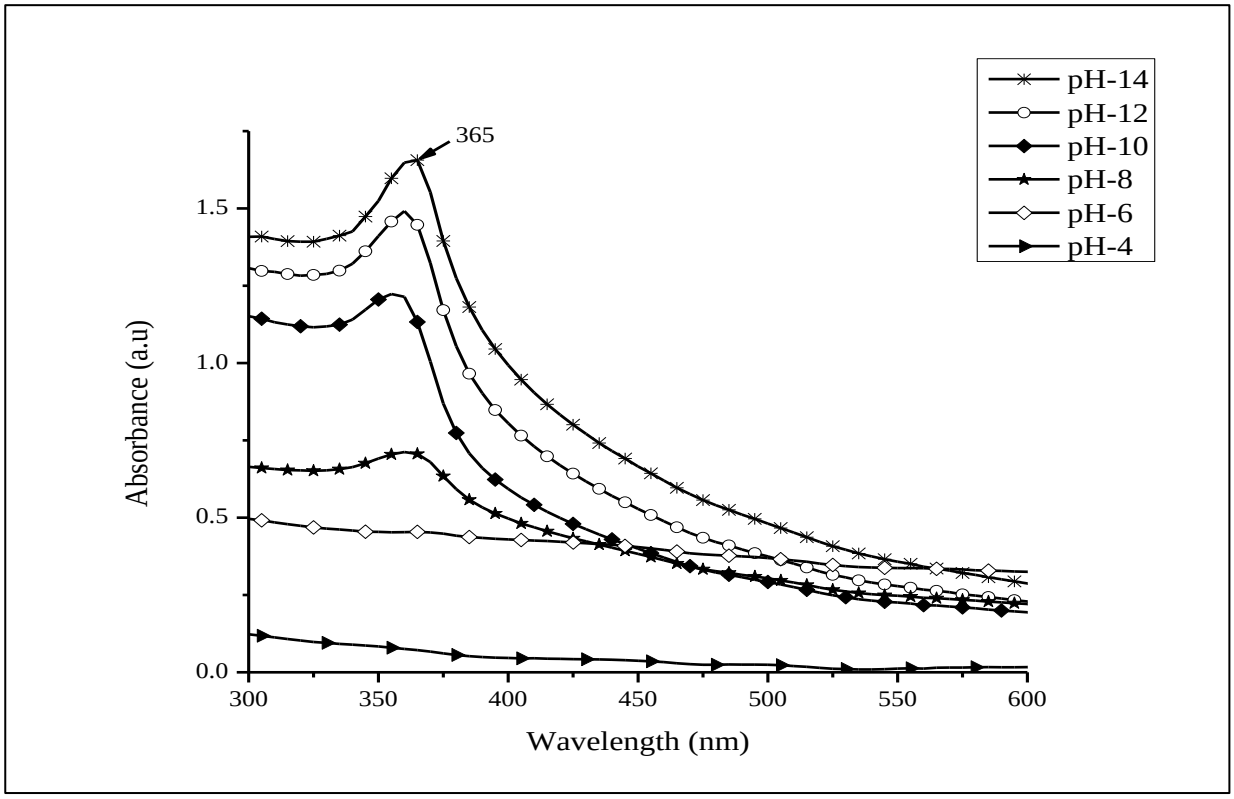

Figure 6: UV/Vis. spectra of ZnONPs synthesized at different pH values (4, 6, 8, 10, 12 and 14) with fixed values for concentration of zinc nitrate hexahydrate solution (1M), zinc nitrate hexahydrate solution to *M. Stenopetala* leaf extracts volume ratio (1:1), temperature (60^0C) and time (2h).

3.3.2. Effect of zinc salt concentration on ZnONPs synthesis

In our study, as clearly depicted in Figure 7, as the concentration of zinc nitrate hexahydrate increased (from 0.1 to 1.0 M), the absorbance intensity was increased. However, further increasing the concentration to 1.5 M was lead to broad and less intense SPR absorption peak.

The increase in SPR band intensity with increasing salt concentration till 1 M was due to the availability of high zinc (II) ions concentration which in turn results higher numbers of ZnONPs formation. But the broad and less intense SPR peak of ZnONPs at the concentration of 1.5 M may be due to the formations of anisotropic NPs. A similar study done by (Shabaani et al., 2020)

showed that a decreased SPR absorption peak when zinc acetate di-hydrate concentration was at higher level of optimum value during green synthesis of ZnONPs. Similarly, during green synthesis of ZnONPs, large anisotropic NPs were formed when concentration of the precursor was increased (Mohammadi and Ghasemi, 2018). During optimized green synthesis of ZnONPs, increasing the concentration of zinc salt concentration beyond the threshold resulted in decrease in absorbance and broadening of peak (Jamdagni et al., 2018). Also, (Chandra et al., 2019) found that there was an increased SPR peak intensity of green synthesized ZnONPs with sharpening as the concentration of zinc acetate dehydrate was increased till 0.01 M which was later changed to broaden peak with reduced intensity when the precursor concentration was further increased to 0.02 M.

In another study, when iron oxide NPs were synthesized by green method, the formation of NPs was decrease as ferric chloride concentration was beyond 50 mM (Kheshtzar et al., 2019). Similarly, when gold NPs were synthesized using green method, increasing the concentration of gold salt up to 0.5 mM was result in SPR band of narrower width with increased absorption intensity which was later changed to broad and less intense peak upon the increment of concentration to 1 mM. This was due to the formation of large anisotropic NPs as confirmed by transmission electron microscope (TEM) (Alam et al., 2014). There was also a decreased absorbance of the reaction mixture when sliver NPs were synthesized by green route with concentration of precursor higher than the optimum value (Velammal et al., 2016). Therefore, for our further studies, 1 M zinc nitrate hexahydrate concentration was selected as optimum value.

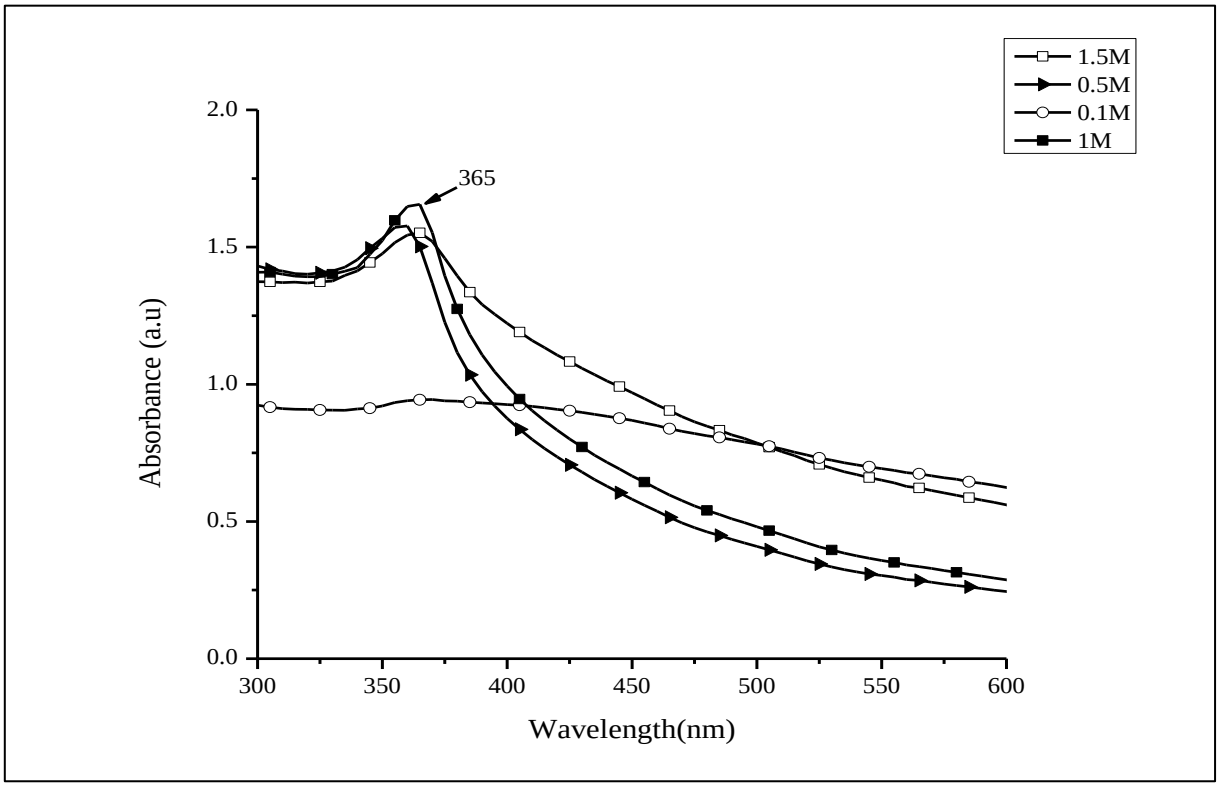

Figure 7: UV–Vis spectra of ZnONPs synthesized at different zinc nitrate hexahydrate solution concentration (0.1, 0.5, 1 and 1.5 M) with fixed values for pH of a mixture (14), zinc nitrate hexahydrate solution to *M. Stenopetala* leaf extracts volume ratio (1:1), temperature (60^0C) and time (2h).

3.3.3. Effect of the amount of *M. Stenopetala* leaf extract on ZnONPs synthesis

In the current study, with increasing the quantity of leaf extract from 1 to 3 proportion (25% to 75%) to 1 to 1 proportion (50% to 50%), there was an increase in SPR peak intensity but further increasing the quantity of leaf extract to 3 to 1 proportion (75% to 25%) resulted in reduced SPR peak intensity, as it is depicted in Figure 8. For lower level of extract concentration than optimum value, the reduced SPR absorption peak was due to the inadequacy of biomolecules for the reduction of metal ions which in turn leads to the formation of less numbers of NPs and increasing the quantity of leaf extract till the optimum value was lead to the formation of more numbers of NPs because of more availability of phytochemicals for reduction and capping.

However, when the quantity of leaf extract was further increased than the optimum value, the SPR peak intensity was again decreased. This may be due to the enhancement of the bridging

effect of phytochemicals because of their availability in excess amount which in turn may leads to the aggregation of NPs (Samari et al., 2019). This result was supported by a study done by (Muthuvel et al., 2020), who synthesized ZnONPs using *Solanum nigrum* leaf extract and the absorption of synthesized NPs was increased up to 15 mL of plant extracts which was later decreased when the volume was further increased to 20 mL. In another study, during optimized green synthesis of ZnONPs, increasing the volume of plant extract beyond the threshold resulted in decreased NP synthesis and their absorbance (Jamdagni et al., 2018). When (Ansari et al., 2020) synthesized ZnONPs, they were found reduced UV light absorbance of synthesized NPs as plant extract volume was increased to 15 mL and even with more reduced absorption intensity when its volume was further increased to 20 mL and above. Similarly, when ZnONPs were synthesized by using *Artocarpus gomezianus* fruit extract, the SPR peak intensity was decreased when the extract was 15 mL and above (Suresh et al., 2015). There was also a reduced SPR peak with red shift for green synthesized ZnONPs when leaf extract concentration was doubled than its initial concentration (Rajiv et al., 2013).

Also, during controllable phyto-synthesis of cupric oxide NPs, there was a reduced SPR intensity of synthesized NPs together with unstable and aggregated NPs in the solution when the volume of extract was further increased beyond the optimum value (Samari et al., 2019). In another study, there was reduced intensity of silver NPs' SPR band when the extract concentration was 25% during and they postulated that the reduced intensity may be due to aggregation of NPs (Aboelfetoh et al., 2017). Similarly, there was a reduced SPR band absorbance of silver NPs when the extract volume was beyond the optimum value (Velammal et al., 2016).

In our result also, in addition to its reduced intensity and broadening, the SPR absorption peak was red shifted when the volume of the extract was three times higher than zinc nitrate solution. This red shift was due to the increased particle size which in turn may be due to aggregation. In concordance with this finding, it was confirmed on SEM micrographs that there was aggregation of ZnONPs when leaf extract volume was increased which in turn resulted in red shifted absorption peak (Handago et al., 2019). Similarly, there was a significant red shift in SPR peak when *aleo vera* extract concentration was increased above 25% during ZnONPs synthesis

(Sangeetha et al., 2011). There were also aggregated NPs when plant extract volume was beyond the optimum value during ZnONPs green synthesis (Nagarajan and Kuppusamy, 2013).

So, the 1:1 volume ratio of zinc nitrate hexahydrate solution to *M. Stenopetala* leaf extract was selected as optimum value for the synthesis of ZnONPs.

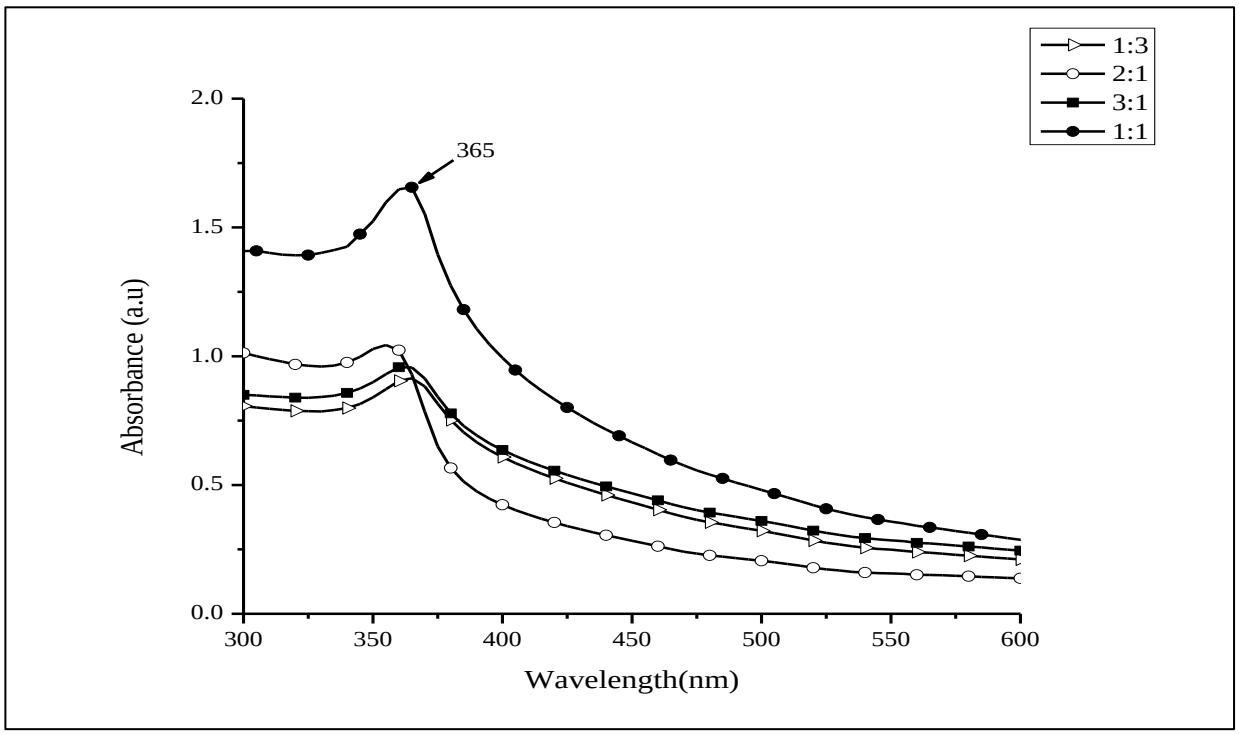

Figure 8: UV–Vis spectra of ZnONPs synthesized at different zinc nitrate hexahydrate solution to *M. Stenopetala* leaf extracts volume ratio (3:1, 2:1, 1:1 and 1:3) with fixed values for pH of a mixture (14), zinc nitrate hexahydrate solution concentration (1 M), temperature (60^0C) and time (2 h).

3.3.4. Effect of temperature on ZnONPs synthesis

In our study, the effect of temperature was demonstrated on the formation of ZnONPs and it was revealed that NP formation was highly affected by temperature. As shown in Figure 9, there were sharp and intense SPR peaks of synthesized NPs accompanied with a blue shift along with temperature increase while a broad and very weak absorption peak intensity of NPs synthesized at room temperature. As the temperature increases, the reactants will be consumed rapidly and smaller particles will be formed (Ibrahim, 2015, Aboelfetoh et al., 2017).

At high temperature also number of nuclei formed increases which results in smaller particles size since metallic NPs formation is dependent on nucleation and growth mechanism (Nagarajan and Kuppusamy, 2013). Ibrahim found similar result, as the temperature of reaction increased, a sharp and narrow peak at lower wave length was observed, and as the reaction temperature decreased, the peak of the NP was found at higher wave length region (Ibrahim, 2015). Similarly, (Aboelfetoh et al., 2017) found less intense SPR peak of silver NPs synthesized at room temperature which later become sharp and intense when the temperature was increased. During green synthesis of silver NPs also, there was a sharp and blue shifted SPR bands as the temperature increased which signifies a decrease in particle size (Yang and Li, 2013). Another study also demonstrated that, there was a broaden and red shifted silver NPs' SPR peak as temperature decreased and there was no characteristics SPR peak for NPs synthesized at room temperature (Avoseh et al., 2017). Hence, in our study, 80^0C was selected as optimum temperature for the synthesis of ZnONPs.

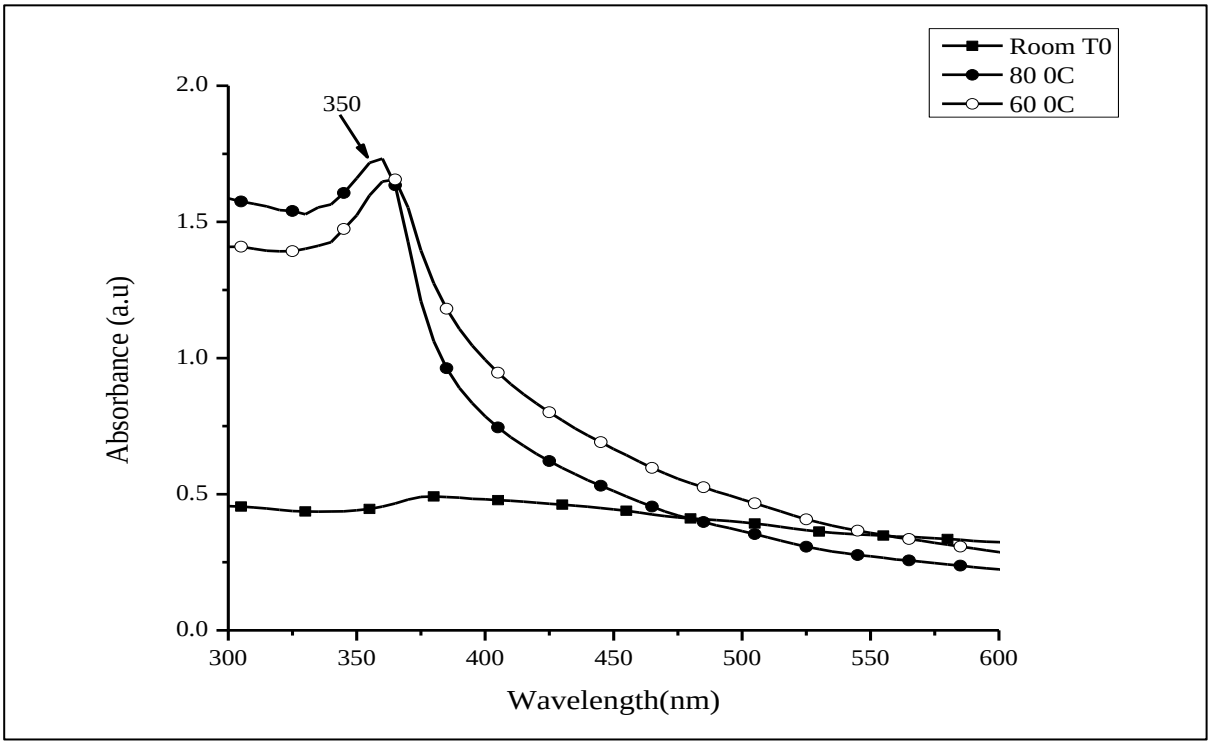

Figure 9: UV–Vis spectra of ZnONPs synthesized at different temperature (room T0, 600C and 800C) with fixed values for pH of a mixture (14), zinc nitrate hexahydrate solution to *M.*

Stenopetala leaf extracts volume ratio (1:1), zinc nitrate hexahydrate solution concentration (1 M) and time (2 h).

3.3.5. Effect of time on ZnONPs synthesis

The quality, quantity, type and characteristics of synthesized NPs by green route are greatly influenced by duration of incubation time for the reaction medium (Patra and Baek, 2014). This effect was also demonstrated in our study; when the incubation time of the reaction medium was increased, SPR peak intensity of synthesized ZnONPs was also increased, since longer incubation time allows production of higher quantity of NPs (Figure 10).

There was a similar finding showing a steadily increased SPR absorbance intensities as incubation time was longer during green synthesis of ZnONPs (Sharmila et al., 2018, Dobrucka and Długaszewska, 2016, Singh et al., 2018), iron oxide NPs (Khatami et al., 2017), silver NPs. (Aboelfetoh et al., 2017, Roy et al., 2010, Mondal et al., 2011) and gold NPs (Ahmad et al., 2016, Mondal et al., 2011, Roy et al., 2010). Therefore, in our study, 3 hours was selected as optimum incubation time for effective synthesis of ZnONPs.

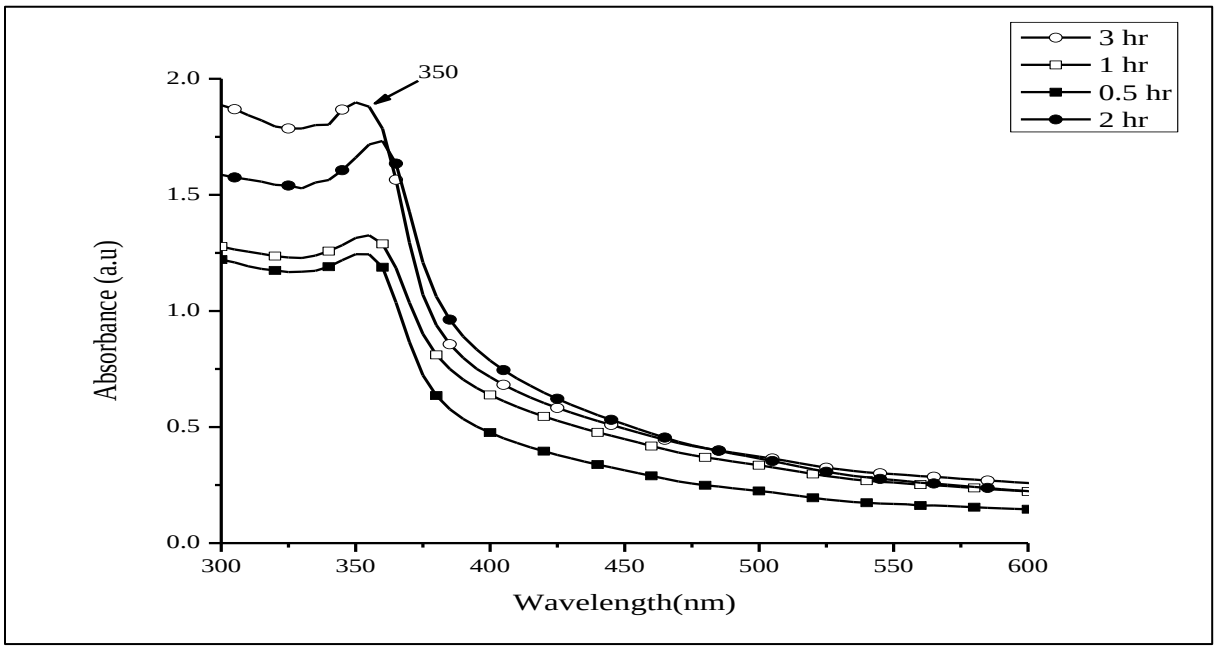

Figure 10: UV–Vis spectra of ZnONPs synthesized at different time period (0.5, 1, 2 and 3 h) with fixed values for pH of a mixture (14), zinc nitrate hexahydrate solution to *M. Stenopetala*

leaf extracts volume ratio (1:1), zinc nitrate hexahydrate solution concentration (1 M) and temperature of 80^0C.

Since the selected optimum values of the preceding factors to be optimized were used to find the optimum values of the succeeding factors, ZnONPs produced at incubation time of 3 hours were synthesized at optimum conditions for all parameters and hence, they were characterized for optical properties, crystal structure, shape and size, and they were utilized for further different applications.

3.4. Characterization of ZnONPs and ciprofloxacin loaded ZnONPs

3.4.1. UV-Visible spectrophotometer

Pure ciprofloxacin showed UV/Vis absorption band at 275 and 315 nm in which the first is being for π-π* transition of the fluorobenzene ring and the latter is for n-π* transition of quinolone ring (Grace and Pandian, 2007). While green synthesized ZnONPs using *M. Stenopetala* leaf extract at optimized conditions were exhibited a peak at 350 nm, as shown in Figure 10. But, after ciprofloxacin loading, there was a new UV/Vis absorption peak at 335 nm keeping the peaks at 275 nm in place for ciprofloxacin and the SPR peak of ZnONPs was shifted to 360 nm, as it is indicated in Figure 11. These peak shifts demonstrated that there was effective loading of ciprofloxacin on ZnONPs which alter their photo-physical property. The red shift of ZnONPs' peak from 350 to 360 nm may be due to the change in surface chemistry of NPs when ciprofloxacin was loaded on it. In line with our finding, there was SPR peak shift of ZnONPs synthesized using microwave irradiation when it was conjugated with ciprofloxacin (Patra et al., 2014). There was also a red shift of UV/Vis. absorption peaks for gold and silver NPs when ampicillin was loaded on them which cause a change in surface chemistry for NPs (Brown et al., 2012). Similarly, there was a red shift of SPR absorption peak of silver NPs (Kaur et al., 2019) and gold NPs (Sulaiman et al., 2020) when vancomycin and hesperidin, respectively were loaded on them.

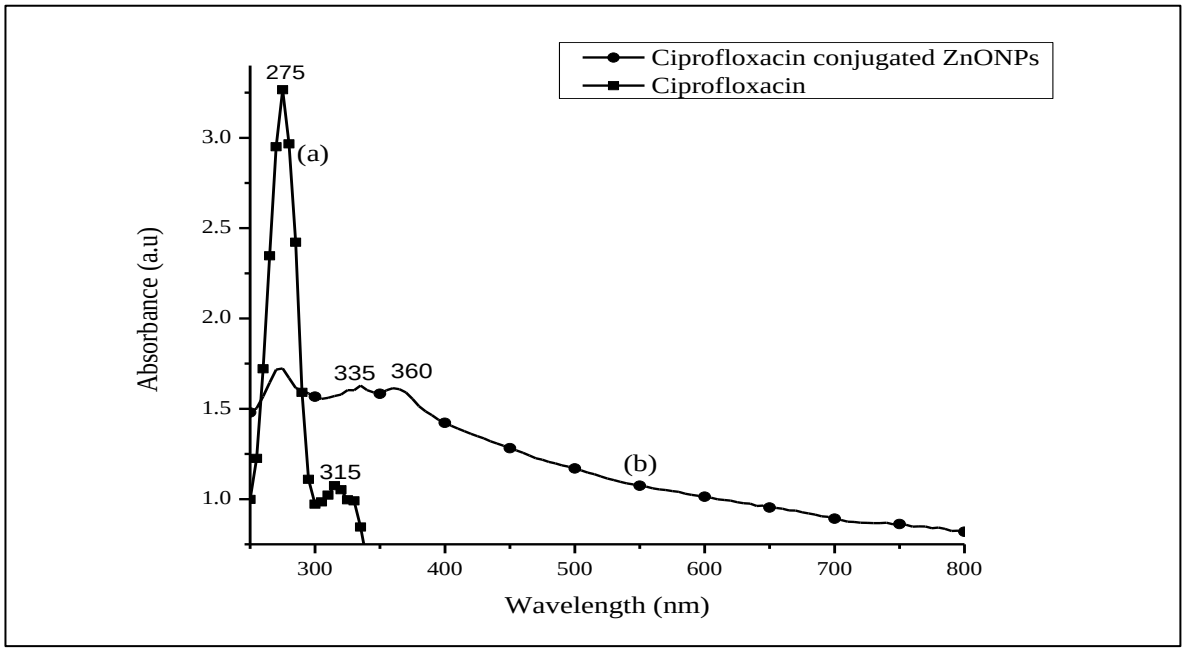

Figure 11: UV/Vis spectra of a) ciprofloxacin b) ciprofloxacin loaded ZnONPs.

3.4.2. Fourier transform-infra red (FTIR) analysis

The main peaks found in the spectra of *M. Stenopetala* leaf extract were shown in Figure 12A. As it is indicated in table 2, these peaks are attributed to different functional groups.

Table 2: FTIR data of *M. Stenopetala* leaf aqueous extract

Wave number (cm^{-1})	**Assignment**	**Reference**
3370	O–H stretching of carboxylic acid	(Stuart, 2004)
	O–H stretching of phenols and alcohols	(Pavia et al., 2014)
2922	C–H stretching of alkanes, aldehydes/ketones	(Stuart, 2004)
1626	N–H bending of amides or –C=C– stretching of aromatic groups	(Stuart, 2004)
1412	C–O–H bending of carboxylic acids	(Stuart, 2004)
1066	C–O stretching of alcohol, phenol/ ester or C–N stretching of aliphatic amines or C–O–C stretching of ether	(Stuart, 2004)
617	C–H bending of alkenes	(Pavia et al., 2014)

While on the FTIR spectrum of ZnONPs, as indicated in Figure 12B, the bands at 3370, 2922, 1626, 1412, 1066 and 617 cm^{-1} on the spectrum of *M. Stenopetala* leaf extract were shifted to 3399, 2911, 1586, 1410, 1056 and 616 cm^{-1}, respectively. These shifts and broadening of bands observed on FTIR spectrum of ZnONPs indicates the participation of the above mentioned functional groups of different phytochemicals in reduction of zinc precursor in to ZnONPs and stabilization of ZnONPs (Gawade et al., 2017).

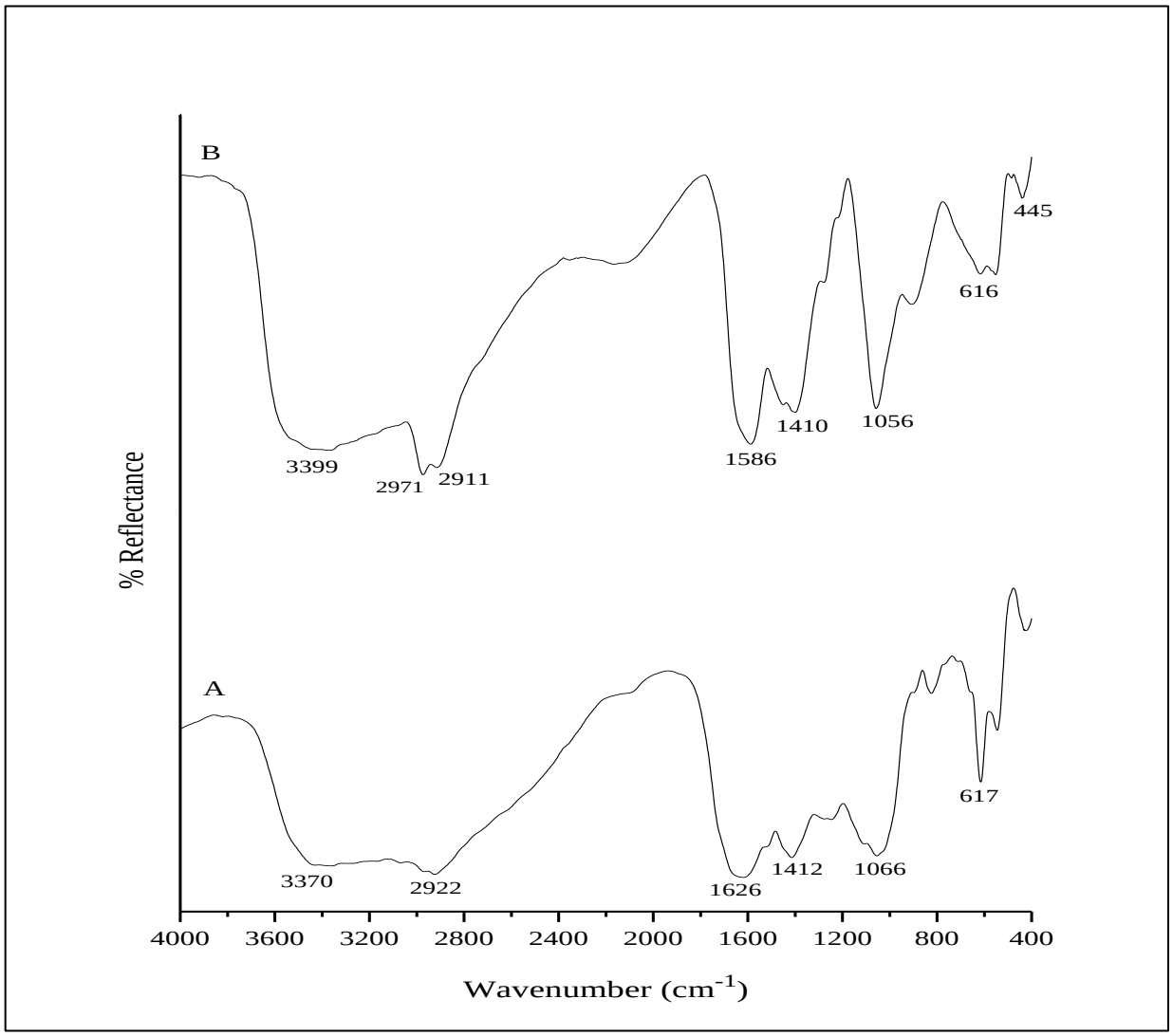

Figure 12: FTIR spectrum of A) *M. Stenopetala* leaf aqueous extract B) ZnONPs synthesized using *M. Stenopetala* leaf extract.

As determined by phytochemical screening test above, the water extracts of *M. Stenopetala* leaf is mainly composed of flavonoids, tannin, saponins, phenols, glycosides, proteins, carbohydrate

and coumarins. Thus, the functional groups related to these organic matters may be engaged in the reduction of zinc salts to ZnONPs as well as in the capping of the formed NPs. In additions to the bands of different functional groups found on spectrum of ZnONPs, there was also a peak found at 445 cm^{-1} which was due to the vibration of metal–oxygen bond of Zn–O as it was observed in earlier reports that the absorptions between 400 and 600 cm^{-1} were characteristics vibration of Zn–O (Sangeetha et al., 2011, Gao et al., 2020, Ahmad and Kalra, 2020). Therefore, FTIR spectrophotometer was also used to confirm the effective synthesis of ZnONPs in addition to functional groups identification.

FTIR result also revealed that the effective loading of ciprofloxacin on green synthesized ZnONPs. According to the FTIR spectra of ciprofloxacin, shown in Figure 13A, the band at 3530 cm^{-1} was due to –OH stretching of carboxyl, at 3379 cm^{-1} was due to N–H stretching of imino moiety of the piperazinyl group, at 1709 cm^{-1} was due to symmetric stretching of C=O of carboxylic acid, at 1625 cm^{-1} was due to symmetric stretching of C=O of pyridone moiety, at 1272 cm^{-1} was due to C–N stretching (Grace and Pandian, 2007, Tom et al., 2004), at 1449 cm^{-1} was due to –CH bending vibration and at 1046 cm^{-1} was due to C–F stretching vibration (Grace and Pandian, 2007).

However, in the case of drug loaded ZnONPs spectra, shown in Figure 13B, the N–H stretching peak of imino moiety of the piperazinyl group was shifted to lower wave length with reduced intensity and the peak intensity of C=O stretching of carboxylic acid was significantly reduced. This finding clearly revealed that ciprofloxacin was form a conjugate with green synthesized ZnONPs through its carboxylic acid functional group and nitrogen atom of the imino piperazinyl group. Since nitrogen atoms of quinolone ring and the one which is ortho- to fluorine are not electron rich due to delocalization of electrons to electron deficient fluoroquinolone ring and are sterically hindered by cyclopropyl and piperazinyl ring, they are less likely to bind with ZnONPs (Tom et al., 2004). In line with our study, there were studies which showed effective loading of ciprofloxacin on amine functionalized ZnONPs using its carboxylic acid group (Patra et al., 2014) and on citrate capped gold NPs using its nitrogen atom of the imino piperazinyl group (Grace and Pandian, 2007). In the other study also, ciprofloxacin was form conjugate with hydroxylated ZnONPs through its nitrogen atom of the imino piperazinyl group by ionic interaction (Banoee et al., 2010). Similarly, there was a disappearance of absorption peaks for

carbonyl group on ciprofloxacin spectrum when it is conjugated with Cu^{+2}, indicating that this functional group was participated in the bonding to this ion (Wu et al., 2003). There was also the disappearance of band for carbonyl group of carboxylic acid when norfloxacin was made complex with Ca^{+2}, Mg^{+2}, Ba^{+2} (Al-Mustafa, 2002), Iron(II) and Iron(III) perchlorate (Al-Mustafa and Tashtoush, 2003) which was indicative for the involvement of carboxyl group for complexation.

Similarly, there was also merging and absorbance intensity reduction of bands of functional groups which were participated during stabilization of silver and gold NPs with ceftriaxone (Shah et al., 2014) and during conjugations of ceftriaxone with green synthesized silver NPs (Harshiny et al., 2015). In the other study, when silver NP was capped with 5-Amino-β-resorcylic acid hydrochloride dihydrate, there was the disappearance of the peak at carbonyl region in 5-Amino-β-resorcylic acid hydrochloride dihydrate spectrum indicated the participation of carboxylic group for electrostatic interaction with silver NPs (Naz et al., 2014). Moreover, during the preparation of doxorubicin functionalized gold NPs, the N–H stretching peak of doxorubicin was shifted to lower wavelength in doxorubicin-gold NPs conjugate spectrum indicating the participation of this functional group for interacting electrostatically with gold NPs (Mirza and Shamshad, 2011). However, in our case, since the NPs were functionalized with many phytochemicals, both of the functional groups namely, nitrogen atom of the imino piperazinyl group and carboxylic acid group of ciprofloxacin were participated for conjugate formation.

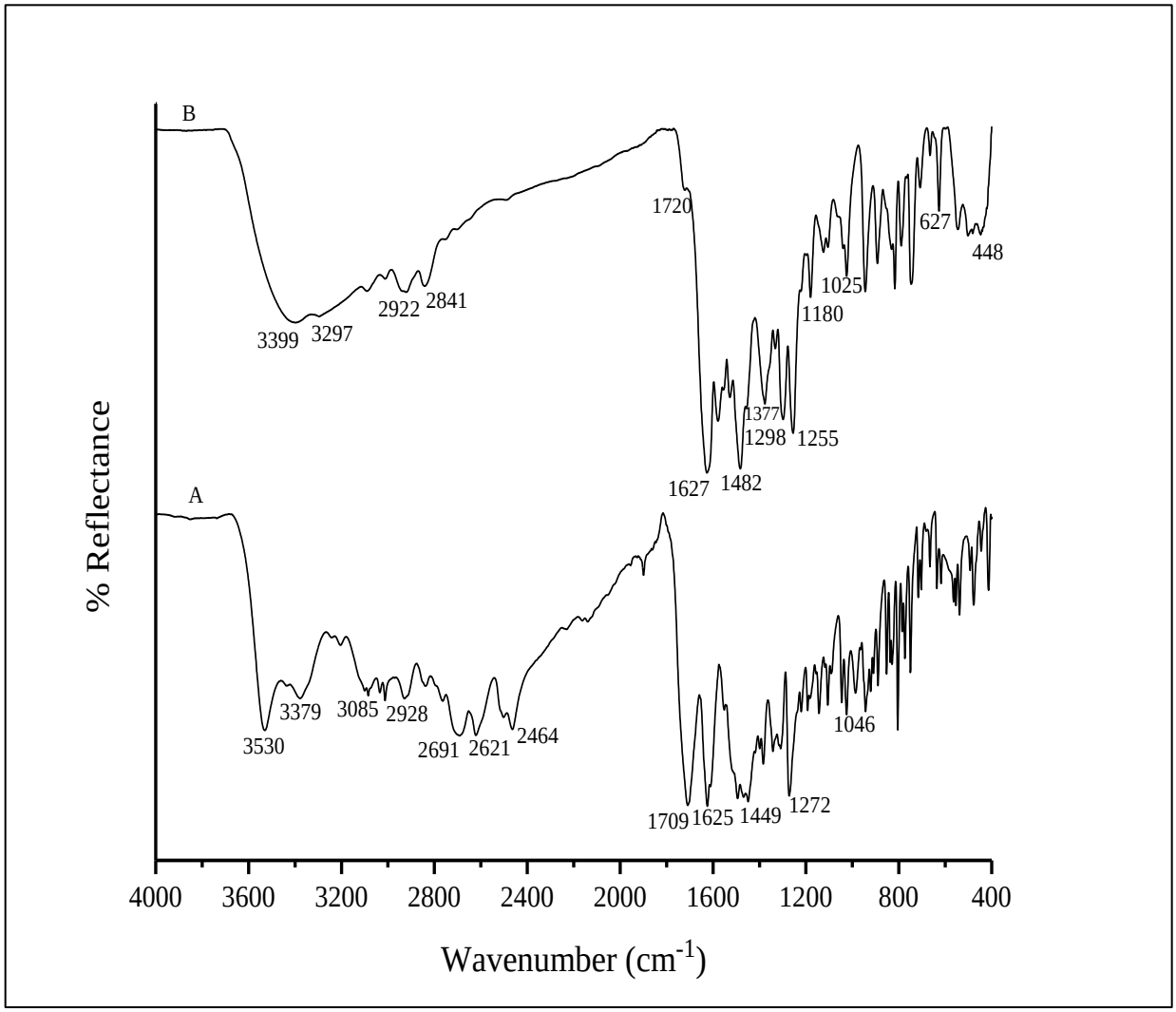

Figure 13: FTIR spectrum of A) ciprofloxacin B) ciprofloxacin loaded ZnONPs.

3.4.3. Powder X-ray diffraction (XRD) analysis

Figure 14 shows the X-ray diffractogram of synthesized ZnONPs which confirmed the formation of biosynthesized ZnONPs. The diffraction peaks appeared at 2θ value of 31.74^0, 34.38^0, 36.23^0, 47.49^0, 56.56^0, 62.79^0, 66.33^0, 67.9^0 and 69.01^0 which corresponds to (100), (002), (101), (102), (110), (103), (200), (112) and (201) crystal planes (h, l, k), respectively, are characteristics peaks for pure ZnONPs. The peaks of the X-ray diffractogram are in line with the previously reported works (Devi and Gayathri, 2014, Nilavukkarasi et al., 2020). As confirmed from the analysis, this typical XRD pattern of ZnONPs is found to possess the hexagonal crystal structure which goes very well (96%) with the value manipulated for hexagonal crystal structure of ZnONPs (Joint Committee on Powder Diffraction Standards: File No. 01-080-0074).

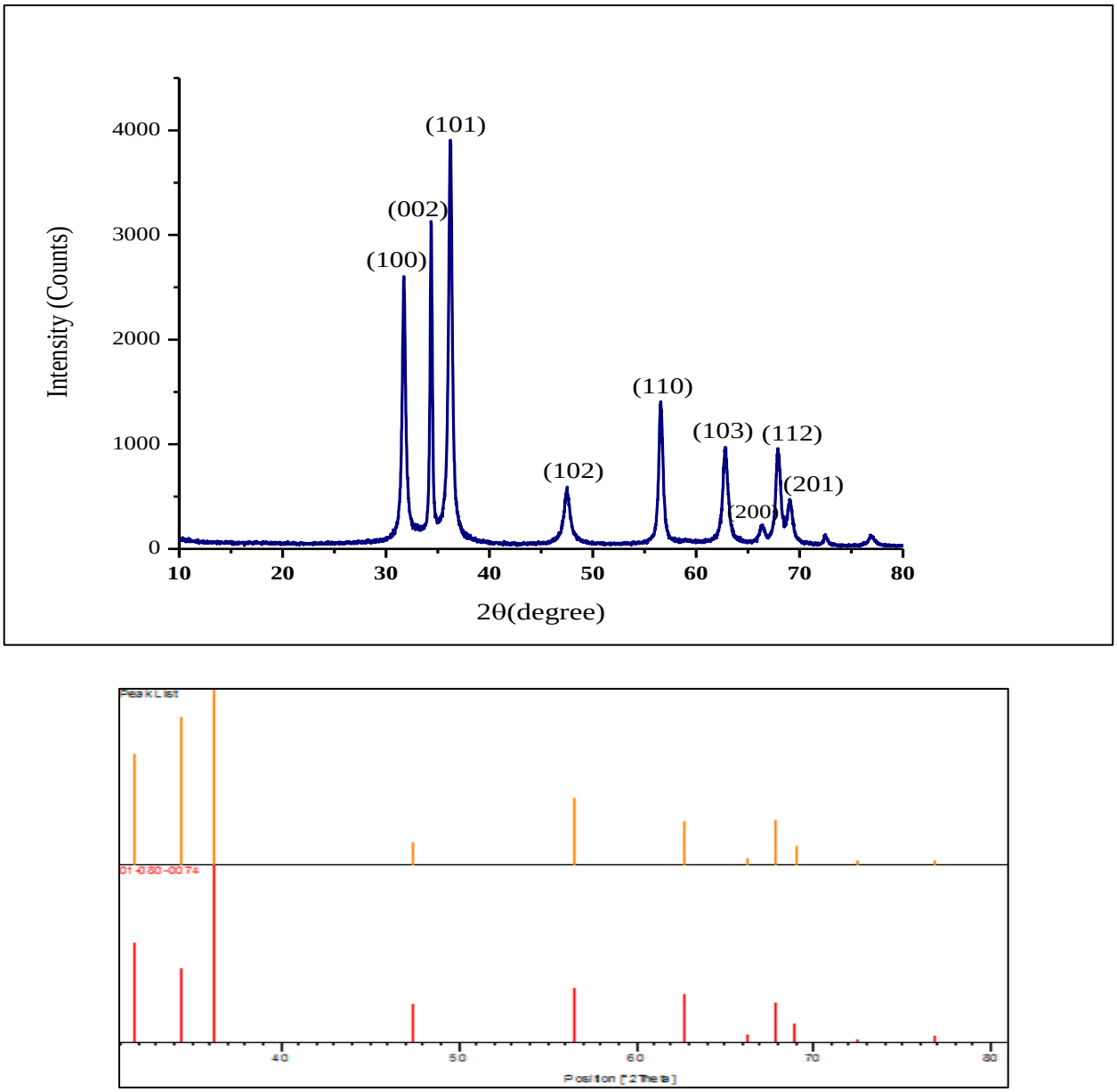

Figure 14: XRD patterns of ZnONPs synthesized using *M. Stenopetala* leaf extract.

Sharp diffraction peaks and absence of any random peaks in XRD pattern depicts a good degree of crystallinity and purity of synthesized ZnONPs, respectively (Agarwal and Shanmugam, 2019).The sharp diffraction peaks are also indicators for the biosynthesis of smaller ZnONPs (Chandra et al., 2019). The average crystal size of biosynthesized ZnONPs was determined using Debye-Scherrer's equation (Eq.1) using the Full-Width Half-Maximum (FWHM) values of the three most intense peaks and it was found 25.4 nm, as presented in Table 3.

Table 3: The average size of synthesized ZnONPs calculated from XRD data using Debye-Scherrer equation

2θ (degree)	d-spacing (d_{hkl})	FWHM (degree)	Diameter (nm)	(*h k l*)
31.707	2.81979	0.428	19.7	(100)
34.345	2.60885	0.239	36.2	(002)
36.195	2.47974	0.420	20.3	(101)
47.462	1.91407	0.646	13.6	(102)
56.536	1.62653	0.417	22.1	(110)
62.772	1.47908	0.518	18.3	(103)
66.328	1.40816	0.510	18.9	(200)
67.875	1.37977	0.475	20.5	(112)
69.004	1.35986	0.541	18.1	(201)

3.4.4. Scanning electron microscope (SEM) analysis

The biosynthesized ZnONPs were inspected by SEM for their size, shape and surface roughness and their electron microscopical images are illustrated on Figure 15 A and B. From these experimental findings, it is possible to see that the fabricated NPs possessed predominately spherical shape (Figure 15A) and they were found together. In concordance with our study, the SEM images of ZnONPs synthesized using *Lippia adoensis* (Koseret) leaf extract showed particles inclined together and the phenomenon was justified as it was due to the presence of many capping agents (Demissie et al., 2020). In addition, the average size of NPs was estimated from SEM image and it was found 58 $\pm$ 0.012 nm. It is somewhat larger than the crystallite size determined using XRD. This difference clearly indicated that the presence or formation of a number of crystallites in a single particle. The surface roughness analysis also revealed that the particles were with rough surfaces (Figure 15B).

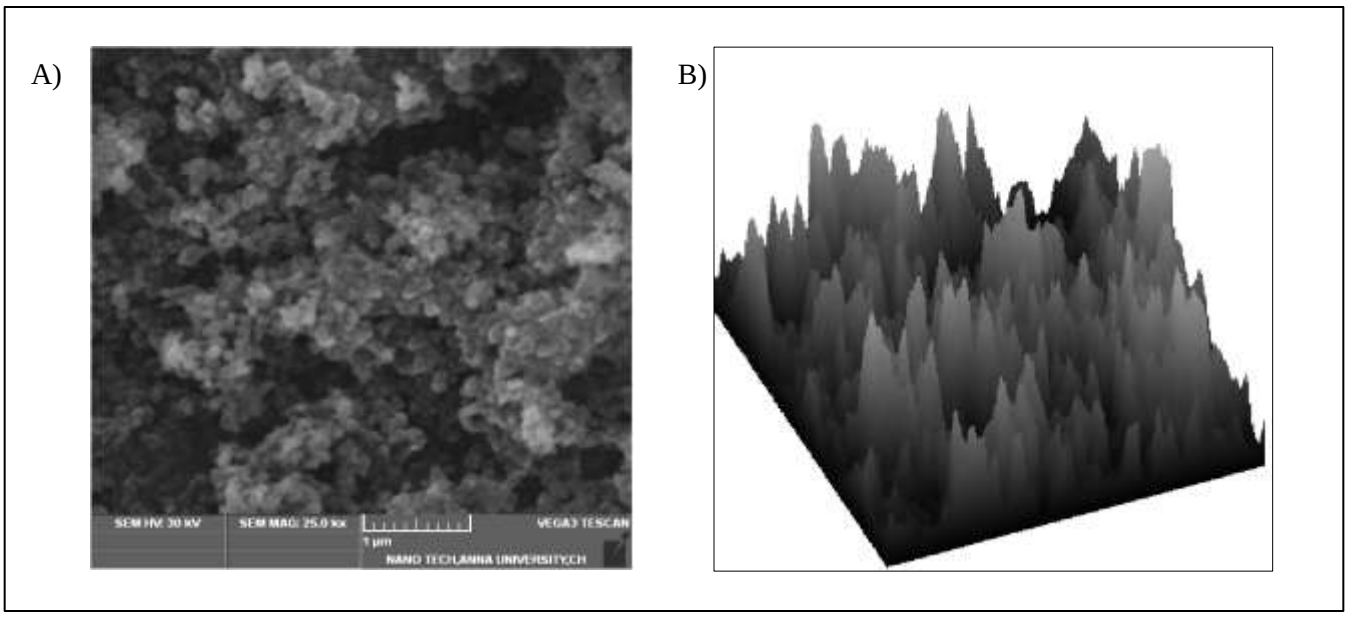

Figure 15: A) SEM image of green synthesized ZnONPs B) Surface roughness analysis.

3.4.5. Dynamic light scattering (DLS) analysis

As shown in Figure 16A and B, the size distribution measurement revealed that the average size of the green synthesized ZnONPs and ciprofloxacin loaded ZnONPs was 134 $\pm$ 0.7 and 148 $\pm$ 0.7 nm, respectively, with a PDI of 0.164 $\pm$ 0.017 for the former and 0.206 $\pm$ 0.014 for the latter. The PDI values of this experiment revealed a homogenous distribution of both blank and drug loaded NPs because values for PDI less than or equal to 0.3 are concidered as indicative of homogenous particle distribution (Eltarahony et al., 2018). It was clearly seen that the resulted particle size from DLS was larger than the particle size obtained from SEM and XRD results. This is due to DLS measures the hydrodynamic radius, a hypothetical hard sphere that diffuses with the same speed as the particles assayed in DLS, which ends up with overestimated particle size (Pryshchepa et al., 2020) and the size of this hydrodynamic radius is dependent on the particle structure, particle shape and roughness (Aldalbahi et al., 2020). There was a similar finding by (Jan et al., 2020) when they measured ZnONPs synthesized using aqueous extracts of *A. pubiflora* by DLS, it was 131 nm which was far from their SEM (34.23 nm) and XRD (9.58 nm) results of size measurement.

Even though DLS is the most recurrently used sizing technique by nanomedicine stakeholders due to its simplicity for use and low cost, it is recognized to be a low resolution method hence, the combination of multiple high-resolution techniques is often required to understand the particle size distribution (PSD) of NPs (Caputo et al., 2019). The technique is also highly biased

towards larger particles in suspension (Modena et al., 2019, Maguire et al., 2018, Faisal et al., 2021). In addition to low resolution power of the equipment, the increased measured size of the NPs may also be due to aggregation of NPs when they dispersed in distilled water. There was aggregation and size increment of commercially obtained ZnO nanopowders when their size was measured by DLS after dispersed in distilled water and other solvents (Vinardell et al., 2017).

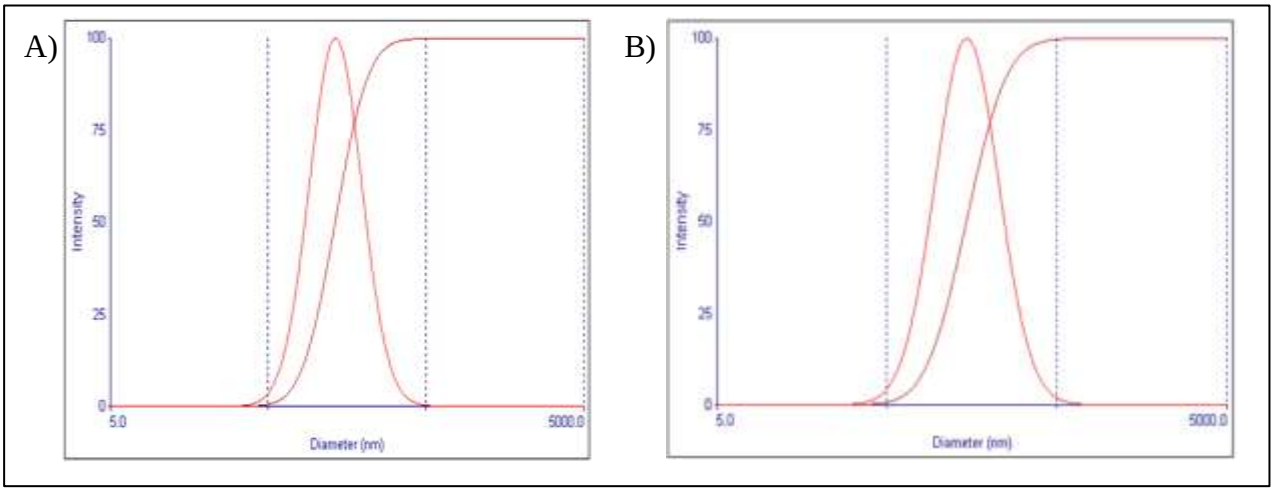

Figure 16: Size distribution of A) ZnONPs and B) ciprofloxacin loaded ZnONPs.

3.4.6. Differential scanning calorimetry /thermogravimetry (DSC-TGA) analysis

The DSC-TGA spectra of synthesized ZnONPs showed continuous weight loss with four major stages of decomposition or mass-loss-events at temperatures of 49.85, 157.47, 240.84 and 411.37^{0}C, as clearly indicated by the endothermic peaks of DSC spectra (Figure 17). The minor weight loss which happened early at 49.85^{0}C was due to the loss of adsorbed ethanol (Faisal et al., 2021, Bhuiyan et al., 2020, Tamaekong et al., 2014) and around 157.47^{0}C was due to the removal of adsorbed water (Faisal et al., 2021, Bhuiyan et al., 2020, Rajendran et al., 2021, Mashrai et al., 2017, Khalil et al., 2014, Ebadi et al., 2019, Kheshtzar et al., 2019). Similarly, the weight loss event around 240.84^{0}C was due to the condensation dehydration of hydroxyls (El-Arab, 2018) and around 411.37^{0}C was due to the decomposition of organic materials (Bhuiyan et al., 2020, Tamaekong et al., 2014, Mashrai et al., 2017, Ebadi et al., 2019, Kheshtzar et al., 2019, Matinise et al., 2017, Fatimah et al., 2016). In general, the decomposition of ZnONPs took place at very slow rate and the total weight loss was negligible (8%) which signify the synthesized NPs were thermally stable.

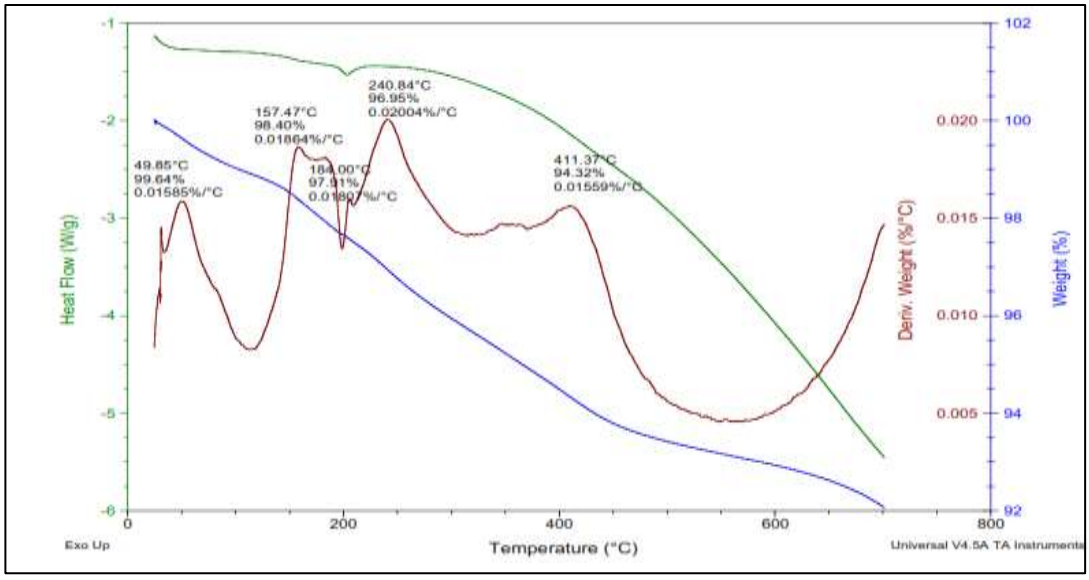

Figure 17: DSC-TGA curve of ZnONPs synthesized using *M. Stenopetala* leaf extract.

3.5. Drug loading on ZnONPs

3.5.1. Construction of calibration curve for drug loading

The absorbance readings were obtained and plotted against concentration. Finally, the calibration curve with a linear regression equation of: Y= 0.1038X + 0.0199 and correlation coefficient (R^2) of 0.9992 was obtained where Y is absorbance and X is concentration in µg/mL (the graph is shown in Appendix I).

3.5.2. Optimization for drug loading

3.5.2.1. Incubation time

As it is indicated in Table 4, the efficiency of ciprofloxacin loading on ZnONPs was increased with the time of experiments. Here, incubation time of 24 hours was selected as optimum time for drug loading.

Table 4: Changes of loading content and entrapment efficiency of ZnONPs with different incubation time

Incubation Time (hrs)	Total amount of drug added (mg)	Amount loaded (mg)	EE (%)	LC (%)
6	4	3.62	90.5	37.6
12	4	3.65	91.2	37.8
24	4	3.68	92.0	38.0

3.5.2.2. Quantity of Ciprofloxacin to be loaded

As it is indicated in Table 5, the efficiency of ciprofloxacin loading on ZnONPs was increased with the quantity of ciprofloxacin and 3 mg/mL (a total of 6 mg) was choosen as optimal quantity. As we can see from these results, the loading efficiency of synthesized ZnONPs was encouraging.

Table 5: Changes of loading content and entrapment efficiency of ZnONPs with different quantity of ciprofloxacin to be loaded.

Ciprofloxacin concentration (mg/mL)	Total amount of drug added (mg)	Amount loaded (mg)	EE (%)	LC (%)
1.5	3	2.80	93.3	31.8
2.0	4	3.68	92.0	38.0
3.0	6	5.79	96.5	49.1

3.6. In-vitro drug release study

3.6.1. Construction of calibration curve for drug release test

For all solutions of ciprofloxacin in all buffer conditions, the absorbance readings were obtained and plotted (Y-axis) against concentration of solutions (X-axis) (Appendix II, A through D). Then, linear regression equations and correlation coefficients were obtained for each calibration curve (Table 6).

Table 6: Linear regression equations and correlation coefficients (R^2) of calibration curves of ciprofloxacin in different buffer solutions

S/No	Buffer solutions' pH	Linear regression equation*	Correlation coefficient (R^2)
1	1.2	Y = 0.0709X + 0.0030	0.9992
2	6.0	Y = 0.0769X – 0.0012	0.9999
3	6.8	Y = 0.0679X + 0.0145	0.9991
4	7.4	Y = 0.0654X + 0.0125	0.9995

*- Y is absorbance and X is concentration in µg/mL.

3.6.2. Drug release test

The result, shown in Figure 18, revealed that the release of ciprofloxacin from ZnONPs was both time and pH dependent. At pH values of 7.4, the drug release rate was slow, only 55% of the drug was released within the first three days and only additional 5% drug (data not shown) was released until the fifth day. This gives evidence about the stability of ciprofloxacin loaded ZnONPs at physiologic pH which is advantageous so that ciprofloxacin will not be released during blood circulation. When the pH value was reduced, the drug release rate was accelerated when compared with a pH of 7.4. At pH 6.8, around 71% and at pH 6.0, around 86% of the drug was released within 72 hours. At much lower pH value, pH 1.2, ciprofloxacin was released completely within the first 5 hours. This implies the drug was dissolved instantly because ciprofloxacin is highly soluble at this pH value. In addition, the higher solubility of ZnONPs in acidic pH (Avramescu et al., 2017, Siddiqi et al., 2018, da Silva et al., 2019) may also facilitate the complete drug release at this specific pH value.

Therefore, from our result, we can conclude that the loaded ciprofloxacin could be efficiently released from ZnONPs at the site of *E.coli* infected uroepithelium environment in a sustained manner, but sufficiently stable in physiological pH conditions. However, the drug loaded NPs were not stable in acidic pH and it needs some levels of modification and protection if it encounters acidic environment like gastric environment, especially when it is desired to release the drug in sustained manner.

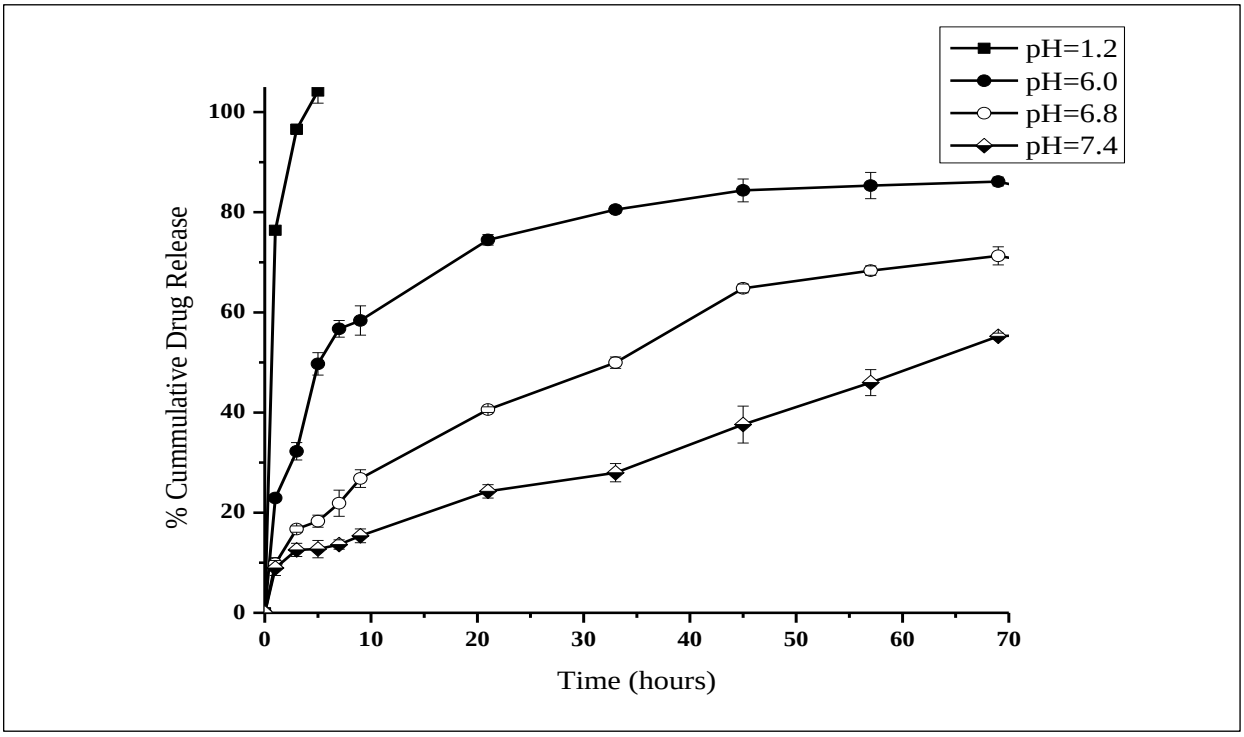

Figure 18: % Cumulative drug releases of ciprofloxacin from ciprofloxacin loaded ZnONPs in different pH conditions.

3.7. In-vitro antibacterial activity study

Many of inorganic metal oxide NPs inhibit the growth of *E.coli*, but ZnONPs are among the most promising for clinical translation because of their high potency against drug resistant strains, reduced toxicity to mammalian cells and its low cost (Kadiyala et al., 2018). ZnONPs are active against gram positive and negative bacteria and even show conciderable activities against more resistant bacterial spores (Jamdagni et al., 2018).

The result showed in Table 7 is the antimicrobial activities of ciprofloxacin, ZnONPs and ciprofloxacin loaded ZnONPs against ciprofloxacin resistant *E.coli*. As it is clearly indicated, green synthesized ZnONPs alone displayed antimicrobial activity against ciprofloxacin resistant *E.coli* and increased the activities of ciprofloxacin when conjugated with it while the negative control showed no inhibitory effect. As it is stated in CLSI, the zone diameter break points, when antimicrobial susceptibility test is conducted for ciprofloxacin against *E.coli* using disc diffusion method, can be categorized as ≥ 26, 25-22 and ≤ 21 which are indicative for the susceptibility, intermediate susceptibility and resistance, respectively, of the bacteria for the drug (CLSI, 2020).

Therefore, according to this guideline, our result demonstrated that *E.coli* was resistant for ciprofloxacin because the diameter of ZOI around ciprofloxacin impregnated disc was 17 ± 0.71.

However, when it was conjugated with green synthesized ZnONPs, the diameter of ZOI was increased to 23 ± 0.92, which falls in the intermediate susceptibility break point category. Hence, it is possible to conclude that ZnONPs can enhance the activity of ciprofloxacin against ciprofloxacin resistant *E.coli*. The supplement of activity of ciprofloxacin by ZnONPs may be due to the destruction of the outer protective membranes of bacteria by the NPs, an action ciprofloxacin alone fails to do that and this cell wall destruction allows easier entrance of it to bacterial cells (Patra et al., 2014). In concordance with our study, (Banoee et al., 2010) was found that there was an increased antimicrobial activity of ciprofloxacin against *E.coli* when it was combined with ZnONPs. There was also a report which showed the dose dependent efficacy of ciprofloxacin conjugated ZnONPs against multi drug resistant bacterial strains including *E.coli* (Patra et al., 2014). It was also reported that ZOI for ciprofloxacin in the presence of ZnONPs was increased by 22% against a tested strain of *E. coli* (Shaikh et al., 2019).

In another study, ZnONPs, prepared by solvothermal method and combined with ciprofloxacin and ceftazidime, showed increased antibacterial activity and uptake of both antibiotics against multidrug resistant *Acinetobacter baumannii* (Ghasemi and Jalal, 2016).

Table 7: Zone of inhibition (mm) of ciprofloxacin, ZnONPs and ciprofloxacin loaded ZnONPs against ciprofloxacin resistant *E.coli*.

S/No	Antimicrobial agents	ZOI diameter[a] (mm)[b]
1	Ciprofloxacin	17 ± 0.71
2	ZnONPs	8 ± 0.43
3	ZnONPs-ciprofloxacin conjugate	23 ± 0.92
4	0.85% Normal saline	6 ± 0.00

[a] -the measured ZOI diameter includes the disc diameter

[b] -the diameter is the mean of three tests

As it is mentioned above, the antimicrobial activities of ZnONPs is proposed through destruction of cell integrity due to its direct contact with cell walls, ROS formation and release of antimicrobial ions mainly Zn^{+2}, though it is yet to be clarified (Shaikh et al., 2019). The contact

of ZnONPs with cell wall is due to the electrostatic attraction because of the bacteria carries negative charge and metal oxides possibly carry positive charge. This may result in destruction of the outer membrane of *E.coli* cell which in turn leads to leakage of materials, proteins and genetic materials (Bekele et al., 2020). This may be facilitated due to the small size of biosynthesized ZnONPs which provides a large surface area for contact with bacteria (da Silva et al., 2019, Rahaiee et al., 2020). This scenario may also work for our case because the average size of our NPs was 25.4 nm (as determined from XRD data) and 58 nm (as determined from SEM data) in which both data indicated that the NPs were small in size. In addition, as it was revealed in SEM image above, the synthesized NPs were with rough surface which in turn can increase the possibility of direct contact killing because surface roughness increases the probability of bacterial adhesion to NPs (Chang et al., 2021).

Regarding reactive oxygen species generation, once it is generated (mostly H_2O_2), it penetrates the bacterial cell wall and can disrupt the metabolic process (Ribut et al., 2018); play an important role in alteration of proteins, enzymes and damage RNA/DNA (Shabaani et al., 2020); while, Zn^{+2} attacks the bacterial cell wall and rupture it (Ribut et al., 2018). As an opportunity also, *E.coli* has a thin peptidoglycan layer that may facilitate the entrance of ions from NPs in to the bacteria which ends up with cell wall destruction (da Silva et al., 2019, Rahaiee et al., 2020, Umar et al., 2019). These broad spectrums of mechanisms create a difficulty to microorganisms to develop resistance for these NPs (Kora and Arunachalam, 2011).

There are a number of studies which shared the above proposed mechanisms as a mechanism of ZnONPs used to exert their antimicrobial effect. For example, the antimicrobial effects of ZnONPs in ciprofloxacin-ZnONPs conjugate, when it was evaluated against multidrug resistant *E. coli*, *Staphylococcus aureus* and *Klebsiella* sp. (resistant to ciprofloxacin, ofloxacine, tetracycline, chloramphenicol and gintamicin), was justified as; ZnONPs were damage the cell membrane of the bacteria through reactive oxygen species generation or due to mechanical damage because of its surface defect. The cell membrane damage was confirmed by release assay which showed the release of RNA, DNA and other materials (Patra et al., 2014). Similarly, there was an evidence for destruction of cell membrane of carbapenem resistant *Acinetobacter baumannii* when there was a leakage of reducing sugars, protein and DNA as a result of its treatment with ZnONPs (Tiwari et al., 2018).

4. CONCLUSIONS

In our study, ZnONPs were synthesized by green method using non-toxic and renewable aqueous extracts of *M. Stenopetala* leaf as a reducing, capping and stabilizing agents. The synthesized NPs were characterized using different techniques to know their properties. The effective formation of ZnONPs were confirmed using UV/Vis. spectrophotometer due to the presence of SPR peak at 350 nm and FTIR spectrophotometers due to the vibration present at 445 cm^{-1}. The synthesized NPs were: pure crystalline as it is indicated from XRD data; predominately spherical in shape as the SEM data revealed; and thermally stable as it is indicated in DSC-TGA thermogram. The estimated crystallite size of NPs was 25.4 nm; their average diameter was 58 nm according to SEM result; and 134 nm according to DLS analysis. The drug loaded NPs were also characterized and hence the effective loading of the drug was confirmed through FTIR and UV/Vis. spectrophotometer analysis, and their hydrodynamic radius was 148 nm which was measured by DLS.

The NPs were also evaluated for their drug loading potential and release characteristics. They were with 96.5% of EE and 49.1% of LC. The drug release test was revealed that the drug loaded NPs were stable at physiological pH and release the drug in sustained manner at a pH value of *E.coli* infected urinary tract environment which makes the NPs good candidate for ciprofloxacin delivery while it was unstable in acidic pH. Finally, AST test was conducted and the results revealed that ZnONPs alone were effective against ciprofloxacin resistant *E.coli* and when conjugated with ciprofloxacin, they enhanced the effect of it against this pathogen.

5. RECOMMENDATIONS

In this study, ZnONPs were synthesized effectively using *M. Stenopetala* leaf extract. They were characterized for their physicochemical characteristics, evaluated for their drug loading efficiency and drug releasing behavior and the findings were promising. It is better if it is known for how long their characteristics and quality stay with them. Therefore, we recommend stability study for both bare ZnONPs and drug loaded ZnONPs.

Likewise, the *in vitro* antimicrobial activity of ZnONPs and drug loaded NPs against ciprofloxacin resistance *E.coli* was evaluated and the result was again promising. Based on this finding, we also recommend the evaluation of *in vivo* antibacterial effect of bare and ciprofloxacin loaded ZnONPs.

REFERENCES

Abdol Aziz, R., Abd Karim, S. F. & Rosli, N. A. The effect of ph on zinc oxide nanoparticles characteristics synthesized from banana peel extract. Key Engineering Materials, 2019. Trans Tech Publ, 271-279.

Abdullah, F., Bakar, N. A. & Bakar, M. A. 2020. Low temperature biosynthesis of crystalline zinc oxide nanoparticles from Musa acuminata peel extract for visible-light degradation of methylene blue. *Optik,* 206**,** 164279.

Abejew, A. A., Denboba, A. A. & Mekonnen, A. G. 2014. Prevalence and antibiotic resistance pattern of urinary tract bacterial infections in Dessie area, North-East Ethiopia. *BMC research notes,* 7**,** 687.

Abiyu, A., Yan, D., Girma, A., Song, X. & Wang, H. 2018. Wastewater treatment potential of Moringa stenopetala over Moringa olifera as a natural coagulant, antimicrobial agent and heavy metal removals. *Cogent Environmental Science,* 4**,** 1433507.

Aboelfetoh, E. F., El-Shenody, R. A. & Ghobara, M. M. 2017. Eco-friendly synthesis of silver nanoparticles using green algae (Caulerpa serrulata): reaction optimization, catalytic and antibacterial activities. *Environmental monitoring and assessment,* 189**,** 1-15.

Abuye, C., Urga, K., Knapp, H., Selmar, D., Omwega, A., Imungi, J. & Winterhalter, P. 2003. A compositional study of Moringa stenopetala leaves. *East African Medical Journal,* 80**,** 247-252.

Agarwal, H., Kumar, S. V. & Rajeshkumar, S. 2017. A review on green synthesis of zinc oxide nanoparticles–An eco-friendly approach. *Resource-Efficient Technologies,* 3**,** 406-413.

Agarwal, H. & Shanmugam, V. K. 2019. Synthesis and optimization of zinc oxide nanoparticles using Kalanchoe pinnata towards the evaluation of its anti-inflammatory activity. *Journal of Drug Delivery Science and Technology,* 54**,** 101291.

Ahmad, T., Irfan, M., Bustam, M. A. & Bhattacharjee, S. 2016. Effect of reaction time on green synthesis of gold nanoparticles by using aqueous extract of Elaise guineensis (oil palm leaves). *Procedia engineering,* 148**,** 467-472.

Ahmad, W. & Kalra, D. 2020. Green synthesis, characterization and anti microbial activities of ZnO nanoparticles using Euphorbia hirta leaf extract. *Journal of King Saud University-Science,* 32**,** 2358-2364.

Ahmed, S., Chaudhry, S. A. & Ikram, S. 2017. A review on biogenic synthesis of ZnO nanoparticles using plant extracts and microbes: a prospect towards green chemistry. *Journal of Photochemistry and Photobiology B: Biology,* 166**,** 272-284.

Akbar, S., Tauseef, I., Subhan, F., Sultana, N., Khan, I., Ahmed, U. & Haleem, K. S. 2020. An overview of the plant-mediated synthesis of zinc oxide nanoparticles and their antimicrobial potential. *Inorganic and Nano-Metal Chemistry,* 50**,** 257-271.

Akbari, A., Amini, M., Tarassoli, A., Eftekhari-Sis, B., Ghasemian, N. & Jabbari, E. 2018. Transition metal oxide nanoparticles as efficient catalysts in oxidation reactions. *Nano-Structures & Nano-Objects,* 14**,** 19-48.

Akbarzadeh, A., Samiei, M. & Davaran, S. 2012. Magnetic nanoparticles: preparation, physical properties, and applications in biomedicine. *Nanoscale research letters,* 7**,** 1-13.

Akintelu, S. A. & Folorunso, A. S. 2020. A review on green synthesis of zinc oxide nanoparticles using plant extracts and its biomedical applications. *BioNanoScience,* 10**,** 848-863.

Al-Mustafa, J. 2002. Magnesium, calcium, and barium perchlorate complexes of ciprofloxacin and norfloxacin. *Acta Chimica Slovenica,* 49**,** 457-466.

Al-Mustafa, J. & Tashtoush, B. 2003. Iron (II) and iron (III) perchlorate complexes of ciprofloxacin and norfloxacin. *Journal of Coordination Chemistry,* 56**,** 113-124.

Alam, M. N., Das, S., Batuta, S., Roy, N., Chatterjee, A., Mandal, D. & Begum, N. A. 2014. Murraya koenegii Spreng. leaf extract: an efficient green multifunctional agent for the controlled synthesis of Au nanoparticles. *ACS Sustainable Chemistry & Engineering,* 2**,** 652-664.

Alawieh, A., Sabra, Z., Bizri, A. R., Davies, C., White, R. & Zaraket, F. A. 2015. A computational model to monitor and predict trends in bacterial resistance. *Journal of global antimicrobial resistance,* 3**,** 174-183.

Aldalbahi, A., Alterary, S., Ali Abdullrahman Almoghim, R., Awad, M. A., Aldosari, N. S., Fahad Alghannam, S., Nasser Alabdan, A., Alharbi, S., Ali Mohammed Alateeq, B. & Abdulrahman Al Mohsen, A. 2020. Greener Synthesis of Zinc Oxide Nanoparticles: Characterization and Multifaceted Applications. *Molecules,* 25**,** 4198.

Alemayehu, T., Ali, M., Mitiku, E. & Hailemariam, M. 2019. The burden of antimicrobial resistance at tertiary care hospital, southern Ethiopia: a three years' retrospective study. *BMC infectious diseases,* 19**,** 585.

Ansari, M. A., Murali, M., Prasad, D., Alzohairy, M. A., Almatroudi, A., Alomary, M. N., Udayashankar, A. C., Singh, S. B., Asiri, S. M. M. & Ashwini, B. S. 2020. Cinnamomum verum bark extract mediated green synthesis of ZnO nanoparticles and their antibacterial potentiality. *Biomolecules,* 10**,** 336.

Arslan, H., Azap, Ö. K., Ergönül, Ö. & Timurkaynak, F. 2005. Risk factors for ciprofloxacin resistance among Escherichia coli strains isolated from community-acquired urinary tract infections in Turkey. *Journal of Antimicrobial Chemotherapy,* 56**,** 914-918.

Assefa, D., Dessalegn, E. & Chauhan, C. 2015. Effect of thermal treatment on phenolic content, antioxidant, and α-amylase inhibition activities of Moringa stenopetala leaves. *Afr J Food Sci,* 9**,** 487-94.

Avoseh, O. N., Oyedeji, O. O., Aremu, O., Nkeh-Chungag, B. N., Songca, S. P., Oyedeji, A. O., Mohan, S. & Oluwafemi, O. S. 2017. Biosynthesis of silver nanoparticles from Acacia mearnsii De Wild stem bark and its antinociceptive properties. *Green Chemistry Letters and Reviews,* 10**,** 59-68.

Avramescu, M.-L., Rasmussen, P., Chénier, M. & Gardner, H. 2017. Influence of pH, particle size and crystal form on dissolution behaviour of engineered nanomaterials. *Environmental Science and Pollution Research,* 24**,** 1553-1564.

Bandeira, M., Giovanela, M., Roesch-Ely, M., Devine, D. M. & Da Silva Crespo, J. 2020. Green synthesis of zinc oxide nanoparticles: A review of the synthesis methodology and mechanism of formation. *Sustainable Chemistry and Pharmacy,* 15**,** 100223.

Banoee, M., Seif, S., Nazari, Z. E., Jafari-Fesharaki, P., Shahverdi, H. R., Moballegh, A., Moghaddam, K. M. & Shahverdi, A. R. 2010. ZnO nanoparticles enhanced antibacterial activity of ciprofloxacin against Staphylococcus aureus and Escherichia coli. *Journal of Biomedical Materials Research Part B: Applied Biomaterials,* 93**,** 557-561.

Banu, K. S. & Cathrine, L. 2015. General techniques involved in phytochemical analysis. *International Journal of Advanced Research in Chemical Science,* 2**,** 25-32.

Bar, H., Bhui, D. K., Sahoo, G. P., Sarkar, P., De, S. P. & Misra, A. 2009. Green synthesis of silver nanoparticles using latex of Jatropha curcas. *Colloids and surfaces A: Physicochemical and engineering aspects,* 339**,** 134-139.

Barui, A. K., Kotcherlakota, R. & Patra, C. R. 2018. Biomedical applications of zinc oxide nanoparticles. *Inorganic Frameworks as Smart Nanomedicines.* Elsevier.

Beg, M. R., Ghodinde, S. & Gupta, V. 2020. Plant mediated green synthesis of Zinc Oxide Nanoparticles for burn wound therapy.

Bekele, E. T., Gonfa, B. A., Zelekew, O. A., Belay, H. H. & Sabir, F. K. 2020. Synthesis of titanium oxide nanoparticles using root extract of kniphofia foliosa as a template, characterization, and its application on drug resistance bacteria. *Journal of Nanomaterials,* 2020.

Bhuiyan, M. S. H., Miah, M. Y., Paul, S. C., Aka, T. D., Saha, O., Rahaman, M. M., Sharif, M. J. I., Habiba, O. & Ashaduzzaman, M. 2020. Green synthesis of iron oxide nanoparticle using Carica papaya leaf extract: application for photocatalytic degradation of remazol yellow RR dye and antibacterial activity. *Heliyon,* 6**,** e04603.

Bhumi, G., Raju, R. & Savithramma, N. 2014. Screening of zinc oxide nanoparticles for cell proliferation synthesized through Adhatoda vasica nees. *Int. J. Drug Dev. & Res,* 6**,** 97-104.

Brown, A. N., Smith, K., Samuels, T. A., Lu, J., Obare, S. O. & Scott, M. E. 2012. Nanoparticles functionalized with ampicillin destroy multiple-antibiotic-resistant isolates of Pseudomonas aeruginosa and Enterobacter aerogenes and methicillin-resistant Staphylococcus aureus. *Applied and environmental microbiology,* 78**,** 2768-2774.

Buazar, F., Bavi, M., Kroushawi, F., Halvani, M., Khaledi-Nasab, A. & Hossieni, S. 2016. Potato extract as reducing agent and stabiliser in a facile green one-step synthesis of ZnO nanoparticles. *Journal of Experimental Nanoscience,* 11**,** 175-184.

Caputo, F., Clogston, J., Calzolai, L., Rösslein, M. & Prina-Mello, A. 2019. Measuring particle size distribution of nanoparticle enabled medicinal products, the joint view of EUNCL and NCI-NCL. A step by step approach combining orthogonal measurements with increasing complexity. *Journal of Controlled Release,* 299**,** 31-43.

Cdc 2019. Antibiotic Resistance Threats in the United States 2019, Atlanta, GA: US Department of Health and Human Services, CDC; 2019.

Chakraborty, S., Farida, J. J., Simon, R., Kasthuri, S. & Mary, N. 2020. Averrhoe carrambola fruit extract assisted green synthesis of zno nanoparticles for the photodegradation of congo red dye. *Surfaces and Interfaces,* 19**,** 100488.

Chandra, H., Patel, D., Kumari, P., Jangwan, J. & Yadav, S. 2019. Phyto-mediated synthesis of zinc oxide nanoparticles of Berberis aristata: Characterization, antioxidant activity and antibacterial activity with special reference to urinary tract pathogens. *Materials Science and Engineering: C,* 102**,** 212-220.

Chandran, K., Song, S. & Yun, S.-I. 2019. Effect of size and shape controlled biogenic synthesis of gold nanoparticles and their mode of interactions against food borne bacterial pathogens. *Arabian Journal of Chemistry,* 12**,** 1994-2006.

Chang, T., Sepati, M., Herting, G., Leygraf, C., Rajarao, G. K., Butina, K., Richter-Dahlfors, A., Blomberg, E. & Odnevall Wallinder, I. 2021. A novel methodology to study antimicrobial properties of high-touch surfaces used for indoor hygiene applications—A study on Cu metal. *Plos one,* 16**,** e0247081.

Chavali, M. S. & Nikolova, M. P. 2019. Metal oxide nanoparticles and their applications in nanotechnology. *SN applied sciences,* 1**,** 1-30.

Crofts, T. S., Gasparrini, A. J. & Dantas, G. 2017. Next-generation approaches to understand and combat the antibiotic resistome. *Nature Reviews Microbiology,* 15**,** 422.

Da Silva, B. L., Abuçafy, M. P., Manaia, E. B., Junior, J. a. O., Chiari-Andréo, B. G., Pietro, R. C. R. & Chiavacci, L. A. 2019. Relationship between structure and antimicrobial activity of zinc oxide nanoparticles: An overview. *International journal of nanomedicine,* 14**,** 9395.

Demissie, M. G., Sabir, F. K., Edossa, G. D. & Gonfa, B. A. 2020. Synthesis of zinc oxide nanoparticles using leaf extract of lippia adoensis (koseret) and evaluation of its antibacterial activity. *Journal of Chemistry,* 2020.

Devi, R. S. & Gayathri, R. 2014. Green synthesis of zinc oxide nanoparticles by using Hibiscus rosa-sinensis. *International Journal of Current Engineering and Technology,* 4**,** 2444-2446.

Devipriya, D. & Roopan, S. M. 2017. Cissus quadrangularis mediated ecofriendly synthesis of copper oxide nanoparticles and its antifungal studies against Aspergillus niger, Aspergillus flavus. *Materials Science and Engineering: C,* 80**,** 38-44.

Dizaj, S. M., Lotfipour, F., Barzegar-Jalali, M., Zarrintan, M. H. & Adibkia, K. 2014. Antimicrobial activity of the metals and metal oxide nanoparticles. *Materials Science and Engineering: C,* 44**,** 278-284.

Dobrucka, R. & Długaszewska, J. 2016. Biosynthesis and antibacterial activity of ZnO nanoparticles using Trifolium pratense flower extract. *Saudi journal of biological sciences,* 23**,** 517-523.

Ebadi, M., Zolfaghari, M. R., Aghaei, S. S., Zargar, M., Shafiei, M., Zahiri, H. S. & Noghabi, K. A. 2019. A bio-inspired strategy for the synthesis of zinc oxide nanoparticles (ZnO NPs) using the cell extract of cyanobacterium Nostoc sp. EA03: from biological function to toxicity evaluation. *RSC advances,* 9**,** 23508-23525.

El-Arab, N. B. 2018. Synthesis and characterization of zinc oxide nanoparticles using green and chemical synthesis techniques for phenol decontamination.

El Shafey, A. M. 2020. Green synthesis of metal and metal oxide nanoparticles from plant leaf extracts and their applications: A review. *Green Processing and Synthesis,* 9**,** 304-339.

Ellen, M. E., Shach, R. & Perlman, S. 2019. Exploring community healthcare providers' perceptions on antimicrobial resistance. *Journal of global antimicrobial resistance,* 18**,** 215-222.

Eltarahony, M., Zaki, S., Elkady, M. & Abd-El-Haleem, D. 2018. Biosynthesis, characterization of some combined nanoparticles, and its biocide potency against a broad spectrum of pathogens. *Journal of Nanomaterials,* 2018.

Emasushan, M. & Britto, J. 2018. Preliminary phytochemical profiling and antifungal activity of the seeds and pericarp of Putranjiva roxburghii Wall. *The Pharma Innovation Journal,* 7**,** 107-110.

Ephi 2018. Ethiopia Antimicrobial Resistance Surveillance: Annual Report July 2017-Augest 2018, Addis Ababa: EPHI; 2018.

European Centre for Disease Prevention and Control. Surveillance of antimicrobial resistance in Europe 2018. Stockholm: ECDC; 2019.

Ezealisiji, K. M., Siwe-Noundou, X., Maduelosi, B., Nwachukwu, N. & Krause, R. W. M. 2019. Green synthesis of zinc oxide nanoparticles using Solanum torvum (L) leaf extract and evaluation of the toxicological profile of the ZnO nanoparticles–hydrogel composite in Wistar albino rats. *International Nano Letters,* 9**,** 99-107.

Fahimmunisha, B. A., Ishwarya, R., Alsalhi, M. S., Devanesan, S., Govindarajan, M. & Vaseeharan, B. 2020. Green fabrication, characterization and antibacterial potential of zinc oxide nanoparticles using Aloe socotrina leaf extract: A novel drug delivery approach. *Journal of Drug Delivery Science and Technology,* 55**,** 101465.

Faisal, S., Jan, H., Shah, S. A., Shah, S., Khan, A., Akbar, M. T., Rizwan, M., Jan, F., Wajidullah & Akhtar, N. 2021. Green synthesis of zinc oxide (ZnO) nanoparticles using aqueous fruit extracts of Myristica fragrans: their characterizations and biological and environmental applications. *ACS omega,* 6**,** 9709-9722.

FAO. 2018. Antimicrobial resistance policy review and development framework - A regional guide for governments in Asia and the Pacific to review, update and develop policy to address antimicrobial resistance and antimicrobial use in animal production. Bangkok. 64 pp.

Fasugba, O., Gardner, A., Mitchell, B. G. & Mnatzaganian, G. 2015. Ciprofloxacin resistance in community-and hospital-acquired Escherichia coli urinary tract infections: a systematic review and meta-analysis of observational studies. *BMC infectious diseases,* 15**,** 1-16.

Fatimah, I., Pradita, R. Y. & Nurfalinda, A. 2016. Plant extract mediated of ZnO nanoparticles by using ethanol extract of Mimosa pudica leaves and coffee powder. *Procedia engineering,* 148**,** 43-48.

Flores-Mireles, A. L., Walker, J. N., Caparon, M. & Hultgren, S. J. 2015. Urinary tract infections: epidemiology, mechanisms of infection and treatment options. *Nature reviews microbiology,* 13**,** 269-284.

Food, Medicine and Health Care Administration and Control Authority standard treatment guidelines for general hospitals; third edition, 2014.

Gao, Y., Xu, D., Ren, D., Zeng, K. & Wu, X. 2020. Green synthesis of zinc oxide nanoparticles using Citrus sinensis peel extract and application to strawberry preservation: A comparison study. *LWT,* 126**,** 109297.

Gawade, V., Gavade, N., Shinde, H., Babar, S., Kadam, A. & Garadkar, K. 2017. Green synthesis of ZnO nanoparticles by using Calotropis procera leaves for the photodegradation of methyl orange. *Journal of Materials Science: Materials in Electronics,* 28**,** 14033-14039.

Geleta, B., Makonnen, E., Debella, A. & Tadele, A. 2016. In vivo antihypertensive and antihyperlipidemic effects of the crude extracts and fractions of Moringa stenopetala (Baker f.) Cufod. leaves in rats. *Frontiers in pharmacology,* 7**,** 97.

Ghasemi, F. & Jalal, R. 2016. Antimicrobial action of zinc oxide nanoparticles in combination with ciprofloxacin and ceftazidime against multidrug-resistant Acinetobacter baumannii. *Journal of global antimicrobial resistance,* 6**,** 118-122.

Global antimicrobial resistance surveillance system (GLASS) report: early implementation 2016-2017. Geneva: World Health Organization; 2017. Licence: CC BY-NC-SA 3.0 IGO.

Grace, A. N. & Pandian, K. 2007. Quinolone antibiotic-capped gold nanoparticles and their antibacterial efficacy against gram positive and gram negative organisms. *Journal of Bionanoscience,* 1**,** 96-105.

Gudkov, S. V., Burmistrov, D. E., Serov, D. A., Rebezov, M. B., Semenova, A. A. & Lisitsyn, A. B. 2021. A Mini Review of Antibacterial properties of ZnO nanoparticles. *Front. Phys. 9: 641481. doi: 10.3389/fphy.*

Gul, R., Jan, S. U., Faridullah, S., Sherani, S. & Jahan, N. 2017. Preliminary phytochemical screening, quantitative analysis of alkaloids, and antioxidant activity of crude plant extracts from Ephedra intermedia indigenous to Balochistan. *The Scientific World Journal,* 2017.

Habtemariam, S. 2017. *The African and Arabian Moringa species: chemistry, bioactivity and therapeutic applications*, Elsevier.

Habtemariam, S. & Varghese, G. K. 2015. Extractability of rutin in herbal tea preparations of Moringa stenopetala leaves. *Beverages,* 1**,** 169-182.

Hamza, T. A. & Azmach, N. N. 2017. The miraculous moringa trees: From nutritional and medicinal point of views in tropical regions. *Journal of Medicinal Plants Studies,* 5**,** 151-162.

Handago, D. T., Zereffa, E. A. & Gonfa, B. A. 2019. Effects of Azadirachta indica leaf extract, capping agents, on the synthesis of pure and Cu doped ZnO-nanoparticles: a green approach and microbial activity. *Open Chemistry,* 17**,** 246-253.

Happy, A., Soumya, M., Kumar, S. V., Rajeshkumar, S., Sheba, R. D., Lakshmi, T. & Nallaswamy, V. D. 2019. Phyto-assisted synthesis of zinc oxide nanoparticles using

Cassia alata and its antibacterial activity against Escherichia coli. *Biochemistry and biophysics reports,* 17**,** 208-211.

Harshiny, M., Matheswaran, M., Arthanareeswaran, G., Kumaran, S. & Rajasree, S. 2015. Enhancement of antibacterial properties of silver nanoparticles–ceftriaxone conjugate through Mukia maderaspatana leaf extract mediated synthesis. *Ecotoxicology and environmental safety,* 121**,** 135-141.

Hassan, S. S., El Azab, W. I., Ali, H. R. & Mansour, M. S. 2015. Green synthesis and characterization of ZnO nanoparticles for photocatalytic degradation of anthracene. *Advances in Natural Sciences: Nanoscience and Nanotechnology,* 6**,** 045012.

Hooper, D. C. 2001. Mechanisms of action of antimicrobials: focus on fluoroquinolones. *Clinical Infectious Diseases,* 32**,** S9-S15.

Hoseinpour, V., Souri, M., Ghaemi, N. & Shakeri, A. 2017. Optimization of green synthesis of ZnO nanoparticles by Dittrichia graveolens (L.) aqueous extract. *Health Biotechnol. Biopharma,* 1**,** 39-49.

Ibrahim, H. M. 2015. Green synthesis and characterization of silver nanoparticles using banana peel extract and their antimicrobial activity against representative microorganisms. *Journal of Radiation Research and Applied Sciences,* 8**,** 265-275.

Ibrahim, R. A., Teshal, A. M., Dinku, S. F., Abera, N. A., Negeri, A. A., Desta, F. G., Seyum, E. T., Gemeda, A. W. & Keficho, W. M. 2018. Antimicrobial resistance surveillance in Ethiopia: Implementation experiences and lessons learned. *African journal of laboratory medicine,* 7**,** 1-4.

Isa, T., Zakaria, Z. a. B., Rukayadi, Y., Mohd Hezmee, M. N., Jaji, A. Z., Imam, M. U., Hammadi, N. I. & Mahmood, S. K. 2016. Antibacterial activity of ciprofloxacin-encapsulated cockle shells calcium carbonate (Aragonite) nanoparticles and its biocompatability in macrophage J774A. 1. *International journal of molecular sciences,* 17**,** 713.

Isık, T., Hilal, M. E. & Horzum, N. 2019. Green Synthesis of Zinc Oxide Nanostructures. *Zinc Oxide Based Nano Materials and Devices.* IntechOpen.

Ivanova, N., Gugleva, V., Dobreva, M., Pehlivanov, I., Stefanov, S. & Andonova, V. 2018. Silver Nanoparticles as Multi-Functional Drug Delivery Systems. *Nanomedicines.* IntechOpen.

Jamdagni, P., Khatri, P. & Rana, J. 2018. Green synthesis of zinc oxide nanoparticles using flower extract of Nyctanthes arbor-tristis and their antifungal activity. *Journal of King Saud University-Science,* 30**,** 168-175.

Jameel, M. S., Aziz, A. A. & Dheyab, M. A. 2020. Green synthesis: Proposed mechanism and factors influencing the synthesis of platinum nanoparticles. *Green Processing and Synthesis,* 9**,** 386-398.

Jan, H., Shah, M., Usman, H., Khan, A., Muhammad, Z., Hano, C. & Abbasi, B. H. 2020. Biogenic Synthesis and Characterization of Antimicrobial and Anti-parasitic Zinc Oxide (ZnO) Nanoparticles using Aqueous Extracts of the Himalayan Columbine (Aquilegia pubiflora). *Frontiers in Materials,* 7**,** 249.

Jelinkova, P., Mazumdar, A., Sur, V. P., Kociova, S., Dolezelikova, K., Jimenez, A. M. J., Koudelkova, Z., Mishra, P. K., Smerkova, K. & Heger, Z. 2019. Nanoparticle-drug conjugates treating bacterial infections. *Journal of Controlled Release*.

Jiru, D., Sonder, K., Alemayehu, L., Mekonen, Y. & Anjulo, A. 2006. Leaf yield and nutritive value of Moringa stenopetala and Moringa oleifera accessions: Its potential role in food security in constrained dry farming agroforestry system. *Proceedings of the Moringa and other highly nutritious plant resources: Strategies, standards and markets for a better impact on nutrition in Africa, Accra, Ghana***,** 16-18.

Johnson, J. R., Kuskowski, M. A., Menard, M., Gajewski, A., Xercavins, M. & Garau, J. 2006. Similarity between human and chicken Escherichia coli isolates in relation to ciprofloxacin resistance status. *The Journal of infectious diseases,* 194**,** 71-78.

Kadiyala, U., Turali-Emre, E. S., Bahng, J. H., Kotov, N. A. & Vanepps, J. S. 2018. Unexpected insights into antibacterial activity of zinc oxide nanoparticles against methicillin resistant Staphylococcus aureus (MRSA). *Nanoscale,* 10**,** 4927-4939.

Kalita, S., Kandimalla, R., Sharma, K. K., Kataki, A. C., Deka, M. & Kotoky, J. 2016. Amoxicillin functionalized gold nanoparticles reverts MRSA resistance. *Materials Science and Engineering: C,* 61**,** 720-727.

Kaur, A., Preet, S., Kumar, V., Kumar, R. & Kumar, R. 2019. Synergetic effect of vancomycin loaded silver nanoparticles for enhanced antibacterial activity. *Colloids and Surfaces B: Biointerfaces,* 176**,** 62-69.

Kavitha, S., Dhamodaran, M., Prasad, R. & Ganesan, M. 2017. Synthesis and characterisation of zinc oxide nanoparticles using terpenoid fractions of Andrographis paniculata leaves. *International Nano Letters,* 7**,** 141-147.

Khalil, M. I., Al-Qunaibit, M. M., Al-Zahem, A. M. & Labis, J. P. 2014. Synthesis and characterization of ZnO nanoparticles by thermal decomposition of a curcumin zinc complex. *Arabian journal of chemistry,* 7**,** 1178-1184.

Khatami, M., Alijani, H., Sharifi, I., Sharifi, F., Pourseyedi, S., Kharazi, S., Lima Nobre, M. A. & Khatami, M. 2017. Leishmanicidal activity of biogenic Fe3O4 nanoparticles. *Scientia pharmaceutica,* 85**,** 36.

Kheshtzar, R., Berenjian, A., Taghizadeh, S.-M., Ghasemi, Y., Asad, A. G. & Ebrahiminezhad, A. 2019. Optimization of reaction parameters for the green synthesis of zero valent iron nanoparticles using pine tree needles. *Green Processing and Synthesis,* 8**,** 846-855.

Kora, A. J. & Arunachalam, J. 2011. Assessment of antibacterial activity of silver nanoparticles on Pseudomonas aeruginosa and its mechanism of action. *World Journal of Microbiology and Biotechnology,* 27**,** 1209-1216.

Król, A., Pomastowski, P., Rafińska, K., Railean-Plugaru, V. & Buszewski, B. 2017. Zinc oxide nanoparticles: Synthesis, antiseptic activity and toxicity mechanism. *Advances in colloid and interface science,* 249**,** 37-52.

Kudinha, T. 2017. The pathogenesis of Escherichia coli urinary tract infection. *Escherichia coli—Recent Advances on Physiology, Pathogenesis and Biotechnological Applications. InTech***,** 45-61.

Lingaraju, K., Naika, H. R., Manjunath, K., Basavaraj, R., Nagabhushana, H., Nagaraju, G. & Suresh, D. 2016. Biogenic synthesis of zinc oxide nanoparticles using Ruta graveolens (L.) and their antibacterial and antioxidant activities. *Applied Nanoscience,* 6**,** 703-710.

Liu, Y. C., Li, J., Ahn, J., Pu, J., Rupa, E. J., Huo, Y. & Yang, D. C. 2020. Biosynthesis of zinc oxide nanoparticles by one-pot green synthesis using fruit extract of Amomum longiligulare and its activity as a photocatalyst. *Optik,* 218**,** 165245.

Maguire, C. M., Rösslein, M., Wick, P. & Prina-Mello, A. 2018. Characterisation of particles in solution–a perspective on light scattering and comparative technologies. *Science and technology of advanced materials,* 19**,** 732-745.

Makhawi, A. & Hamadnalla, H. 2019. Phytochemical screening of leaves and roots of stylochiton borumensis: A medicinal plant. 2**,** 1-5.

Marrs, C. F., Zhang, L. & Foxman, B. 2005. Escherichia coli mediated urinary tract infections: are there distinct uropathogenic E. coli (UPEC) pathotypes? *FEMS microbiology letters*, 252**,** 183-190.

Martín-Gutiérrez, G., Rodríguez-Beltrán, J., Rodríguez-Martínez, J. M., Costas, C., Aznar, J., Pascual, Á. & Blázquez, J. 2016. Urinary tract physiological conditions promote ciprofloxacin resistance in low-level-quinolone-resistant Escherichia coli. *Antimicrobial agents and chemotherapy,* 60**,** 4252-4258.

Mashrai, A., Khanam, H. & Aljawfi, R. N. 2017. Biological synthesis of ZnO nanoparticles using C. albicans and studying their catalytic performance in the synthesis of steroidal pyrazolines. *Arabian Journal of Chemistry,* 10**,** S1530-S1536.

Matinise, N., Fuku, X., Kaviyarasu, K., Mayedwa, N. & Maaza, M. 2017. ZnO nanoparticles via Moringa oleifera green synthesis: Physical properties & mechanism of formation. *Applied Surface Science,* 406**,** 339-347.

Mehar, S., Khoso, S., Qin, W., Anam, I., Iqbal, A. & Iqbal, K. 2019. Green Synthesis of Zinc oxide Nanoparticles from Peganum harmala, and its biological potential against bacteria. *Front. Nanosci. Nanotech,* 6**,** 1-5.

Mirza, A. U., Kareem, A., Nami, S. A., Bhat, S. A., Mohammad, A. & Nishat, N. 2019. Malus pumila and Juglen regia plant species mediated zinc oxide nanoparticles: synthesis, spectral characterization, antioxidant and antibacterial studies. *Microbial pathogenesis,* 129**,** 233-241.

Mirza, A. Z. & Shamshad, H. 2011. Preparation and characterization of doxorubicin functionalized gold nanoparticles. *European journal of medicinal chemistry,* 46**,** 1857-1860.

Mitiku, A. A. & Yilma, B. 2017. Antibacterial and antioxidant activity of silver nanoparticles synthesized using aqueous extract of Moringa stenopetala leaves. *African J. Biotechnol,* 16**,** 1705-1716.

Modena, M. M., Rühle, B., Burg, T. P. & Wuttke, S. 2019. Nanoparticle characterization: what to measure? *Advanced Materials,* 31**,** 1901556.

Moges, F., Endris, M., Belyhun, Y. & Worku, W. 2014a. Isolation and characterization of multiple drug resistance bacterial pathogens from waste water in hospital and non-hospital environments, Northwest Ethiopia. *BMC research notes,* 7**,** 215.

Moges, F., Endris, M., Mulu, A., Tessema, B., Belyhun, Y., Shiferaw, Y., Huruy, K., Unakal, C. & Kassu, A. 2014b. The growing challenges of antibacterial drug resistance in Ethiopia. *Journal of global antimicrobial resistance,* 2**,** 148-154.

Mohammadi, F. M. & Ghasemi, N. 2018. Influence of temperature and concentration on biosynthesis and characterization of zinc oxide nanoparticles using cherry extract. *Journal of Nanostructure in Chemistry,* 8**,** 93-102.

Mondal, S., Roy, N., Laskar, R. A., Sk, I., Basu, S., Mandal, D. & Begum, N. A. 2011. Biogenic synthesis of Ag, Au and bimetallic Au/Ag alloy nanoparticles using aqueous extract of mahogany (Swietenia mahogani JACQ.) leaves. *Colloids and surfaces B: biointerfaces,* 82**,** 497-504.

Muhie, O. A. 2019. Antibiotic use and resistance pattern in ethiopia: systematic review and meta-analysis. *International journal of microbiology,* 2019.

Murali, M., Siva, S. & Sahitya, P. 2014. Effect of ultrasound on protein metabolism in the silkworm, Bombyx mori (L.). *Ethiopian Journal of Science and Technology,* 7**,** 67-84.

Muthuvel, A., Jothibas, M. & Manoharan, C. 2020. Effect of chemically synthesis compared to biosynthesized ZnO-NPs using Solanum nigrum leaf extract and their photocatalytic, antibacterial and in-vitro antioxidant activity. *Journal of Environmental Chemical Engineering,* 8**,** 103705.

Nagarajan, S. & Kuppusamy, K. A. 2013. Extracellular synthesis of zinc oxide nanoparticle using seaweeds of gulf of Mannar, India. *Journal of nanobiotechnology,* 11**,** 1-11.

Naz, S. S., Shah, M. R., Islam, N. U., Khan, A., Nazir, S., Qaisar, S. & Alam, S. S. 2014. Synthesis and bioactivities of silver nanoparticles capped with 5-Amino-?-resorcylic acid hydrochloride dihydrate. *Journal of nanobiotechnology,* 12**,** 1-8.

Nielsen, K. L., Stegger, M., Kiil, K., Godfrey, P. A., Feldgarden, M., Lilje, B., Andersen, P. S. & Frimodt-Møller, N. 2017. Whole-genome comparison of urinary pathogenic Escherichia coli and faecal isolates of UTI patients and healthy controls. *International Journal of Medical Microbiology,* 307**,** 497-507.

Nilavukkarasi, M., Vijayakumar, S. & Prathipkumar, S. 2020. Capparis zeylanica mediated bio-synthesized ZnO nanoparticles as antimicrobial, photocatalytic and anti-cancer applications. *Materials Science for Energy Technologies,* 3**,** 335-343.

Ny, S., Edquist, P., Dumpis, U., Gröndahl-Yli-Hannuksela, K., Hermes, J., Kling, A.-M., Klingeberg, A., Kozlov, R., Källman, O. & Lis, D. O. 2019. Antimicrobial resistance of Escherichia coli isolates from outpatient urinary tract infections in women in six European countries including Russia. *Journal of global antimicrobial resistance,* 17**,** 25-34.

O'neill, J. 2014. Antimicrobial resistance: tackling a crisis for the health and wealth of nations. *Rev. Antimicrob. Resist,* 20**,** 1-16.

Olivera, M. E., Manzo, R. H., Junginger, H., Midha, K., Shah, V., Stavchansky, S., Dressman, J. & Barends, D. 2011. Biowaiver monographs for immediate release solid oral dosage forms: Ciprofloxacin hydrochloride. *Journal of pharmaceutical sciences,* 100**,** 22-33.

Osman, M., Al Mir, H., Rafei, R., Dabboussi, F., Madec, J.-Y., Haenni, M. & Hamze, M. 2019. Epidemiology of antimicrobial resistance in Lebanese extra-hospital Settings: an overview. *Journal of global antimicrobial resistance,* 17**,** 123-129.

Patra, J. K. & Baek, K.-H. 2014. Green nanobiotechnology: factors affecting synthesis and characterization techniques. *Journal of Nanomaterials,* 2014.

Patra, P., Mitra, S., Debnath, N., Pramanik, P. & Goswami, A. 2014. Ciprofloxacin conjugated zinc oxide nanoparticle: A camouflage towards multidrug resistant bacteria. *Bulletin of Materials Science,* 37**,** 199-206.

Pavia, D. L., Lampman, G. M., Kriz, G. S. & Vyvyan, J. A. 2014. *Introduction to spectroscopy*, Cengage Learning.

Pham, T. D., Ziora, Z. M. & Blaskovich, M. A. 2019. Quinolone antibiotics. *Medchemcomm,* 10**,** 1719-1739.

Piccinno, F., Gottschalk, F., Seeger, S. & Nowack, B. 2012. Industrial production quantities and uses of ten engineered nanomaterials in Europe and the world. *Journal of Nanoparticle Research,* 14**,** 1-11.

Praburaman, L., Jang, J.-S., Muthusamy, G., Arumugam, S., Manoharan, K., Cho, K.-M., Min, C., Kamala-Kannan, S. & Byung-Taek, O. 2016. Piper betle-mediated synthesis,

characterization, antibacterial and rat splenocyte cytotoxic effects of copper oxide nanoparticles. *Artificial cells, nanomedicine, and biotechnology,* 44**,** 1400-1405.

Pryshchepa, O., Pomastowski, P. & Buszewski, B. 2020. Silver nanoparticles: Synthesis, investigation techniques, and properties. *Advances in Colloid and Interface Science***,** 102246.

Rad, S. S., Sani, A. M. & Mohseni, S. 2019. Biosynthesis, characterization and antimicrobial activities of zinc oxide nanoparticles from leaf extract of Mentha pulegium (L.). *Microbial pathogenesis,* 131**,** 239-245.

Rahaiee, S., Ranjbar, M., Azizi, H., Govahi, M. & Zare, M. 2020. Green synthesis, characterization, and biological activities of saffron leaf extract-mediated zinc oxide nanoparticles: A sustainable approach to reuse an agricultural waste. *Applied Organometallic Chemistry,* 34**,** e5705.

Raj, L. A. & Jayalakshmy, E. 2015. Effect of zinc oxide nanoparticle produced by Zingiber Officinale against pathogenic bacteria. *Journal of Chemical and Pharmaceutical Sciences,* 8**,** 124-127.

Raja, A., Ashokkumar, S., Marthandam, R. P., Jayachandiran, J., Khatiwada, C. P., Kaviyarasu, K., Raman, R. G. & Swaminathan, M. 2018. Eco-friendly preparation of zinc oxide nanoparticles using Tabernaemontana divaricata and its photocatalytic and antimicrobial activity. *Journal of Photochemistry and Photobiology B: Biology,* 181**,** 53-58.

Rajendran, N. K., George, B. P., Houreld, N. N. & Abrahamse, H. 2021. Synthesis of Zinc Oxide Nanoparticles Using Rubus fairholmianus Root Extract and Their Activity against Pathogenic Bacteria. *Molecules,* 26**,** 3029.

Rajiv, P., Rajeshwari, S. & Venckatesh, R. 2013. Bio-Fabrication of zinc oxide nanoparticles using leaf extract of Parthenium hysterophorus L. and its size-dependent antifungal activity against plant fungal pathogens. *Spectrochimica Acta Part A: Molecular and Biomolecular Spectroscopy,* 112**,** 384-387.

Rajivgandhi, G., Maruthupandy, M., Muneeswaran, T., Ramachandran, G., Manoharan, N., Quero, F., Anand, M. & Song, J.-M. 2019. Biologically synthesized copper oxide nanoparticles enhanced intracellular damage in ciprofloxacin resistant ESBL producing bacteria. *Microbial pathogenesis,* 127**,** 267-276.

Rajoriya, P., Misra, P., Singh, V. K., Shukla, P. K. & Ramteke, P. W. 2017. Green synthesis of silver nanoparticles. *Biotech Today,* 7**,** 7-20.

Rao, K. J. & Paria, S. 2015. Aegle marmelos leaf extract and plant surfactants mediated green synthesis of Au and Ag nanoparticles by optimizing process parameters using Taguchi method. *ACS Sustainable Chemistry & Engineering,* 3**,** 483-491.

Reis, A. C. C., Santos, S. R. D. S., Souza, S. C. D., Saldanha, M. G., Pitanga, T. N. & Oliveira, R. R. 2016. Ciprofloxacin resistance pattern among bacteria isolated from patients with community-acquired urinary tract infection. *Revista do Instituto de Medicina Tropical de São Paulo,* 58.

Reta, A., Bitew Kifilie, A. & Mengist, A. 2019. Bacterial Infections and Their Antibiotic Resistance Pattern in Ethiopia: A Systematic Review. *Advances in preventive medicine,* 2019.

Ribut, S. H., Abdullah, C. a. C., Mustafa, M., Yusoff, M. Z. M. & Azman, S. N. A. 2018. Influence of pH variations on zinc oxide nanoparticles and their antibacterial activity. *Materials Research Express,* 6**,** 025016.

Robino, L., Scavone, P., Araujo, L., Algorta, G., Zunino, P., Pírez, M. C. & Vignoli, R. 2014. Intracellular bacteria in the pathogenesis of Escherichia coli urinary tract infection in children. *Clinical Infectious Diseases,* 59**,** e158-e164.

Roope, L. S., Smith, R. D., Pouwels, K. B., Buchanan, J., Abel, L., Eibich, P., Butler, C. C., San Tan, P., Walker, A. S. & Robotham, J. V. 2019. The challenge of antimicrobial resistance: what economics can contribute. *Science,* 364**,** eaau4679.

Roy, N., Mondal, S., Laskar, R. A., Basu, S., Mandal, D. & Begum, N. A. 2010. Biogenic synthesis of Au and Ag nanoparticles by Indian propolis and its constituents. *Colloids and Surfaces B: Biointerfaces,* 76**,** 317-325.

Safdari, R., Ghazisaeedi, M., Masoumi-Asl, H., Rezaei-Hachesu, P., Mirnia, K. & Samad-Soltani, T. 2017. A national framework for an antimicrobial resistance surveillance system within Iranian healthcare facilities: Towards a global surveillance system. *Journal of global antimicrobial resistance,* 10**,** 59-69.

Samari, F., Baluchi, L., Salehipoor, H. & Yousefinejad, S. 2019. Controllable phyto-synthesis of cupric oxide nanoparticles by aqueous extract of Capparis spinosa (caper) leaves and application in iron sensing. *Microchemical Journal,* 150**,** 104158.

Sangeetha, G., Rajeshwari, S. & Venckatesh, R. 2011. Green synthesis of zinc oxide nanoparticles by aloe barbadensis miller leaf extract: Structure and optical properties. *Materials Research Bulletin,* 46**,** 2560-2566.

Sati, S. C., Kour, G., Bartwal, A. S. & Sati, M. D. 2020. Biosynthesis of Metal Nanoparticles from Leaves of Ficus palmata and Evaluation of Their Anti-inflammatory and Anti-diabetic Activities. *Biochemistry,* 59**,** 3019-3025.

Selvam, G. G. & Sivakumar, K. 2015. Phycosynthesis of silver nanoparticles and photocatalytic degradation of methyl orange dye using silver (Ag) nanoparticles synthesized from Hypnea musciformis (Wulfen) JV Lamouroux. *Applied Nanoscience,* 5**,** 617-622.

Shabaani, M., Rahaiee, S., Zare, M. & Jafari, S. M. 2020. Green synthesis of ZnO nanoparticles using loquat seed extract; Biological functions and photocatalytic degradation properties. *LWT,* 134**,** 110133.

Shah, M. R., Ali, S., Ateeq, M., Perveen, S., Ahmed, S., Bertino, M. F. & Ali, M. 2014. Morphological analysis of the antimicrobial action of silver and gold nanoparticles stabilized with ceftriaxone on Escherichia coli using atomic force microscopy. *New Journal of Chemistry,* 38**,** 5633-5640.

Shaikh, S., Nazam, N., Rizvi, S. M. D., Ahmad, K., Baig, M. H., Lee, E. J. & Choi, I. 2019. Mechanistic insights into the antimicrobial actions of metallic nanoparticles and their implications for multidrug resistance. *International journal of molecular sciences,* 20**,** 2468.

Shaker, M. A. & Shaaban, M. I. 2017. Formulation of carbapenems loaded gold nanoparticles to combat multi-antibiotic bacterial resistance: in vitro antibacterial study. *International journal of pharmaceutics,* 525**,** 71-84.

Sharma, N., Singh, V., Pandey, A. K., Mishra, B. N., Kulsoom, M., Dasgupta, N., Khan, S., El-Enshasy, H. A. & Haque, S. 2019. Preparation and Evaluation of the ZnO NP–Ampicillin/Sulbactam Nanoantibiotic: Optimization of Formulation Variables Using RSM Coupled GA Method and Antibacterial Activities. *Biomolecules,* 9**,** 764.

Sharma, P. C., Jain, A., Jain, S., Pahwa, R. & Yar, M. S. 2010. Ciprofloxacin: review on developments in synthetic, analytical, and medicinal aspects. *Journal of enzyme inhibition and medicinal chemistry,* 25**,** 577-589.

Sharma, R., Garg, R. & Kumari, A. 2020. A review on biogenic synthesis, applications and toxicity aspects of zinc oxide nanoparticles. *EXCLI journal,* 19**,** 1325.

Sharmila, G., Muthukumaran, C., Sandiya, K., Santhiya, S., Pradeep, R. S., Kumar, N. M., Suriyanarayanan, N. & Thirumarimurugan, M. 2018. Biosynthesis, characterization, and antibacterial activity of zinc oxide nanoparticles derived from Bauhinia tomentosa leaf extract. *Journal of Nanostructure in Chemistry,* 8**,** 293-299.

Siddiqi, K. S., Ur Rahman, A. & Husen, A. 2018. Properties of zinc oxide nanoparticles and their activity against microbes. *Nanoscale research letters,* 13**,** 1-13.

Siddiqui, M. N., Redhwi, H. H., Achilias, D. S., Kosmidou, E., Vakalopoulou, E. & Ioannidou, M. D. 2018. Green synthesis of silver nanoparticles and study of their antimicrobial properties. *Journal of Polymers and the Environment,* 26**,** 423-433.

Singh, A. K., Pal, P., Gupta, V., Yadav, T. P., Gupta, V. & Singh, S. P. 2018. Green synthesis, characterization and antimicrobial activity of zinc oxide quantum dots using Eclipta alba. *Materials Chemistry and Physics,* 203**,** 40-48.

Sirelkhatim, A., Mahmud, S., Seeni, A., Kaus, N. H. M., Ann, L. C., Bakhori, S. K. M., Hasan, H. & Mohamad, D. 2015. Review on zinc oxide nanoparticles: antibacterial activity and toxicity mechanism. *Nano-micro letters,* 7**,** 219-242.

Sivaraj, R., Rahman, P. K., Rajiv, P., Salam, H. A. & Venckatesh, R. 2014. Biogenic copper oxide nanoparticles synthesis using Tabernaemontana divaricate leaf extract and its antibacterial activity against urinary tract pathogen. *Spectrochimica Acta Part A: Molecular and Biomolecular Spectroscopy,* 133**,** 178-181.

Sreedharan, S. M. & Singh, R. 2019. Ciprofloxacin Functionalized Biogenic Gold Nanoflowers as Nanoantibiotics Against Pathogenic Bacterial Strains. *International Journal of Nanomedicine,* 14**,** 9905.

Steiger, S. N., Comito, R. R. & Nicolau, D. P. 2017. Clinical and economic implications of urinary tract infections. *Expert review of pharmacoeconomics & outcomes research,* 17**,** 377-383.

Stuart, B. H. 2004. *Infrared spectroscopy: fundamentals and applications*, John Wiley & Sons.

Sulaiman, G. M., Waheeb, H. M., Jabir, M. S., Khazaal, S. H., Dewir, Y. H. & Naidoo, Y. 2020. Hesperidin loaded on gold nanoparticles as a drug delivery system for a successful

biocompatible, anti-cancer, anti-inflammatory and phagocytosis inducer model. *Scientific reports,* 10**,** 1-16.

Suresh, D., Shobharani, R., Nethravathi, P., Kumar, M. P., Nagabhushana, H. & Sharma, S. 2015. Artocarpus gomezianus aided green synthesis of ZnO nanoparticles: luminescence, photocatalytic and antioxidant properties. *Spectrochimica Acta Part A: Molecular and Biomolecular Spectroscopy,* 141**,** 128-134.

Suresh, J., Pradheesh, G., Alexramani, V., Sundrarajan, M. & Hong, S. I. 2018. Green synthesis and characterization of zinc oxide nanoparticle using insulin plant (Costus pictus D. Don) and investigation of its antimicrobial as well as anticancer activities. *Advances in Natural Sciences: Nanoscience and Nanotechnology,* 9**,** 015008.

Sutradhar, P. & Saha, M. 2016. Green synthesis of zinc oxide nanoparticles using tomato (Lycopersicon esculentum) extract and its photovoltaic application. *Journal of Experimental Nanoscience,* 11**,** 314-327.

Sweileh, W. M., Al-Jabi, S. W., Sa'ed, H. Z., Sawalha, A. F. & Abu-Taha, A. S. 2018. Global research output in antimicrobial resistance among uropathogens: A bibliometric analysis (2002–2016). *Journal of global antimicrobial resistance,* 13**,** 104-114.

Tamaekong, N., Liewhiran, C. & Phanichphant, S. 2014. Synthesis of thermally spherical CuO nanoparticles. *Journal of Nanomaterials,* 2014.

Tc, P., Mathew, L., Chandrasekaran, N., Raichur, A. M. & Mukherjee, A. 2010. Biomimetic synthesis of nanoparticles: science, technology & applicability. *Biomimetics: Learning from Nature***,** 1, 1-18.

Tekle, A., Belay, A., Kelem, K., Wodajo, B. & Tesfaye, Y. 2015. Nutritional profile of Moringa stenopetala species samples collected from different places in Ethiopia. *European Journal of Nutrition & Food Safety***,** 1100-1101.

Thatoi, P., Kerry, R. G., Gouda, S., Das, G., Pramanik, K., Thatoi, H. & Patra, J. K. 2016. Photo-mediated green synthesis of silver and zinc oxide nanoparticles using aqueous extracts of two mangrove plant species, Heritiera fomes and Sonneratia apetala and investigation of their biomedical applications. *Journal of Photochemistry and Photobiology B: Biology,* 163**,** 311-318.

Tielen, P., Narten, M., Rosin, N., Biegler, I., Haddad, I., Hogardt, M., Neubauer, R., Schobert, M., Wiehlmann, L. & Jahn, D. 2011. Genotypic and phenotypic characterization of

Pseudomonas aeruginosa isolates from urinary tract infections. *International Journal of Medical Microbiology,* 301**,** 282-292.

Tiwari, V., Mishra, N., Gadani, K., Solanki, P. S., Shah, N. & Tiwari, M. 2018. Mechanism of anti-bacterial activity of zinc oxide nanoparticle against carbapenem-resistant Acinetobacter baumannii. *Frontiers in microbiology,* 9**,** 1218.

Tom, R. T., Suryanarayanan, V., Reddy, P. G., Baskaran, S. & Pradeep, T. 2004. Ciprofloxacin-protected gold nanoparticles. *Langmuir,* 20**,** 1909-1914.

Tuem, K. B., Desta, R., Bitew, H., Ibrahim, S. & Hishe, H. Z. 2019. Antimicrobial resistance patterns of uropathogens isolated between 2012 and 2017 from a tertiary hospital in Northern Ethiopia. *Journal of global antimicrobial resistance,* 18**,** 109-114.

Uma, C. & Sekar, K. 2014. Phytochemical analysis of a folklore medicinal plant Citrullus colocynthis L (bitter apple). *Journal of pharmacognosy and Phytochemistry,* 2, 195-202.

Umar, H., Kavaz, D. & Rizaner, N. 2019. Biosynthesis of zinc oxide nanoparticles using Albizia lebbeck stem bark, and evaluation of its antimicrobial, antioxidant, and cytotoxic activities on human breast cancer cell lines. *International journal of nanomedicine,* 14**,** 87.

Van Giau, V., An, S. S. A. & Hulme, J. 2019. Recent advances in the treatment of pathogenic infections using antibiotics and nano-drug delivery vehicles. *Drug design, development and therapy,* 13**,** 327.

Velammal, S. P., Devi, T. A. & Amaladhas, T. P. 2016. Antioxidant, antimicrobial and cytotoxic activities of silver and gold nanoparticles synthesized using Plumbago zeylanica bark. *Journal of Nanostructure in Chemistry,* 6**,** 247-260.

Venkatesh, N., Bhowmik, H. & Kuila, A. 2018. Metallic nanoparticle: a review. *Biomedical Journal of Scientific & Technical Research,* 4**,** 3765-3775.

Vijayakumar, S., Arulmozhi, P., Kumar, N., Sakthivel, B., Kumar, S. P. & Praseetha, P. 2020. Acalypha fruticosa L. leaf extract mediated synthesis of ZnO nanoparticles: Characterization and antimicrobial activities. *Materials Today: Proceedings,* 23**,** 73-80.

Vijayakumar, S., Vaseeharan, B., Malaikozhundan, B. & Shobiya, M. 2016. Laurus nobilis leaf extract mediated green synthesis of ZnO nanoparticles: characterization and biomedical applications. *Biomedicine & Pharmacotherapy,* 84**,** 1213-1222.

Vimala, K., Sundarraj, S., Paulpandi, M., Vengatesan, S. & Kannan, S. 2014. Green synthesized doxorubicin loaded zinc oxide nanoparticles regulates the Bax and Bcl-2 expression in breast and colon carcinoma. *Process biochemistry,* 49**,** 160-172.

Vinardell, M. P., Llanas, H., Marics, L. & Mitjans, M. 2017. In vitro comparative skin irritation induced by nano and non-nano zinc oxide. *Nanomaterials,* 7**,** 56.

Vineetha, N., Vignesh, R. & Sridhar, D. 2015. Preparation, standardization of antibiotic discs and study of resistance pattern for first-line antibiotics in isolates from clinical samples. *International Journal of Applied Research,* 1**,** 624-631.

Wahab, R., Kim, Y.-S. & Shin, H.-S. 2009. Synthesis, characterization and effect of pH variation on zinc oxide nanostructures. *Materials transactions,* 50**,** 2092-2097.

Walsh, C. & Collyns, T. 2017. The pathophysiology of urinary tract infections. *Surgery (Oxford),* 35**,** 293-298.

Woźniak-Budych, M. J., Przysiecka, Ł., Langer, K., Peplińska, B., Jarek, M., Wiesner, M., Nowaczyk, G. & Jurga, S. 2017. Green synthesis of rifampicin-loaded copper nanoparticles with enhanced antimicrobial activity. *Journal of Materials Science: Materials in Medicine,* 28**,** 42.

Wu, G., Wang, G., Fu, X. & Zhu, L. 2003. Synthesis, crystal structure, stacking effect and antibacterial studies of a novel quaternary copper (II) complex with quinolone. *Molecules,* 8**,** 287-296.

Yang, N. & Li, W.-H. 2013. Mango peel extract mediated novel route for synthesis of silver nanoparticles and antibacterial application of silver nanoparticles loaded onto non-woven fabrics. *Industrial Crops and Products,* 48**,** 81-88.

Yusof, H. M., Mohamad, R. & Zaidan, U. H. 2019. Microbial synthesis of zinc oxide nanoparticles and their potential application as an antimicrobial agent and a feed supplement in animal industry: a review. *Journal of animal science and biotechnology,* 10**,** 57.

Yuvakkumar, R., Suresh, J., Nathanael, A. J., Sundrarajan, M. & Hong, S. 2014. Rambutan (Nephelium lappaceum L.) peel extract assisted biomimetic synthesis of nickel oxide nanocrystals. *Materials Letters,* 128**,** 170-174.

Zheng, J., Zhou, C., Yu, M. & Liu, J. 2012. Different sized luminescent gold nanoparticles. *Nanoscale,* 4**,** 4073-4083.

Zhou, G. & Lv, X. 2020. Ciprofloxacin Resistance in Hospital and Community-acquired Urinary Tract Infections by Escherichia coli: A Systematic Review and Meta-analysis. *bioRxiv*.

Zhu, X., Pathakoti, K. & Hwang, H.-M. 2019. Green synthesis of titanium dioxide and zinc oxide nanoparticles and their usage for antimicrobial applications and environmental remediation. *Green Synthesis, Characterization and Applications of Nanoparticles.* Elsevier.

APPENDICES

Appendix I. Calibration curve for drug loading

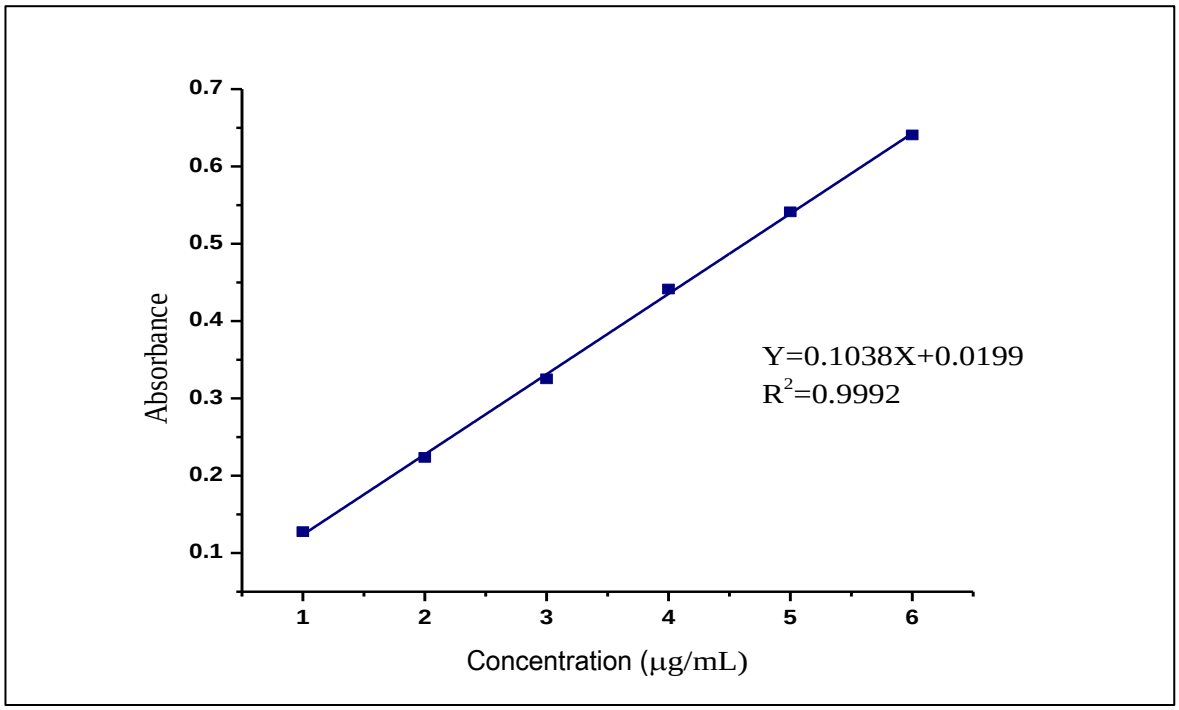

Appendix II. Calibration curves for drug release

A) Standard calibration curve of pure ciprofloxacin at λmax of 276 nm in buffer solution with pH value of 1.2.

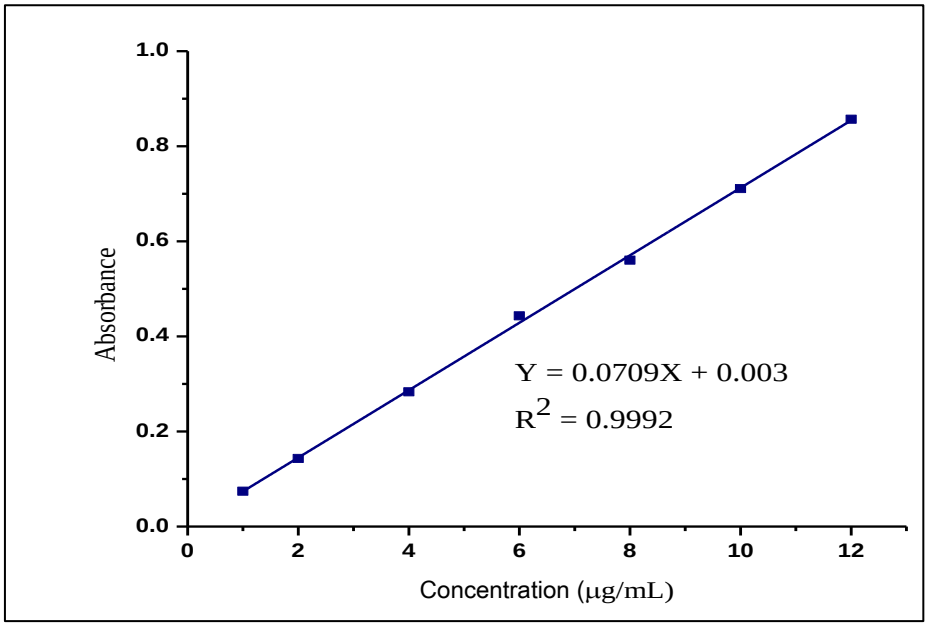

B) Standard calibration curve of pure ciprofloxacin at λ_{max} of 276 nm in buffer solution with pH value of 6.0.

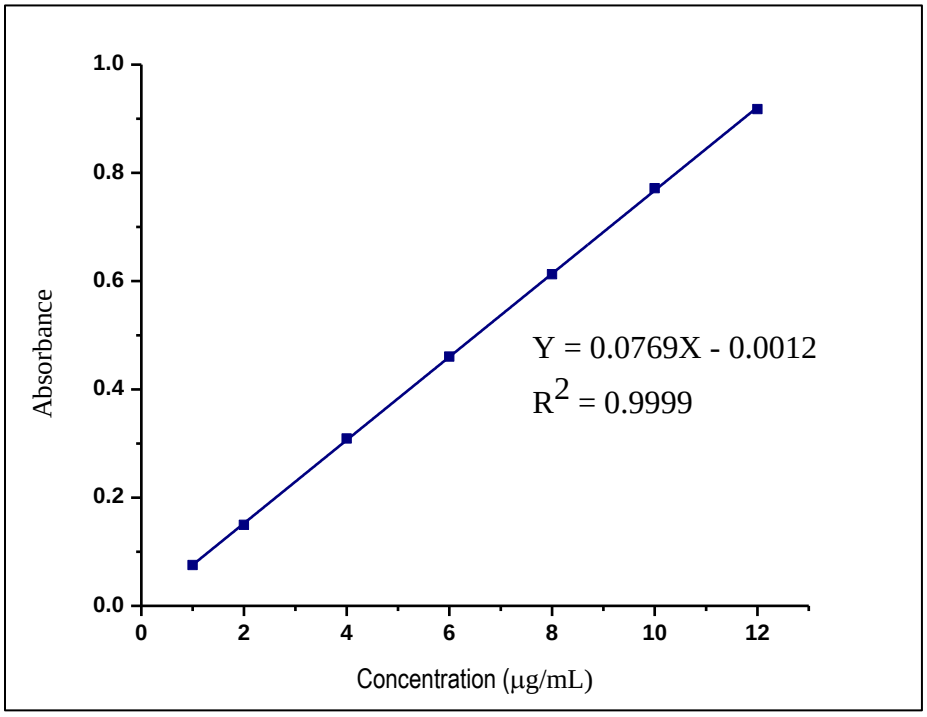

C) Standard calibration curve of pure ciprofloxacin at λ_{max} of 270 nm in buffer solution with pH value of 6.8.

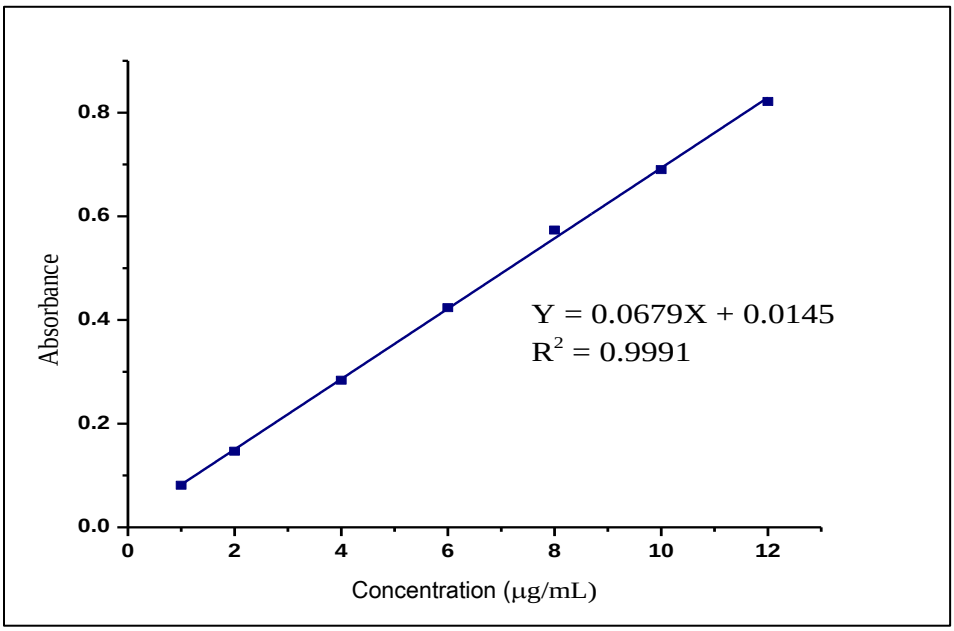

D) Standard calibration curve of pure ciprofloxacin at λ_{max} of 268 nm in buffer solution with pH value of 7.4.